Characterization and Simulation of the Deformation Behaviour of Elastomer Particle Filled Polypropylene Compounds

Master Thesis

by

Ermei Wang

at the

Institute of Materials Science and Testing of Plastics

University of Leoben

Supervisor: Dipl.-Ing. Dr.mont. Zoltan Major

Academic Adviser: O. Univ.-Prof. Dipl.-Ing. Dr. Reinhold W. Lang

Leoben, 2008-09-10

ACKNOWLEDGMENT

At the beginning, I would like to express my heartfelt gratitude to o.Univ.-Prof. Dipl.-Ing. Dr.mont. Reinhold W. Lang and to Dipl.-Ing. Dr.mont. Zoltan Major who kindly helped me to finish my academic work. Prof. Lang is the academic advisor of my bachelor thesis and master thesis. I am very grateful to his valuable revision and supervision of my work. I am most indebted to Mr. Major for his continuous motivation and support during my whole study. As my supervisor, he taught me how to deal with the problems in practice, and showed me how to apply the theory that I have learned. Without him, this work would not have today's form. I sincerely acknowledge his numerous suggestions, corrections and ideas so that I could begin and finish this work. Moreover, he helped me to overcome various difficulties in my study as well as in daily life, and I appreciate all his dedication for me. Furthermore, I appreciate very much the friendship afforded to me by Mr. Major and his family.

I would also like to express my thankfulness to people who facilitated the accomplishment of this work. The most challenging part of this work was the TEM (transmission electron microscopy) investigation. It couldn't have been possible to obtain the necessary micrographs for this work without the commitment and expertise of three ladies at the Austrian Centre for Electron Microscopy and Nanoanalysis (i.e. the Institute for Electron Microscopy of the Graz University of Technology, Graz Centre for Electron Microscopy). My special thanks go to Mrs. Elisabeth Ingolic, Mrs. Claudia Mayrhofer and Mrs. Maria Belegratis. Mr. Armin Zankel and Mr. Peter Pölt at the University of Technology, Graz, have provided me with useful literature about microscopy and are to be gratefully acknowledged, too. As to microscopy, I would like to take this opportunity to extend my special thanks to Mr. Walter Rath for showing me the fundamental operation of several kinds of microscopes and for his humour that made the work even more interesting. For the mechanical experiments, I am very grateful to Mr. Juergen Föttinger for having manufactured plenty of specimens. Thanks also go to Mr. Michael Jerabek and Mr. Simon Gastl for their help in uniaxial tensile tests. Mr. Jerabek has also made control of the experimental data for my work and gave valuable advice. Mr. Gastl carried out the simulation for this work, which was of great importance for my discussion and interpretation of the test results. Without Mr. Gabor Molnar, I would not have managed it to carry out the biaxial tensile tests. Thanks a lot for your readiness to help. For the biaxial tensile tests, Mr. Erwin Mach has provided me with useful references and should be acknowledged here, too. The help in the biaxial tensile tests by Mr. Maximilian Tonjecs and Mr. Georg Chaloupka is also acknowledged. Mr.

Georg Chaloupka and Mr. Zoltan Major have made the pure shear tensile tests together with me; I would like to thank them for their contribution. As to the DMA experiments, Mr. Bernd Schrittesser taught me how to set up the machine, to choose the relevant parameters and to handle the data, therefore my best thanks to him as well. I am especially indebted to Dr. Erika Augustin for proof reading the English test of this thesis and for many helpful suggestions and corrections regarding English grammar and style.

Furthermore, I wish to express my sincere gratitude for their valuable advice and friendship, respectively, to the following persons:

Ao. Univ.-Prof. Dipl.-Ing. Dr. techn. Brigitte Weinhardt, Mag. Martin Payer, Miss Ines Ragger, Miss Kerstin Kriszt, MMag. Jana Maurer, Mrs. Seraphine Janisch, Mrs. Michaela Ersl, Prof. Dipl.-Ing. Dr.mont. Walter Friesenbichler, Dipl.-Ing. Artur Fertschej, Mrs. Ernestine Vojacek, Mag. Nina Pongratz, Mag. Helmut Kozarac, Miss Hannelore Mattausch, Miss Marlene Knausz, Miss Katharina Bruckmoser, DI. Cornelia Kock, Dipl.-Ing. Resch Katharina, Mr. Ivaylo Mitev, Mr. Hausberger Andreas, Mr. Bernd Haar, Mr. Christof Kucher, Dipl.-Ing. Martin Reiter, Dipl.-Ing. Dr.mont. Christian Feichter, Dipl.-Ing. Andreas Frank, Mr. Alexander Lovas, Dipl.-Ing. Markus Wolfahrt, DI. Daniel Tscharnuter, Mr. Robert Karpf and many others whose names are not mentioned here.

I gratefully thank the companies and Institutions that enabled me to undertake apprenticeship in a variety of technique fields:

University of Leoben, Leoben, Austria

Polymer Competence Center Leoben GmbH (PCCL, Austria), Leoben, Austria

Institute of Materials Science and Testing of Plastics, University of Leoben, Austria

Institute of Plastics Processing, University of Leoben, Austria

Siemens Transportation Systems GmbH & Co KG (STS), Graz, Austria

Semperit Technische Produkte GmbH. Wimpassing, Austria

Economos Austria GmbH, Judenburg, Styria, Austria

Borealis Austria GmbH, Linz, Austria

Keba AG, Linz, Austria

Particular thanks go to the **Afro-Asiatisches Institut (AAI)**, Graz, Austria, for the scholarship and for the inspiration of “Eine-Welt (One-World)”.

At last, I express the deepest love and highest respect to my parents. Their support and confidence in me underly every my improvement. Their support and confidence enabled me to proceed on my way and all my efforts were dedicated to them. Whatever I achieve in future I will owe to them.

The research work of this thesis **"Characterization and Simulation of the Deformation Behaviour of Elastomer Particle Filled Polypropylene Compounds"** was performed within the Kplus-project **„Effect of Constituent Properties on Material Laws of Heterogeneous Thermoplastic Compounds" (project-no.: II-1.03)** at the Polymer Competence Center Leoben GmbH (PCCL, Austria) within the framework of the Kplus-program of the Austrian Ministry of Traffic, Innovation and Technology with contributions by the Institute of Materials Science and Testing of Plastics at the University of Leoben and Borealis GmbH Austria. The PCCL is funded by the Austrian Government and the State Governments of Styria and Upper Austria.

AFFIDAVIT

I declare in lieu of oath, that I wrote this thesis and performed the associated research myself, using only literature cited in this volume.

Date

Signature

1 INTRODUCTION AND OBJECTIVES

Polypropylene (PP) is a highly versatile material offering a wide range for modification and in its performance profile and with cost advantages. PP is available not only as homopolymers or copolymers but also in form of blends and compounds, being tailored to particular applications. Through physical or chemical blending with numerous different materials, multiphasic compounds can be generated. Compounding broadens the property range of the neat PP and yields additional or enhanced properties for special applications [Karger-Kocsis, 1995; Moore, 1996].

To meet the increasing requirements for material performance, diverse fillers are used to improve certain properties of the neat PP and consequently to enlarge its application extent. Typical fillers for polymeric materials are natural organic materials such as wood, cloth and inorganic minerals like chalk or talc, and glass, carbon and so on. Compounding is a procedure of mixing of constituents (fillers and matrix materials) into a heterogenous or homogenous blend [Karger-Kocsis, 1995; Moore, 1996; Wypych, 1999]. The components are commonly dry-mixed, melting processed and then followed by extrusion or moulding of the mixture. Generally, we distinguish between physical and chemical blending. The convenience of physical blending in terms of both composition development and industrial production makes it a prominent processing approach.

The elastomers are known as hyperelastic polymeric materials with lower stiffness and glass transition temperature, and are widely used as modifiers for toughening of polymers (commodity polymers like PS, PVC, PE, PP). A modification of PP with elastomers improves low temperature behaviour and impact resistance, while maintaining the mechanical properties of PP at the same time [Moore, 1996; Van der Wal et al., 1998 and 1999].

However, PP-elastomer compounds are of great complexity because the two constituents are principally immiscible even in the molten state [Utracki, Dumoulin and Karger-Kocsis, 1995]. The component properties and the processing have to be studied scientifically in the product design to achieve the desirable end-use quality. Therefore coupled with experimental testing the computational simulation has been employed instead of carrying out time or cost intensive testings and enables unlimited research work of material engineers and designers.

This work is a part of the research project carried out in cooperation by the Borealis Austria GmbH (Linz, Austria) and the Polymer Competence Center Leoben GmbH (PCCL, Leoben, Austria), where it is attempted to predict the composite properties by means of simulation in the software DIGIMAT [Gastl, 2008] based on information on the characteristic values of both constituents and compounds from

monotonic and dynamic mechanical experiments and study of the micro morphology.

In this work, experimental tests results of both constituents and compounds of an elastomer filled PP with two different filler volume fractions are presented and discussed. Furthermore, some simulations were performed under simplified conditions, as the preliminary approach of exploring the availability and the constraint of the simulation and modeling in design of PP composites.

2 BACKGROUND

2.1 Introduction to modification of Polypropylene (PP)

Polypropylene (PP) is a semicrystalline thermoplastic viscoelastic material. Isotactic polypropylene (iPP) has a density, ρ, of around 0.9 g/cm³ at 25 °C, a tensile modulus, E, about 1600 MPa at 25 °C, a glass transition temperature, T_g, of 0 °C, and a melting temperature, T_m, about 165 °C [Saechtling, 1995]. Due to its excellent cost-performance ratio, PP has been supplied extensively as commercial and engineering material for decades. In addition to its conventional applications, diverse PP based copolymers, terpolymers and composites have been developed to extend the useful property range of PP. Wypych introduced a variety of fillers and their properties, effects and processing techniques [Wypych, 1999]. In the following sections some important and most frequent used fillers for reinforcement of polypropylene will be briefly summarized.

2.1.1 Deformation characteristics of neat polypropylene - the matrix

The material microstructure of PP and the load conditions, including the temperature, the rate, the mode and amplitude of the load, the environment and the specimen configuration are basic factors that influence the deformation and failure behaviour of neat PP. Two modes of irreversible microdeformation are commonly observed in a polymeric material, namely the shear yielding and the craze formation [Narisawa, 1999; Van der Wal et al., 1999]. The two mechanisms occur alternatively or more often simultaneously with one of them as dominant. Depending on which of them will be promoted by the loading magnitude, loading rate, temperature and the material composition, the material fails macroscopically in a brittle or ductile manner.

Crazing is generally considered to be caused by normal forces or stresses. The appearance of brittle breakage of material has its origin in crazing, where molecules will be stretched in direction of local stress (**Fig. 1** (a)). A craze consists of micro fibrils and voids. The fibrils bridge the two inner surfaces of a craze, and a crack will be ultimately produced, if the fibrillous strands are broken with increasing elongation parallel to the stress direction. The formation and growth of crazes contribute to energy absorption. Once the critical size and amount of micro crazes have been reached, the material fails in a catastrophic way. As a consequence, brittle fracture surface of material will be shaped [Birley et al., 1992; Moore, 1996; Strobl, 1996].

Another competitive deformation mechanism to crazing is the more desirable shear yielding. Shear bands occur on a plane of maximum resolved shear stress, that is at 45° to the main stress (**Fig. 1** (b)). Compared to craze yielding, shear yielding does not induce change of the material volume. Ductile deformation of unfilled

polymers under load corresponds usually to the formation of shear bands, thus shear yielding is a favorable flow of material in practice [Birley et al., 1992; Moore, 1996; Strobl, 1996]. The craze and shear yielding of polymer molecule chains are illustrated in **Fig. 1**:

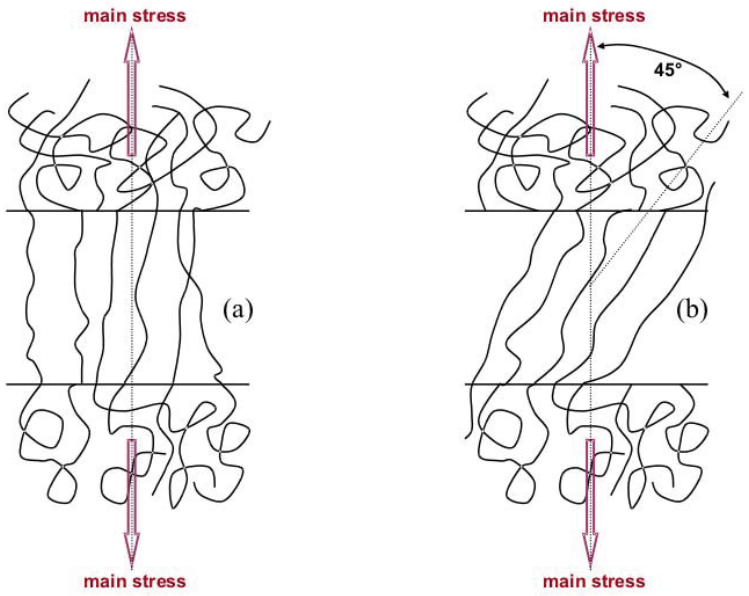

Fig. 1: Deformation mechanisms in polymers: (a) craze yielding (b) shear yielding (with reference to [Hertzberg, 1995]).

2.1.2 Deformation characteristics of elastomer - the filler

A compound can be described as a multiphasic material, in which the dispersed phases are physically or chemically mixed in the resin material. Most of the fillers have a volume fraction of up to 20 % [Moore, 1996]. Roughly the filler particles can be classified as hard and soft particles. The typical hard particles which are used to reinforce PP are glass fibres, minerals like talc, mica and calcium carbonates, while diverse elastomers are the most representative soft fillers.

2.1.2.1 The hard fillers

Fillers in polymeric blends have generally two functions [Karger-Kocsis, 1995; Moore, 1996; Wypych, 1999]. Passive fillers such as clay or kaolin are incorporated into the compounds to reduce their volume cost; in principle, the loading of passive filler does not aim to affect the material performance. In contrast to passive fillers, the active fillers enhance the performance of neat polymers or even introduce certain physical properties into the resin material, and thus gain great importance.

As to PP, talc is one of the most frequent added inorganic filler, which offers many consistent properties like high stiffness, high yield strain, better surface-scratch resistance and low thermal expansion coefficient, low shrinkage [Moore 1996; Bucknall and Paul, 1999]. In the literature it is also reported that talc might be a

nucleating agent for PP. In some observations, a change of crystallite type from ß to α of the processed PP has also been identified due to the existence of the talc [Varga and Schulek-Toth, 1991].

Another widely used filler for PP formulation is calcium carbonate ($CaCO_3$). The loading of $CaCO_3$ in a PP composition approaches up to 40 % by weight. It is available in fine or coarse particles with chemical surface treatment or coupling agent. $CaCO_3$ filled PP compounds exhibit well-established mechanical properties: increased elongation at fracture, higher notched impact strength. The cost of $CaCO_3$ filled PP is even lower than talc filled PP at equivalent filler content [Moore, 1996; Bucknall and Paul, 1999].

Furthermore, possibilities of adding rigid but finer inorganic fillers, including mica, dolomite, wollastonite, to PP were also intensively investigated [Karger-Kocsis, 1995], because these filler particles possess higher aspect ratio and smaller size, which cause considerable adaptations of mechanical properties of a PP composition due to the size effect on processing and on crystallinity of the PP resin.

Glass fillers must be mentioned especially, because of their sufficient enhancement to not only PP but also many other engineering polymers. Glass in itself is a rigid solid, whose tensile modulus is between 40000 MPa and 90000 MPa at room temperature. Its glass transition temperature is over 400 °C. Glass filler is available in spheric or fibrous form. Long glass fibres with high aspect ratio are compounded into polymers to increase the elastic modulus and tensile strength to a higher degree. With short glass fibres a relatively isotropic reinforcement can be reached. Due to the excellent mechanical performance and low market price of glass reinforced PP, the glass-PP compounds replace polycarbonate (PC), acryl-butadiene-styrol (ABS), polyester in many applications such as automotive, housing, panels, etc [Moore, 1996; Bucknall and Paul, 1999; Wypych, 1999].

Pukanszky has reported the performance of different hard particle filled polypropylenes [Pukanszky, 1995]. The change of flexural modulus of PP modified by glass fibre, talc and $CaCO_3$ is shown in **Fig. 2**. The change of tensile yield stress of PP modified by $CaCO_3$ with various treatments is presented in **Fig. 3**. Recently, Grein has depicted the alteration of the tensile modulus and toughness of ß-PP filled with $CaCO_3$ as function of filler content in weight in a three-dimensional plot, as shown in **Fig. 4**. Further, Pukanszky has presented the effect of filler particle size on the tensile yield stress of PP composites as shown in **Fig. 5**.

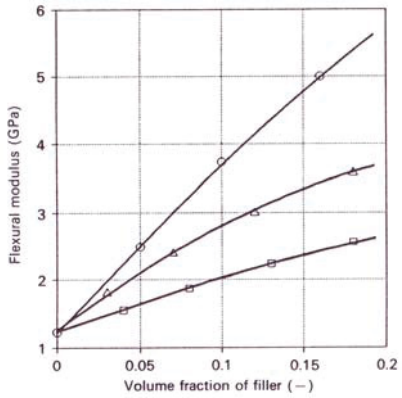

Fig. 2: Flexural modulus of PP composites in function of filler volume fraction: (o) glass fiber, (Δ), talc, (▫) CaCO3 [Pukanszky, 1995].

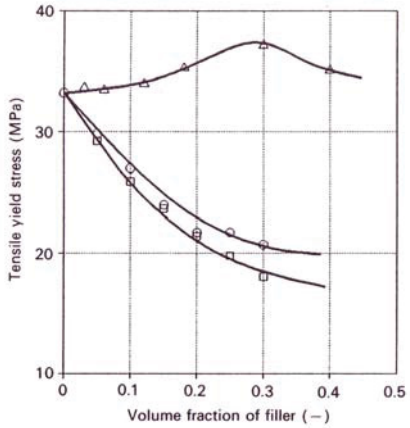

Fig. 3: Tensile yield stress of PP/$CaCO_3$ composites in function of filler volume fraction: (o) non-treated, (Δ) stearic acid treated, (▫) MA-PP modified [Pukanszky, 1995].

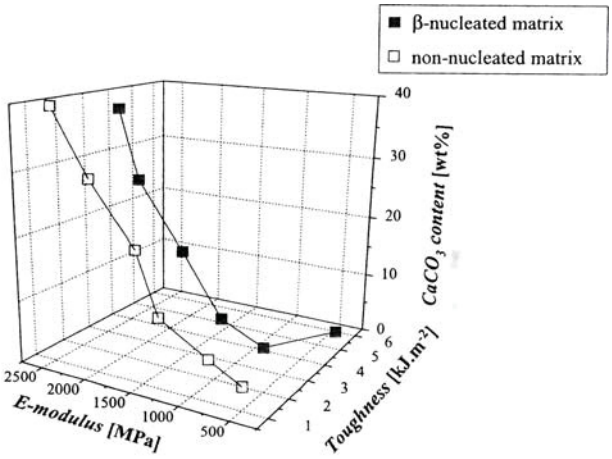

Fig. 4: Evolution of the tensile modulus, E, and notched impact strength of composites based on PP (MFI: 40 g/min) with increasing amounts of $CaCO_3$. [Tjong, 1997; Grein, 2005]

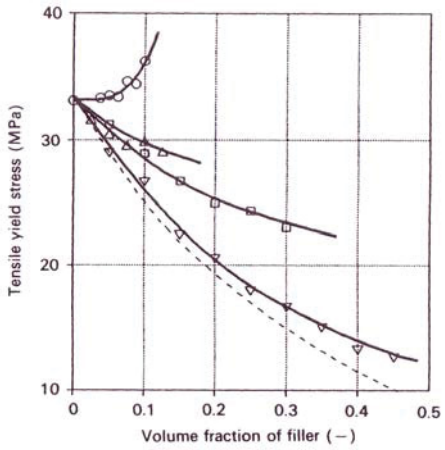

Fig. 5: Effect of hard filler particle size on the tensile yield stress of PP composites. Particle diameter: (O) 0.01 µm, (Δ) 0.08 µm, (▫) 3.3 µm, (∇) 58.0 µm and (---) theoretical prediction [Pukanszky, 1995].

2.1.2.2 The soft fillers

After the brief review of hard particle fillers which improve principally the stiffness and strength of PP, soft fillers and the toughening mechanism will be introduced in detail. The impact strength of neat PP exhibits embrittlement at lower temperatures. The elastomers are added to PP to provide an enhancement in impact.

The simplest compound is a binary system comprised of two constituents. The constituent with higher content is the continuous phase, and it is called the matrix. The second constituent dispersed in the continuous phase is the discrete phase, the filler. The common elastomer fillers for PP are natural rubber (NR), butadiene rubber (BR), ethylene propylene rubber (EPR), ethylene propylene diene copolymer (EPDM), styrene butadiene rubber (SBR) and so on. Compared to the hard particles the elastomers change their shape, size, orientation, dispersion, and distribution in greater dependence on process conditions like temperature, shear stress, and the flow velocity. But because of the unique toughening effect of the elastomer phase, elastomer-modified PPs have become an interesting group of polypropylene based compounds. Thus a lot of investigations of the elastomer-PP compounds have been carried out in the past [Karger-Kocsis, 1995; Van der Wal et al., 1998 and 1999], and more will be performed in the future employing modern techniques.

There are two types of elastomer-modified PP compounds, depending on whether the elastomeric phase is vulcanized or not [Moore, 1996]. The vulcanized elastomers are cross-linked rubbers that stay solid after chemical cross-linking of molecules and will not melt under heat any more [Moore, 1996]. Since the elegant

processing techniques have been developed, the fabrication of PP-based elastomer vulcanizates can be performed in one reactor; that is, in other words, to carry out the mixing of two phases and the cross-linking of elastomeric phase at the same time or in a multistep process in one set-up [Moore, 1996]. The performance characteristics of such a compound system are for example lower compression set, improved fatigue and failure behaviour, good resistance to heat, humidity and chemicals. The hardness of the compound with vulcanized elastomeric phase can even be extended to that of PP [Moore, 1996].

The thermoplastic elastomers are non-crosslinked; they undergo repeatable melting and solidification procedures by variation of temperature. A thermoplastic elastomer-modified PP composition can be manufactured by mechanical blending or direct polymerization in a reactor. Besides good resistance to solvents, chemicals, and thermal stability, compounds from PP and thermoplastic elastomers are economically more interesting than the composition with vulcanizates [Karger-Kocsis, 1995; Coran and Patel, 1995; Moore, 1996].

No matter whether vulcanized, the elastomers that are incorporated into PP lead to dramatically improved toughness of PP compounds at lower temperatures, at relatively small expense of stiffness and strength. For reference, the change of the tensile modulus, E, and yield stress, σ_y, of polyisobutylene (PIB) modified PP is demonstrated as a function of PIB percentage in **Fig. 6** [Martuscelli, 1995]. In a three-dimensional chart by [Varga, 1994] in **Fig. 7**, it can be seen how the impact strength can be enhanced by the rubber phase, regarding the temperature dependence.

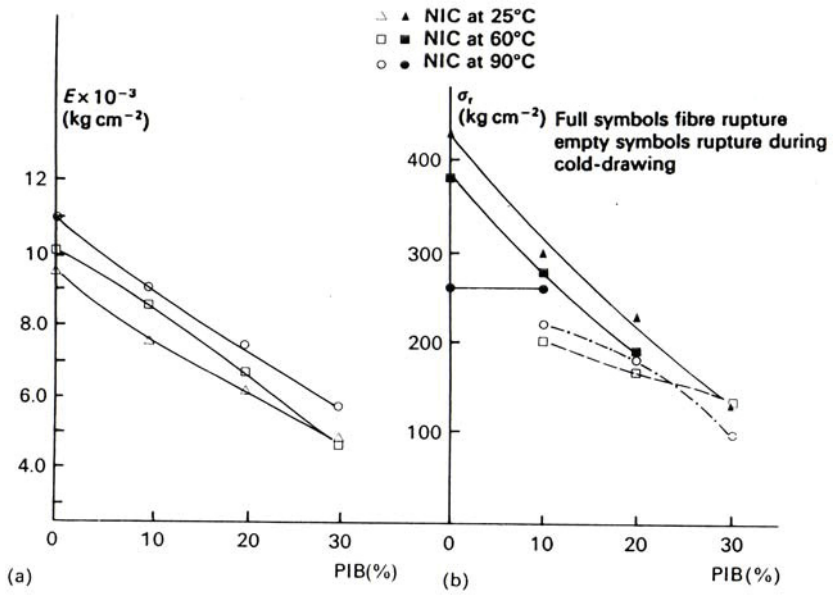

Fig. 6: Tensile modulus, E, (left) and yield stress, σ_y, (right) of PIB modified PP as a function of PIB percentage [Martuscelli, 1995].

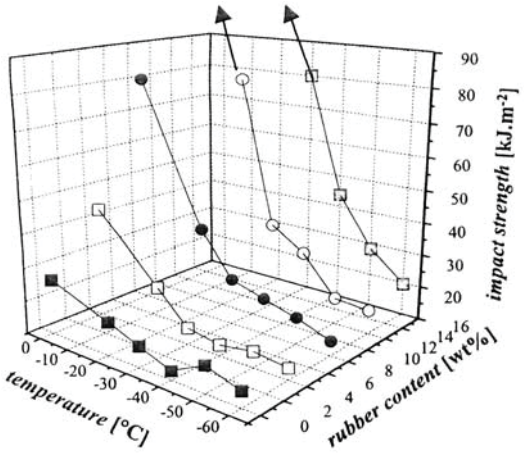

Fig. 7: Flexural impact strengths of ß-modified rubber toughened PP plotted versus the amount of rubber content of the blends and the testing temperature. The arrows indicate samples that did not break [Varga, 1994; Grein, 2005].

2.1.2.3 Rubber elasticity

Compared to other solid materials, elastomeric materials possess the following mechanical properties: (1) Elastomers undergo large reversible elastic deformation up to maximum of about 1000 %, whilst the reversible deformation of thermoplastics is under 10 % and of metal is normally only 1 %. (2) Elastomers exhibit comparably small modulus values in the order of 10^{-1}-10 MPa, while the modulus of thermoplastics is in the order of 10^{3} MPa and that of metal about 10^{6} MPa. (3) The deformation of elastomers is exothermal and restoration endothermal, where the recovery of elongation or compression is a relaxation procedure that is time dependent [Ma et al., 1981]. The large elastic deformation behaviour of rubber is about 90 % entropic in its nature.

An elastomer can be envisaged as an irregular three-dimensional network whose molecule chains are correlated by cross-links. The motion of the chain segment between two cross-links can be demonstrated by the tube model in **Fig. 8** that goes back to Edwards and de Gennes [Vilgis, 2003]. In a network, the elastomer chains are random cross-linked and entangled as shown in **Fig. 8**a. A chain segment between two joint points can be considered like trapped in tube, the chain motion being more or less restricted by the neighbouring structure (**Fig. 8**b and 8c). Through cross-linking the micro deformation of elastomer chain segments synchronizes with the macro deformation of the material.

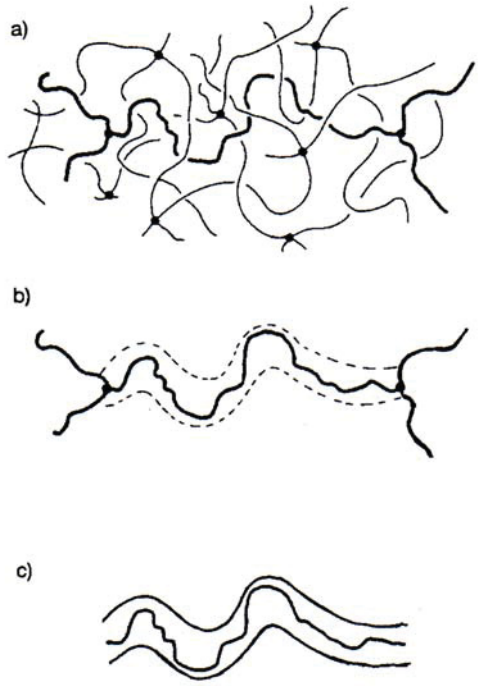

Fig. 8: Tube model that illustrates the motion space of a chain segment between two cross-links in an elastomer network [Vilgis, 2003].

The one-dimensional elongation of a polymer chain can be illustrated by **Fig. 9**, where the chain deforms along the x-axis, if the chain is exposed to an external force in the x direction. The three-dimensional description of the chain deformation is the affine theory, shown in **Fig. 10**.

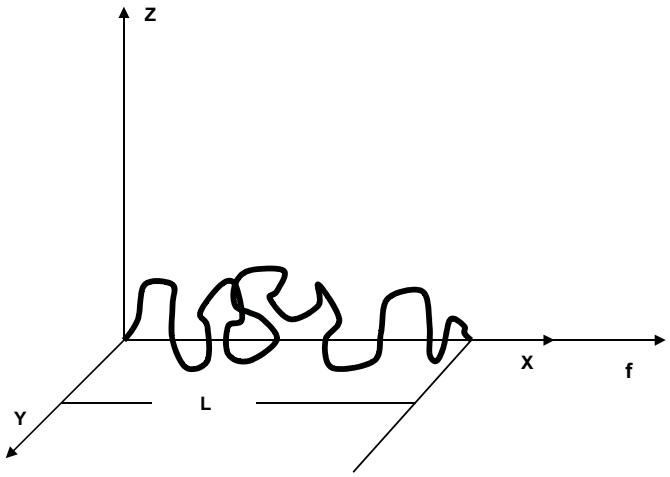

Fig. 9: A polymer chain whose ends are fixed by external force f in x-direction.

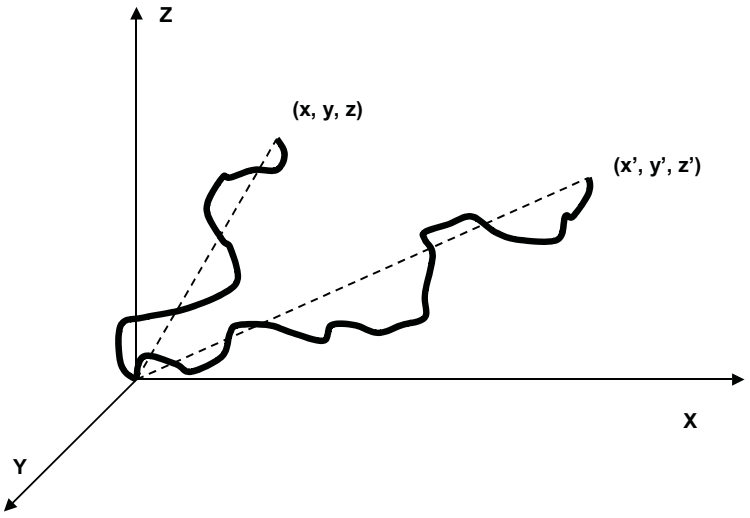

Fig. 10: Affine deformation of a polymer chain.

The statistical theory of rubber elasticity, which regards the chain of elastomers as a Gaussian chain, is based on the following assumptions according to [Treloar, 1975]:

1. The network contains N Gaussian chains per unit volume, a chain being defined as the segment of molecule between successive points of cross-linkage.
2. The mean-square end-to-end distance for the whole ensemble of chains in the undeformed state is the same as for a corresponding set of free chains.
3. The volume is constant on deformation.
4. The junction points between chains move on deformation as if they were embedded in an elastic continuum. As a result the components of length of each chain change in the same ratio as the corresponding dimensions of the bulk rubber (Affine deformation assumptions).
5. The entropy of the network is the sum of the entropies of the individual chains.

The work of deformation, W, can be then given by [Treloar, 1975]:

$$W = \frac{1}{2} NkT(\lambda_1^2 + \lambda_2^2 + \lambda_3^2 - 3) \qquad (1)$$

where N is the number of chains per unit volume, k is Boltzmann's constant, and T the temperature.

The stretch ratio λ_i is defined as:

$\lambda_i = (1+\varepsilon)$ (2)

W represents the work of deformation or elastically stored free energy per unit volume of the rubber. It can be also written in the form:

$$W = \frac{1}{2}G(\lambda_1^2 + \lambda_2^2 + \lambda_3^2 - 3) \quad (3)$$

where G is the shear modulus:

$G = NkT$ (4)

Obviously, the work of deformation, W, only depends on stretch ratio and the number of chains per unit volume, N, taking account of the influence of temperature. The work of deformation of elastomer in this sense does not relate to the chemical structure of elastomer itself. It is of significance that the statistical theory correlates the deformation of the molecule chain with the macro network deformation.

The statistical theory was later amended by James and Guth (1943) who suggest that the junction points in the elastomer network are not fixed but take part in the micro-Brownian motion of the associated chain elements or links [Treloar, 1975]. Only those junction points which are located on the boundary surfaces of the rubber are specified as fixed. A very large number of joint points are fluctuating in the network. In addition, regarding the existence of network imperfections like interloping or physical entanglement between chains that exert comparably like a cross-link, the closed loop as a result of the linkage of two points on a single chain and chains with a free end, Gase (1960), Scanlan (1960) and Gordon, Kucharik, and Ward (1970) developed diverse theories to represent the network deformation [Treloar, 1975].

A breakthrough in the attempt to describe deformation behaviour of elastomer network should be the phenomenological theory [Treloar, 1975]. The phenomenological theory is an approach that is based not on the molecular or structural concepts but on the merely mathematical reasons. Thus it is possible to obtain a more accurate mathematical formulation of the general properties of elastomers [Treloar, 1975].

In practice, the performance of elastomers at higher elongations is of major interest. The large deformation behaviour of hyperelastic materials like elastomers can be characterized by the strain energy functions; the one used in this work is the simplified Mooney-Rivlin strain energy function [Treloar, 1975]:

$$W = C_{10}(I_1 - 3) + C_{01}(I_2 - 3) \quad (5)$$

where W is the strain energy density, C_{10}, C_{01} are constants and I_1, I_2 and I_3 are

Cauchy strain invariants, which can be expressed as:

$$I_1 = \lambda_1^2 + \lambda_2^2 + \lambda_3^2 \tag{6}$$

$$I_2 = \lambda_2^2\lambda_3^2 + \lambda_3^2\lambda_1^2 + \lambda_1^2\lambda_2^2 \tag{7}$$

$$I_3 = \lambda_1^2\lambda_2^2\ \lambda_3^2 \tag{8}$$

The two basic assumptions of the Mooney-Rivlin theory are: the elastomers are incompressible and isotropic if not deformed; the simple shear deformation can be described by Hooke's law [Treloar, 1975]. Because of the incompressibility of elastomer, I_3 is equal to 1.

There are different strain states a material may be submitted to during stretch. In general, the following three modes of strain states will be investigated in research works to establish data set for the strain energy function:

1.) Uniaxial tension: $\lambda_1 = \lambda$ $\lambda_2 = \lambda_1^{-1/2}$ $\lambda_3 = \lambda_1^{-1/2}$

2.) Pure shear: $\lambda_1 = \lambda$ $\lambda_2 = 1$ $\lambda_3 = \lambda_1^{-1}$

3.) Equibiaxial tension: $\lambda_1 = \lambda$ $\lambda_2 = \lambda_1$ $\lambda_3 = \lambda_1^{-2}$

The usual specimen configurations for tests in the introduced three strain states are illustrated in **Fig. 11** and the material behaviour for each state is schematically plotted in **Fig. 12**. The testing methods and corresponding results will be shown in the later sections.

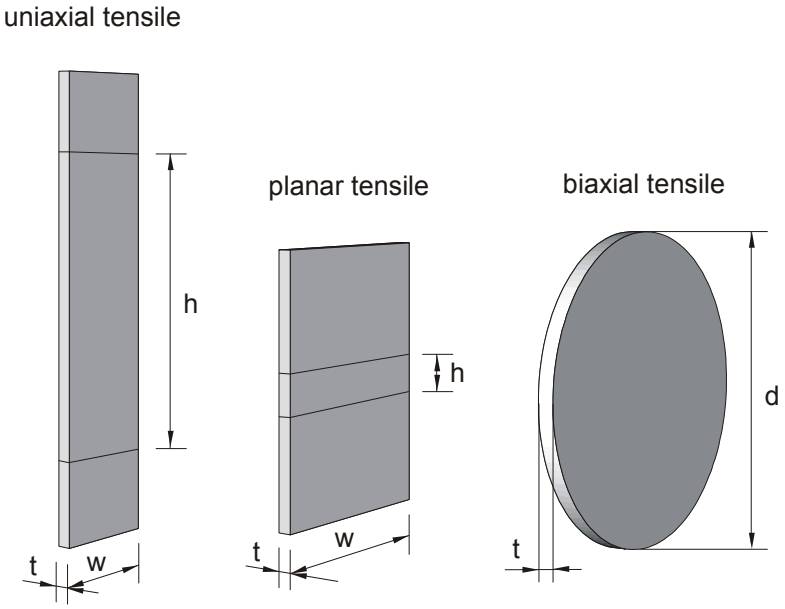

Fig. 11: Illustration of specimens for uniaxial, planar, and biaxial strain conditions. (image copied from the script "Kunststoffeigenschaften und Bauteilverhalten" edited by [Major, 2007])

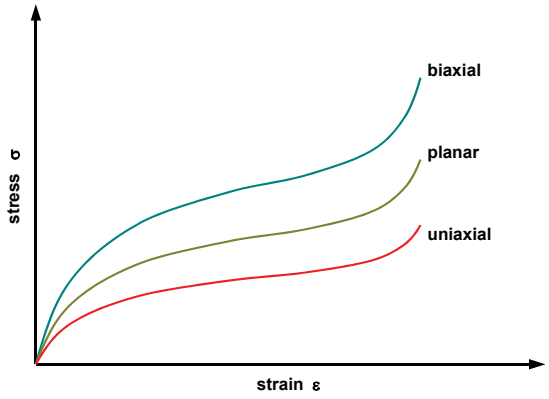

Fig. 12: Schemea of stress-strain relationship under different strain states.

Mooney (1940) has devised the semiemperical formulas that are consistent with each strain state. According to Treloar the two-constant formula for uniaxial tension can be written in the form:

$$Y = \frac{f}{2\left(\lambda - 1/\lambda^2\right)} = C_1 + \frac{C_2}{\lambda} \qquad (9)$$

where f is the force per unit of undeformed area.

The formula (9) was deduced from the functions (5) to (8) (see Section 2.1.4). The two material constants C_1 and C_2 are identical to the C_{10} and C_{01}, respectively in the general formulation which is valid not only for uniaxial tension state but also for pure shear and biaxial tension. The plot of Y against 1/λ is the so-called Mooney plot (**Fig. 13**). It is a straight line in the region of larger strains. The slope of the Mooney plot results in the constant C_2 and the intercept on the vertical axis shows the value of C_1. Generally accepted explanation proposes that the C_1 = E/6 is a function of network structure, while C_2 is associated with the flexibility of the network and is primarily dependent on the crosslink density [Ha-Anh and Vu-Khanh, 2005]

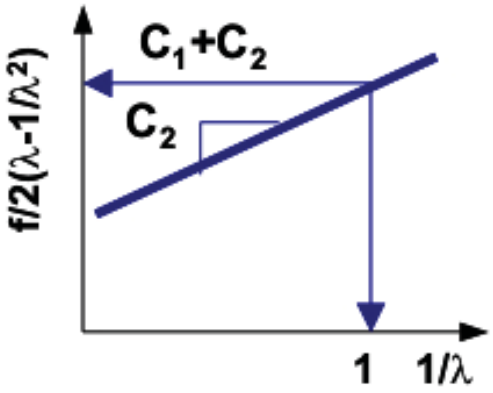

Fig. 13: Estimation of C_1 and C_2 in Mooney plot.

2.1.3 Deformation characteristics of elastomer filled PP compounds

In the previous sections, the deformation behaviour of each constituent of an elastomer-modified PP composition has been summarized. The improvement of the ductility of such a toughening system has been discussed in literature based on the study of a rich diversity of PP compounds with different elastomers. A widely accepted explanation of micro deformation mechanisms of elastomer toughening is the multiple crazing theory [Bucknall and Smith, 2006]. The multiple crazing theory describes the impact energy dissipation during deformation in terms of the interactive micro-mechanisms which are derived from the respective constituent properties but show some new features in the compound.

Beside crazing and shear bands that are introduced in the preceding Section 2.1.1, voids in the elongated elastomeric domains of compounds have been found in great quantities. If the compound is submitted to mechanical loading, the rigid PP matrix makes it difficult to release energy by expanding the elastomer particles; the energy may then be absorbed through formation of cavitations inside the elastomer domain. According to the strength of the interfacial adhesion between the elastomer phase and PP phase, voids that occur in the interface lead directly to debonding. Debonding is the disjunction of the matrix and the filler, it causes decrease of the effective cross section of a sample perpendicular to the loading direction, since the stress will be less sufficiently transported between constituents of a compound. Debonding weakens the performance of a particle-filled compound and should be avoided, reduced or delayed in applications. For this reason, the interfacial adhesion has been intensively investigated, and many surface treatments for filler particles and coupling agents have been developed as well [Wool, 1995; Kimberly et al., 2000]. G'Sell et al. have studied the plastic deformation of polypropylene/polyamide 6/polyethylene-octene elastomer (PEO) blends and proposed the different formation mechanisms of cavitation inside the elastomer particle and of interfacial debonding as in **Fig. 14** [G'Sell et al., 2004].

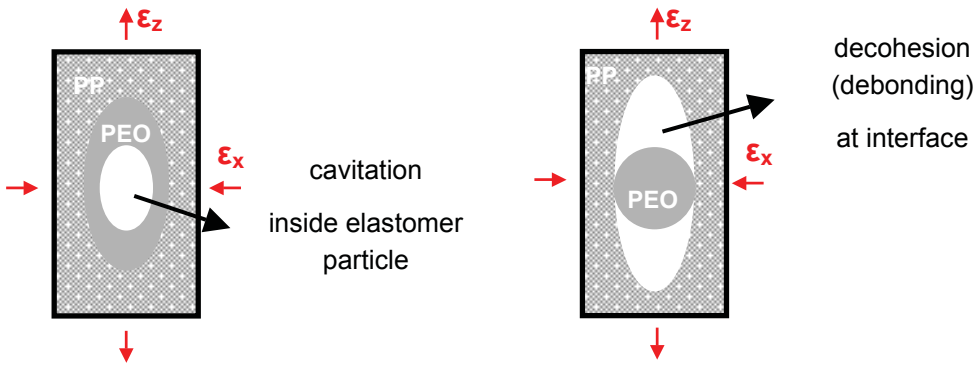

Fig. 14: Schemes of cavitation ($-\varepsilon_x/\varepsilon_z \approx ½$) and debonding ($-\varepsilon_x/\varepsilon_z << ½$) formation mechanisms [G'Sell et al., 2004].

Polypropylene matrix fails at lower temperature by crazing without large plastic flow. The elastomer inclusions in PP matrix play two roles in the energy absorption so that the impact performance can be sufficiently improved. On the one hand, they contribute to trigger the formation of micro-crazes in subcritical size so that the energy can be absorbed. Owing to the low modulus, the elastomer particles that are dispersed in polypropylene act as stress concentrator [McCrum et al., 1988]. On the other hand, the growth of micro-crazes stops, if the craze tip meets another elastomer particle, preventing the crack formation. The dimension of elastomer particles dispersed in matrix is important for both initiation and termination of micro-crazes. Particles should have appropriate size to provide stress concentration that is needed to initiate micro-crazes. In turn the elastomer particles must be able to hinder the propagation of crazes to avoid crack initiation. The interaction between crazes and elastomer fillers is the essential toughening mechanism. In addition the elongation and the rupture of elastomer particles contribute to the overall energy dissipation and absorption, too.

Shear bands were also identified in brittle fracture though in small amount. They can devote to a minor part of energy dissipation. Moreover, in sense of toughening, if placed in front of micro crazes, shear bands may also act as kicker against craze growth. Furthermore, it has been suggested that the local stress field introduced by shear bands may compensate the stress concentration around filler particles or crazes to certain degree [Yokoyama, 1998]. In fact, the closer the stress fields around elastomer particles, PP crystallites, crazes and shear bands are, the stronger the interaction between these local stress fields shall be.

Between the above mentioned deformation phenomena, one of them may be preponderant in most cases, depending on the individual matrix nature principally. Since the compound is a more or less heterogenous system, the interaction between those mechanisms must take place at different deformation stages and parts of a product. If taking the loading and environmental conditions into consideration, it is not possible to bring out universal prediction of material behaviour. Many research works [Herbst, 2008; Jerabek, 2008] therefore employ computer modeling and simulation to differentiate between or combine those complicated processes selectively; this approach brings new comfort and advantages for material engineers and designers in the investigation of elastomer toughened polymer systems.

2.1.4 Influence of processing on compounds

As for the performance of elastomer-toughened polypropylene, one must take account of the individual processing factors that play roles not only in the production but also in the application of end products. Since the elastomeric and the polypropylene phases are immiscible, a proper processing must be adjusted

carefully to achieve the intended end product properties. In this section, we are going to have a short look of the complexity and the influencing factors of the processing of elastomer PP compounds.

The elastomer and the polypropylene are blended normally in the molten state. In some cases, elastomer phase will be polymerized in the polypropylene phase in the reactor. The thermodynamics of mixing of two phases can be normally described by the Flory-Huggins theory [Strobl, 1996]. The “Gibbs free energy of mixing” is the change of the energy of the system that is generated through combination of two distinct components, and denoted ΔG. The “Gibbs free energy of mixing” is given by $\Delta G=\Delta H-T\Delta S$, where the ΔH is the change of enthalpy, and the ΔS is the change of entropy. As a necessary requirement for the occurrence of mixing, the “Gibbs free energy of mixing” ΔG must be negative. For polymers, the change of entropy is usually small during mixing and therefore negligible. Decisive is, whether the term ΔH is negative or positive and whether the absolute value of ΔH is smaller than that of the term $T\Delta S$ in the case of a positive ΔH. In most cases of elastomer-modified polypropylenes the elastomeric phase is immiscible with the polypropylene phase. Hence, many efforts have been made to obtain fine and quasi-uniform dispersed phase structure through adjusting processing parameters. As to miscibility and compatibility of the phases of a polymer blend in fluid state, Bucknall et al. have introduced diverse models in details [Bucknall et al., 1999].

As is well known, particle size and particle size distribution are of major significance to the efficiency of toughening effect of the elastomeric phase [Karger-Kocsis, 1995]. In the pioneer work of Taylor in 1934, the break-up process of a liquid drop suspended in a liquid continuous phase has been discussed at first. Later, based on the model proposed by Taylor, Rayleigh and Tomotika have contributed to describe the break-up of droplet in flow field, taking account of the viscosities of both droplet (or thread, if largely elongated) and surrounding fluid. During the course of processing of polymer compounds, the particle size and particle size distribution are usually controlled by the following factors [Briscoe et al., 1999]:

1. the initial particle radius;
2. the magnitude and type of the applied strain field;
3. the flow history;
4. the relative viscosities of the continuous and dispersed phase; and
5. the interface tension between the two melts.

Recent research [Briscoe et al., 1999] highlighted a considerable influence of:

6. the experimental geometry; and
7. the influence of a third species, such as a surfactant.

If one is concerned with the relationship between processing and blend morphology, the viscosity ratio is one of the two main processing relevant parameters. The viscosity ratio, η_r, is the ratio of the viscosity of the dispersed phase to the viscosity of the continuous phase, defined as $\eta_r=\eta_{dispersed}/\eta_{matrix}$.

The Weber number, We (also called Capilary number, Ca), represents the ratio of the viscous forces that facilitate the deformation of droplet to the interfacial tension, σ, which promotes the restoration of droplets. The Weber number is the second processing relevant parameter in terms of particle deformation in flow field, and is given by $We=\dot{\gamma}*\eta_{matrix}*a/\sigma$, where *a* is the radius of the undeformed drop, the $\dot{\gamma}$ is the local shear rate. The critical Weber number, We_{cr}, is a function of η_r and the type of flow field. If $We>We_{cr}$, droplet break-up takes place, as the deforming viscous force overwhelms the constraining interfacial tension.

It is known that in injection moulding, there are shear flow and extensional flow in the mould. In case of simple shear flow, if $\eta > \eta_r$, no droplet break-up will be triggered, irrespective of shear rate, $\dot{\gamma}$. And in case of extensional flow, droplet break-up occurs at smaller We_{cr}, irrespective of η_r [Moore, 1996].

The relationship between the Weber number and viscosity ratio has been represented by the Taylor dispersion [Moore, 1996; Briscoe et al., 1999]. This relationship is plotted in **Fig. 15**, where the upper part of the chart refers to instability of droplet, that is to say the droplet tends to be divided into smaller ones. Martuscelli has introduced the Rayleigh-Taylor-Tomotika theory in his book in detail [Martuscelli, 1990]. According to the study of Martuscelli of PP/EPR and PA 6/ EVA blends, the dependence of the dispersed particle size upon the phase viscosity ratio, η_r, can be illustrated as in **Fig. 16**, which yields good agreement with the prediction of Tomotika theory.

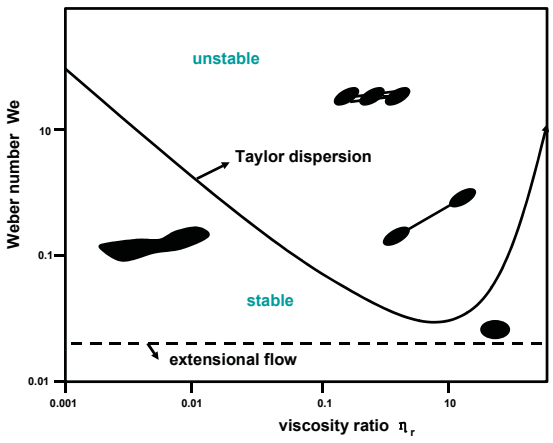

Fig. 15: The relationship between Weber number, We, and the viscosity ratio, η_r. The solid line shows the Taylor dispersion, while the dashed line describes the case of extensional flow [Moore, 1996].

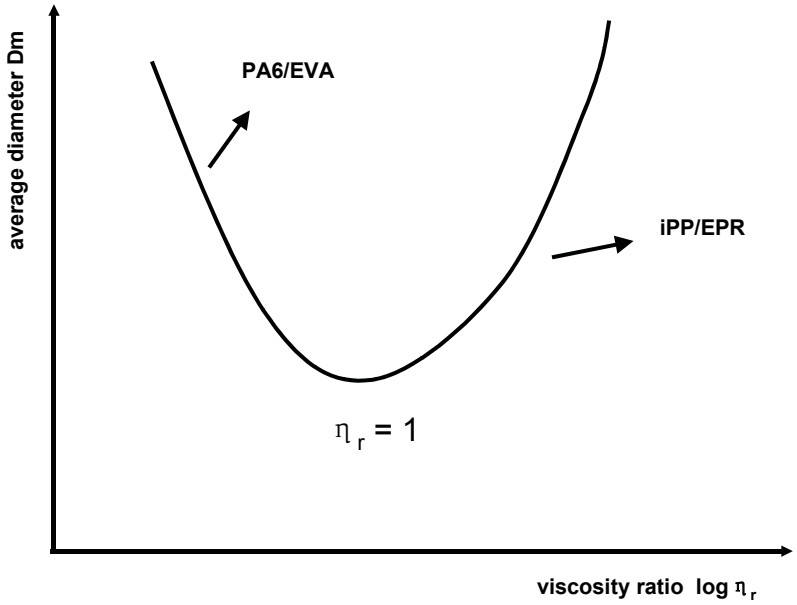

Fig. 16: Average diameter, D_m, of dispersed particles as a function of the Log η_r. Trend as predicted by Tomotika theory [Martuscelli and Karger-Kocsis, 1995].

2.1.5 Properties of elastomer-modified polymers

There are a great number of different elastomeric toughеners and the diverse resin materials fail by different mechanisms according to their inherent structures. Moreover, the parametric sensibility of the characteristic values like fracture toughness, K_{IC}, fracture energy, G_{IC}, etc. may be changed by particular test conditions like temperature and test rate, It is difficult to evaluate the toughening effect of elastomers quantitatively. Generally, the improvement of impact behaviour is more or less at the expense of other mechanical properties like stiffness and tensile strength. The elastomer content in commercial polymer products does not exceed 20 %, since greater quantities of elastomer phase in the compound result in an undesirable softening of the material to be toughened [Moore, 1996]. Lovell et al. have identified a decrease of tensile modulus of PMMA from 3 GPa to 1 GPa as the rubber volume fraction increases from 0 vol% to 30 vol%. They also reported that the yield strength of PMMA is reduced from less than 60 MPa to 30 MPa as the rubber volume fraction increases from 0 vol% to 30 vol%. But at the same time the PMMA with 10-15 vol% rubber modifier has trebled its fracture toughness, K_{IC}, and fracture energy, G_{IC}, compared with neat PMMA [Lovell et al., 1993]. Verchere et al. have suggested that at rubber volume fraction of 30 vol%, the G_{IC} of the diepoxide based on bisphenol A diglycidyl ether cured with a cycloaliphatic diamine in the presence of ETBN is almost three times as much as the G_{IC} of the epoxy

resin [Verchere et al., 1993]. Moore has also mentioned in his book that the elongation of impact modified PS reaches 40 % instead of 3 % [Moore, 1996]. Rezaifard et al. have investigated a novel rubber, poly (methyl methacrylate)-g-natural rubber (Hevea-plus MG) as toughening agent for bisphenol A diglycidyl ether (BPA) and found that the G_{IC} of the BPA can be elevated up to more than 6000 J/m^{-2} at 10 phr (parts per hundred) MG content instead of 1000 J/m^{-2} [Rezaifard et al., 1993].

In terms of the effect of elastomer particle size on the compounds performance, the optimum particle size for impact resistance should decrease with increasing ductility of the plastic. It is found by Morton et al. that 1.2 µm represents the largest particle size possible by emulsion polymerization. An optimum had been suggested in the rubber particle size of about 1-2 µm for high-impact PS. For PS, no toughening exists if particle size is less than 1.2 µm. They have also concluded that rubbers with lower T_g show stronger toughening effect [Morton et al., 1984]. To get an idea of the order of the effective elastomer particle size, it is recognized that the optimum particle size of elastomeric toughener for PVC is about 0.1-0.2 µm, for SAN around 0.3-0.8 µm, for PS about 1-2 µm, and for polypropylene (PP) about 0.4 µm, based on various observations [Morton et al., 1984; Moore, 1996]. It can be seen that elastomer-modified polymer system is far more than complicated; a general statistical plot of the influence of elastomers has not been found in literature.

The properties of the elastomer-toughened PP are strongly related to the two components; therefore it is helpful to keep in mind the individual material behaviour of the elastomer and of the PP while discussing the performance of the compound. Here we simply compare the tensile behaviour and the variation of the modulus in relationship to temperature of the two constituents with each other. The tensile stress-strain relationship of the PP and elastomer at room temperature are drawn in **Fig. 17** approximately. **Fig. 18** illustrates the modulus as a function of temperature of PP and elastomer Schemetically. The upper and lower limits of the corresponding compound property range are given by the two constituents. This will be shown by the experimental test results in the later sections.

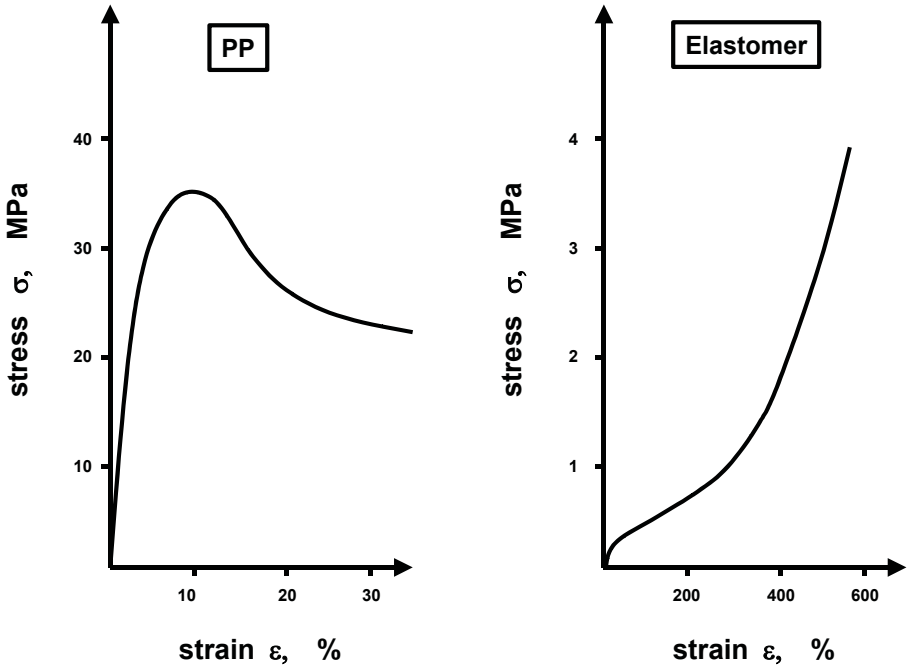

Fig. 17: Scheme of the tensile stress-strain relationship of PP and elastomer.

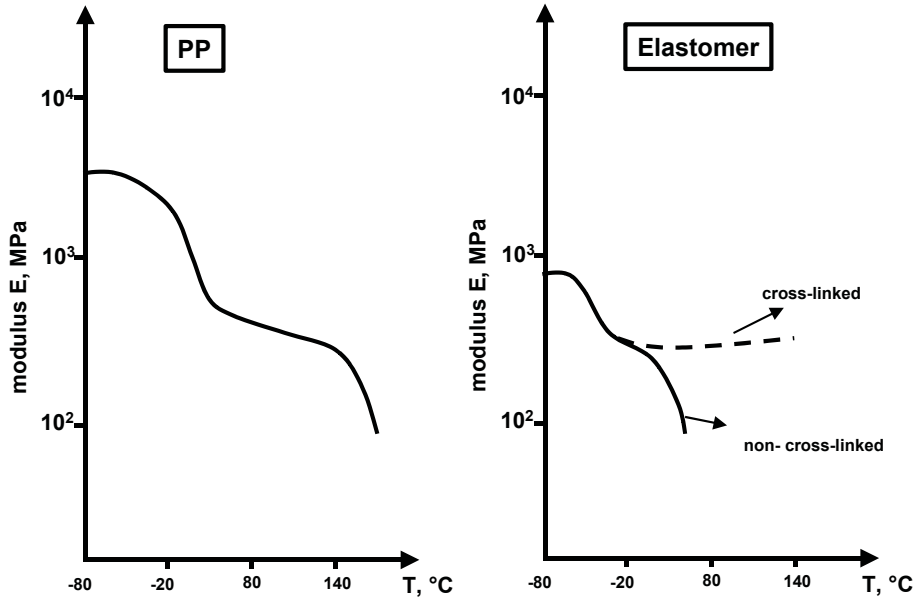

Fig. 18: Scheme of temperature dependence of modulus of PP and elastomer.

In the above sections we have reviewed the reinforcements of PP. The fundamental deformation mechanisms of the PP, elastomer, and their compound were interpreted in general. As shown in **Fig. 19** the polymer experiences linear-viscoelastic deformation, yielding, post-yielding (necking), and sometimes hardening during stretching. In this work, the mechanical experiments and the simulation only focus on the small strain behaviour, where the linear viscoelasticity dominates. The plastic deformation and fracture behaviour of the relevant compounds will be discussed elsewhere [Major, to be published].

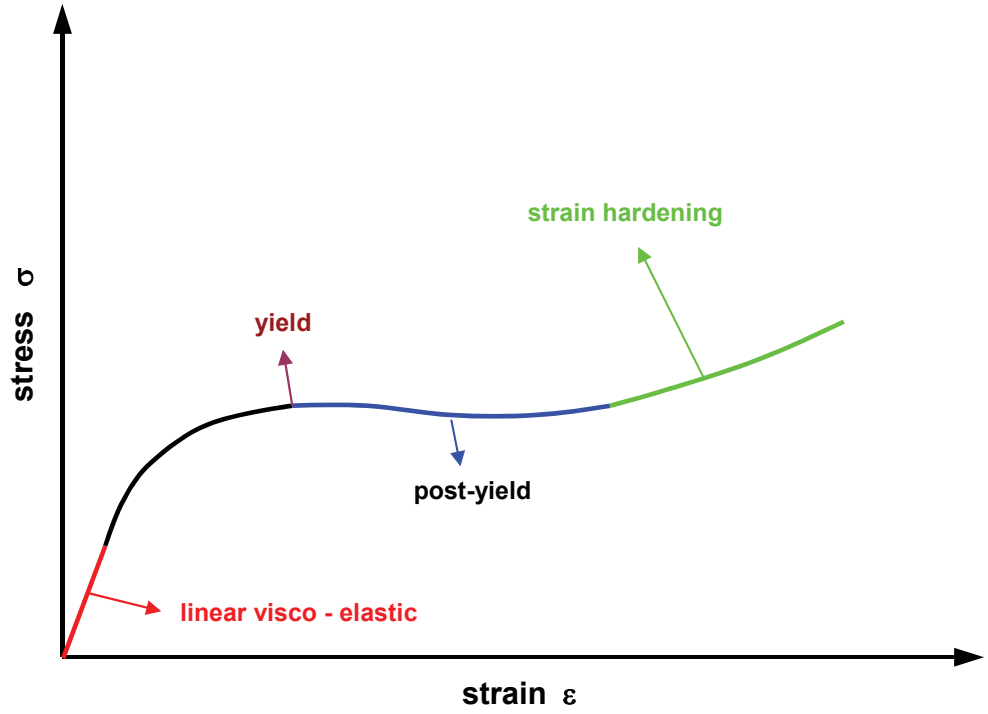

Fig. 19: Scheme of the deformation stages of polymer material under tension.

The different modifying effects of hard and soft particles are schematically illustrated in **Fig. 20**. Due to their rigidity, the hard particles as dispersed phase enhance the stiffness and the strength of the PP matrix, but accompanied by embrittlement in most cases. Hard particle modified PP fractures at comparably smaller strain. In contrast, the soft particles contribute mainly to the toughness of PP. Although the stiffness and strength will be accordingly affected, PP with elastomeric phase bears large plastic deformation and fractures at higher strain. Either particles have merit and demerit in terms of modification of PP, some researchers also tried to combine the hard and soft fillers [Zebarjad et al., 2006].

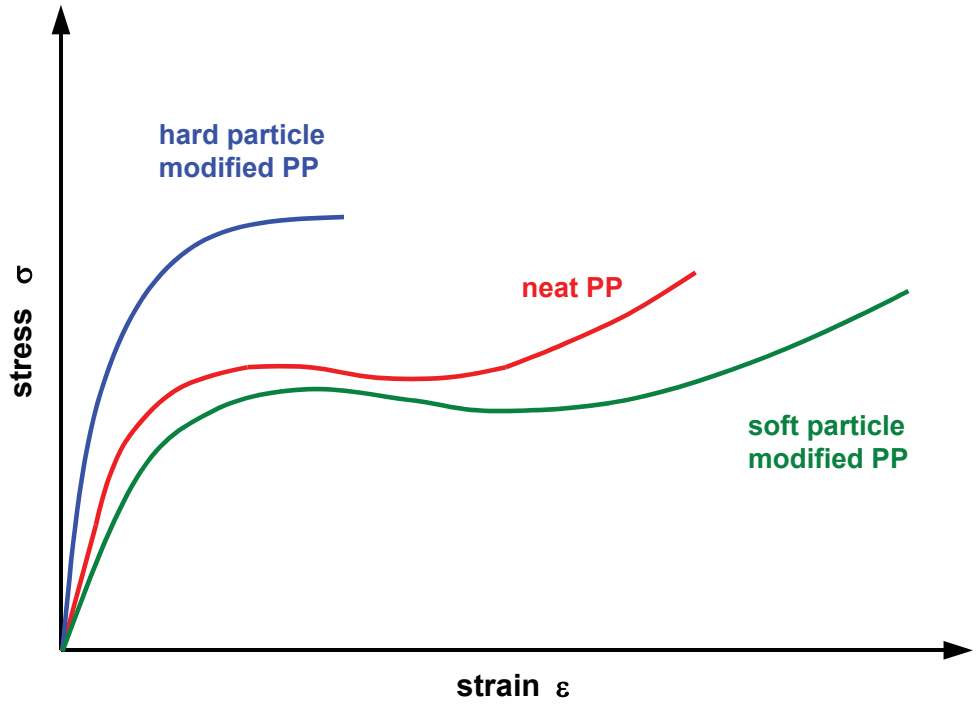

Fig. 20: Comparison of tensile behaviour of hard and soft particle filled PP with neat PP.

The material behaviour of the soft elastomer particle modified polypropylene will be discussed in details in later sections based on results of various mechanical experiments. The illustrated toughening effect of elastomer particles on the tensile behaviour of the PP-based compounds will be shown in Section 5.1.1, where the uniaxial tensile experiments show good agreement with results that are as expected (**Fig. 20**).

2.2 Fundamentals of microscopic investigations of material structure

The microscopy techniques are systematically described in the Handbook of Microscopy (Volumes I, II, and III) and in the Electron Microscopy. These two literature contributions are edited by [Amelinckx et al., 1997]. A comparison between the TEM and REM in terms of the investigation of modified polypropylene has been made by [Poelt, Ingolic, Gahleitner et al., 2000]. Below only those aspects relevant to the present work are summarised.

Three-dimensional micro and macro structure of a material can be investigated by two-dimensional microscopy, in the way of observing from at least two mutually perpendicular angles of view. Taking the investigation of an injection moulded tensile specimen for example (**Fig. 21**), one distinguishes between three directions:

the flow direction (**FD**), the transverse to flow direction (**TD**) and the thickness direction (**ND**). Each two of the three directions constitute a cross section. If the material is comprised of filler and polypropylene for instance, the filler and the spherulites of PP will be oriented due to flow field during injection and exhibit therefore an anisotropy of morphology in the three directions. To visualize the three-dimensional structure of such a tensile specimen, one can take specimens from each cross section and make micrographs of them. On the basis of the two-dimensional analyses from different view angles, the steric structural information can then be deduced.

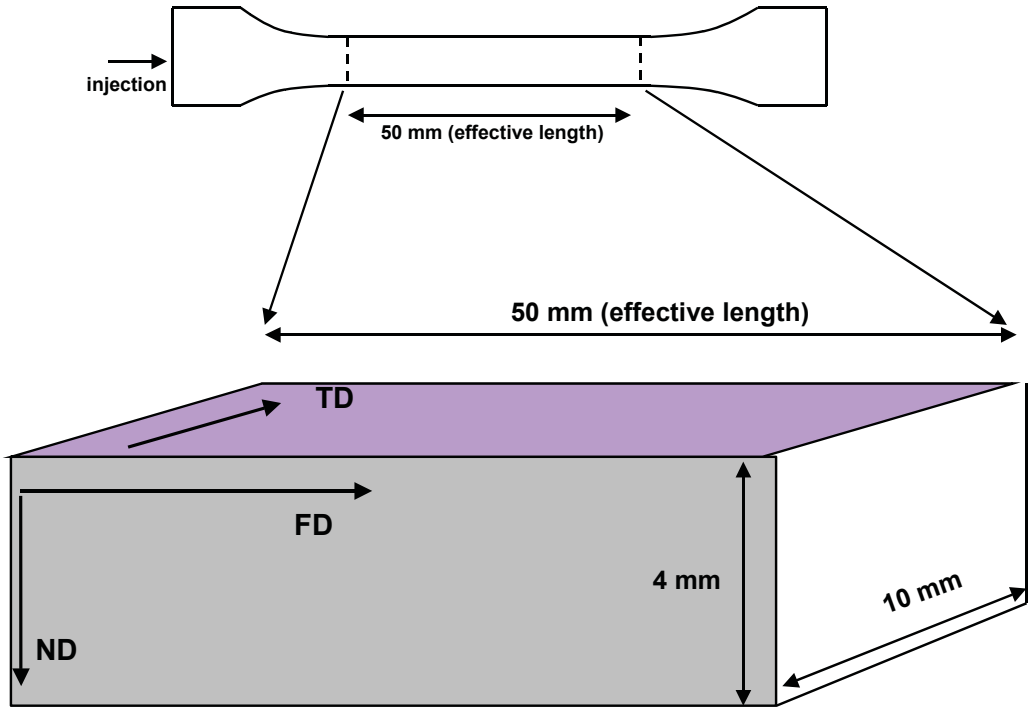

Fig. 21: Three directions and three cross sections of an injection moulded tensile specimen.

An extra brief overview of the conventional microscopes used in material manufacturing factories and research institutions will be given in this section, because the comprehensive knowledge of basic macro and micro structures of material as well as the documentation and interpretation of the fracture surface of material are always required in material engineering. It is recommended to learn the general functions of each type of microscope, which is sometimes very helpful for information resourcing and morphological analyses.

Although the types of microscope are expanding due to the association of computation and invention of new imaging techniques, the price of

high-performance microscopes and the technical know-how and experiences required for the operation restrict their widespread use. But if the advantages and shortcomings of popular microscopes, light microscope (LM), scanning electron microscope (SEM) and transmission electron microscope (TEM), are well handled, information can be extracted successfully, too [Amelinckx et al., 1997].

2.2.1 Light microscopy

No matter what kind of microscope is used, there are some basic concepts one must know. The resolution, magnification and the depth of focus will be defined in the following part, because they are involved in the operation of all types of microscope [Amelinckx et al., 1997].

The resolution (also called resolving power) of a microscope is defined as the shortest distance between two points on a surface that can still be distinguished by the observer or camera system as separate entities. I.e. being able to tell the difference between two closely positioned bright objects, or between one big object and its surrounding is the resolution. The **Fig. 22** helps to understand.

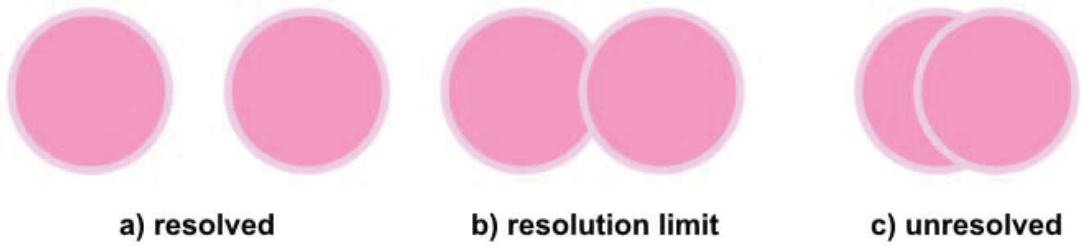

Fig. 22: Illustration of resolution and limit of resolution.

The resolution of a microscope is the most important feature of an optical system and influences the ability to differentiate between fine details of a particular specimen. The primary factor in determining resolution is the objective numerical aperture, but resolution is also dependent upon the type of specimen, coherence of illumination and other factors such as contrast enhancing methodology either for the optical system of the microscope or for the specimen itself. The best resolution for a light optical microscope is about 0.2 µm (micrometers) = 200 nm (nanometers) [Amelinckx et al., 1997].

The magnification is not the resolution but the power of a microscope to enlarge an object. The power of a microscope is described with a number followed by the letter "x". For example, if we can see something 10 times larger than actual size through a microscope, its magnification power is 10x. In a similar way, to get the total magnification of an image that is viewed through the microscope, we take the power of the objective (4x, 10x, 40x, etc.) and multiply it by the power of the eyepiece, usually 10x.

In addition, the depth of focus should not be confused with the depth of field in the

use of light microscope. The depth of focus refers to the range over which the image plane can be moved while a certain accuracy is maintained. In contrast, the depth of field is the thickness of the sample that is acceptably accurate at a given focus level. One should especially be aware of this while doing stereomicroscopy.

A light (optical) microscope uses the light as the probe and generates patterns of the object through interaction, reflection, refraction, scattering, absorption and polarization of the light beam. Light microscopy, including the 3D stereo imaging system, is often used in the polymer material science to study the crystallinity, the fracture surface, surface defects etc. primarily on macroscopic scale.

2.2.2 Scanning electron microscopy

The most popular microscopy technique is the SEM (scanning electron microscopy), because of its relatively user-friendly operation, the simplicity of image interpretation and above all a lot of information that can be obtained. In an SEM investigation, electrons will be emitted from electrode and accelerated; they interact then with the sample that is placed on the stage in vacuum. The reflected electrons and the secondary electrons which come from the atoms of sample will be detected and recorded to reveal the details of sample in size between less than 1 nm and 20 nm [Amelinckx at el., 1997]. Nowadays, the resolution ability of high-performance SEM even rivals that of a TEM. With additional available analytical equipments, the SEM is really a very versatile tool for morphological investigations in material science. With respect to material engineering, ductile/brittle proportions of the fracture surface, crystal morphology, micro material defects and etc. can be imaged by SEM.

Depending on the object features and the intended results, specimens are to be prepared in different ways. The relevant preparation techniques are introduced here [Amelinckx at el., 1997]. Sectioning is the first step through which a small representative fraction will be separated from the object. Mounting is chiefly used to support the further handling of the specimen. Usually the specimen is embedded in an epoxy resin with similar abrasive properties of the specimen material. After mounting, the impregnated specimen can be ground and polished. Grinding and polishing are multistep procedures. According to single material, optimum steps of grinding will be applied with abrasives like silicon carbide in different particle sizes that are bound to a paper substrate. Water is used during grounding to avoid heat due to friction. The ground specimen may be subsequently polished using cloths that are impregnated with fine diamond suspensions to obtain an optically flat surface. After each step of grinding or polishing, the specimen surface must be cleaned thoroughly to remove the debris.

Sometimes, etching will be carried out to visualize the microstructural features preferentially, in the way of bringing the sample into a chemical or electrical

chemical environment. After selective reaction of the surface material with the etchant, the contrast between the coexisting phases or structures, for example, between the fillers and matrix of a compound, can be enhanced. For individual material or purpose suitable etchant will be needed.

Moreover, polymeric materials are nonconductive and have to be sputtering coated with gold or palladium to eliminate charging in SEM. The thickness of the metal layer ranges between 3-30 nm [Amelinckx at el., 1997]. In some cases, carbon coverage will be applied to surface that should not be significantly obscured by coating. The carbon sputtering technique can be employed to prepare sample for back scatter electron (BSE) analysis. Back-scattered electrons form an image that is often used in analytical SEM along with the spectra made from the characteristic x-rays as clues to the elemental composition of the sample (www.wikipedia.com). For instance, BSE images of a glass fibre reinforced polymer composite present distinctly in black and white contrasted phases. Such images are called binary images, which are convenient for example for the determination of phase distribution. And the volume fraction of glass fibres can be evaluated by automatic image analysis. However the BSE technique cannot be applied to polymeric multiphasic systems that consist of components of the same atomic composition. The compound to be investigated in this work is one of such materials, as both of its two constituents the PP and the elastomer (ethylene octene copolymer) consist of the same elements, namely C (carbon) and H (hydrogen). To solve this problem, TEM that is to be introduced in the coming section is an alternative approach.

2.2.3 Transmission electron microscopy

The TEM (transmission electron microscope) is a high magnification and high resolution imaging instrument. The principle of image formation is the electron diffraction. As its name suggests, the electron beam penetrates through an ultra thin specimen, where interaction between electrons and specimen material takes place and diffraction patterns will be formed and magnified. Compared to SEM, the TEM can resolve details of the order of 0.1 nm. Microstructures, even atomic structures can be characterized by TEM [Amelinckx at el., 1997].

The most important step of sample preparation for TEM observation is staining. To contrast the phase structure of interest, the polymer samples are commonly stained with chemicals. The staining technique for polymers is demonstrated in detail in the book “Polymer blends” by Bucknall and Paul and in the cited references of this book [Bucknall and Paul, 1999].

Of the available stains, osmium tetroxide OsO_4 and ruthenium tetroxide RuO_4 are pre-eminent reagents used for polymeric materials. OsO_4 reacts specifically with double bonds to form an osmate ester and leads in most cases to hardening of the sample. In staining, vapour or solution of OsO_4 stain will be applied to the sample

for a certain time. Satisfactory staining was achieved by reacting with the etchant over a night in normal case. A raise of staining temperature to about 60°C may enhance the uptake of stains. To remove residual stain, the sample should be carefully washed after staining. OsO_4 staining offers successful phase contrasting of high-impact polystyrene (HIPS), acryl-butadien-styrol copolymere (ABS), rubber-modified polyvinyl chloride (PVC), EPDM-PP blends, and many other blends containing unsaturated rubber components [Bucknall and Paul, 1999].

The RuO_4 staining is also frequently used to contrast polymeric components, because of its reactivity with alcohol, ether, aromatic, or amine groups. RuO_4 is less selective and less stable than OsO_4, and diffuses less readily compared with OsO_4. But it deserves attention, since it can be used to stain multiple phases differently. Furthermore, a larger number of polymer components can be stained by OsO_4 treatment. Samples are exposed to RuO_4 vapour or solution for 10-60 seconds, in contrast to OsO_4 staining, prior to sectioning (microtomy) [Bucknall and Paul, 1999].

In some cases, an optimized contrast will be revealed preferentially by combination of the two above introduced stains, sometimes also with the aid of other chemicals. In one word, before carrying out staining of complex sample, it is recommended to clarify how the components react with various stains and under which conditions (time, temperature, concentrate and composition of the solution).

Bucknall and Paul further mentioned the discovery of possibility to develop contrast in microtomed thin sections of polymer by direct irradiation in the electron beam. This technique has been firstly applied to the PMMA-SAN blends by Thomas and Talmon [Thomas and Talmon, 1978; Bucknall and Paul, 1999]. This may open a new chapter in the contrasting technique for material engineering.

Sectioning will be performed in specimen preparation for TEM, because the object that is to be investigated in TEM is normally smaller than 1x1 mm. Thus the sample shall be microtomed into very tiny parts before given into the vacuum chamber of TEM. Prior to ultramicrotomy, a slab of sample is cut off and embedded in an epoxy resin. Then the embedded sample will be contrasted by treatment with special stains or mixtures of stains. For TEM observation of polymeric material, cryopreparation will be applied, where ultra thin specimens are cut by microtomy at liquid nitrogen temperature, which is also termed cryogenic temperature (below –100 °C). The low-temperature microtomy is generally required for polymers to prevent the microstructures from melting under heat while cutting. Glass or diamond microtome is used to obtain (ultra) thin slices that are only 10-100 nm thick. The ultra thin slice will then be carried by a substrate, usually a copper mesh. Due to the small size of the sample obtained, normally several samples will be needed to ensure the universality of conclusion extracted from TEM investigations.

For further information about TEM investigation and corresponding specimen

preparation technique please refer to the homepage of Austrian Centre for Electron Microscopy and Nanoanalysis, Institute for Electron Microscopy of the Graz University of Technology, Graz Centre for Electron Microscopy (www.felmi-zfe.tugraz.at). Bucknall and Paul have also depicted the microscopy techniques with particular aspect to morphology characterization of polymer blends in their book “Polymer blends” [Bucknall and Paul, 1999].

In **Table 1** the general information about the LM, SEM and TEM is summarized to help to choose the appropriate instrument to explore the structure-property relationship in material science.

Table 1: List of the three types of microscopes.

	LM	SEM	TEM
Resolution ability	**> 200 nm**	**1-20 nm**	**< 0.1 nm**
Source of Radiation for Image Formation	**visible light**	**electrons**	**electrons**
Medium	**air**	**vacuum**	**vacuum**
Specimen	**no preparation required or thin microtomed film**	**coating, eventually etching**	**(ultra) thin slices**
Costs	**€1500**	**more than €100.000**	**more than €500,000**

Since the limitation of SEM and TEM on one side (a good vacuum is required, allowing no real atmosphere conditions; specimen preparation affects directly the results) and the limitation of LM on the other side (a lower resolution property) can be complementary, a combination of those methods may be more fruitful.

3 EXPERIMENTAL

In this work a polypropylene (PP) homopolymer from the manufacturer Borealis Austria GmbH, Linz, Austria, was used as the resin. The PP homopolymer was blended with an ethylene-octene copolymer, an elastomer from the DOW chemical company, Horgen, CH.

The mechanical behaviour of each resin, filler and compounds have been tested to obtain the basic knowledge of the component-property relationship. The monotonic tensile tests that have been made to establish the stress-strain data set were the uniaxial tensile tests with dumbbell specimens and the pure shear tests with FWPS (faint-waist pure shear) specimens. The multipurpose dumbbell tensile specimens were delivered by Borealis Austria GmbH. The FWPS specimens were injection moulded from granulates by the ECONOMOS Austria GmbH, Judenburg, Austria. The biaxial tensile tests with special test set-up deliver information of deformation behaviour under biaxial strain state (see Section 2.1.3). The biaxial test specimens are discs provided by Borealis Austria GmbH. The dynamic tensile tests, the DMA (dynamic mechanic analysis) determined the material response under cyclic tensile loading. The DMA helps to understand the material performance in realistic application, as most of the time a material is subjected to dynamic loading conditions. For the tensile DMA to be discussed in this work, multipurpose tensile specimens used were the same as those for uniaxial tensile test.

Morphological relationship of filler and resin in a compound reflects the processing quality and is also important for determination of the interaction property of the components of the compound. The microscopic investigations are important instruments for the study of macro- and microstructure and the examination of the fracture cross-sections. The TEM investigation of the compounds has been performed by experts at the Austrian Centre for Electron Microscopy and Nanoanalysis, Institute for Electron Microscopy of the Graz University of Technology, Graz Centre for Electron Microscopy (www.felmi-zfe.tugraz.at).

The simulation of material behaviour has been carried out at the Institute of Materials Science and Testing of Plastics, University of Leoben, Austria. The identified stress-strain relationship of tensile tests on the constituents together with the aspect ratio of elastomer particles were used as input signals for the simulation of the mechanical behaviour of the compound. The simulated and measured values of tensile modulus and Poisson’s ratio of the compounds will then be compared.

3.1 Materials and test specimens

In this section, the constituents and the compounds that were selected for the investigations and the various test specimens together with their preparations are summarized. Please note the abbreviations of materials in **Table 2**. In this work, only these abbreviations will be used.

3.1.1 The materials

In this work polypropylene homopolymer (PP(H)) is a model material offered by Borealis Austria GmbH, Linz, of which the density is 0.904 g/cm³. The melt flow index MFI of PP(H) is 15.7 dg/min, at 190 °C/2.16kg. The T_g of PP(H) is 0 °C, and its T_m is 168 °C. The PP(H) is one constituent that is used as resin in the compounds. The second constituent is the elastomer (R(PEO)) which is the filler of the compounds. R(PEO) is the polyolefin elastomer Engage 8100 of DOW chemical company. Its density is 0.870 g/cm. The MFI of R(PEO) is 1.0 dg/min at 190 °C/2.16kg. Its T_g is –52 °C and T_m is 60 °C. Please refer to the data sheet of DOW in the appendix for other characteristic material parameters. The compounds RPP(3.5) and RPP(7) were loaded with 3.5 vol% and 7 vol% elastomers, respectively. The material parameters of the compounds have been estimated by experiments (see experimental sections). The abbreviation, manufacturer, description of material for constituents and compounds are listed in **Table 2**.

Table 2: The list of materials investigated (constituents and compounds).

	abbreviation	manufacturer	type	remark
constituents	PP(H)	Borealis Linz, Austria, Europe	HH 450 SP modeling material	PP homopolymer
	R(PEO)	DOW chemical company, Horgen, CH, Europe	Engage 8100	ethylene-octene copolymer (see appendix)
compounds	RPP(3.5)	Borealis Linz, Austria, Europe	PP(H)+ R(PEO) (3.5vol%)	physically blended
	RPP(7)	Borealis Linz, Austria, Europe	PP(H)+ R(PEO) (7vol%)	physically blended

3.1.2 The specimens

The fabrication and the delivery of each specimen have been already introduced in previous sections. The tests and corresponding specimens together with the dimensions and processing of each specimen are summarized in **Table 3**.

Table 3: The specimens for each type of test.

test	specimen	dimension	Processing
uniaxial tensile	**multipurpose dumbbell specimen**	**4x10x50 (effective length) mm**	**Injection moulded by Borealis**
planar tensile	**FWPS specimen**	**see Fig. 24**	**Injection moulded by Economos**
equibiaxial tensile	**disc**	**thickness 1 mm, diameter 140 mm**	**Injection moulded by Economos**
dynamic mechanical analysis (DMA)	**multipurpose dumbbell specimen**	**4x10x50 (effective length) mm**	**Injection moulded by Borealis**
light microscopy (LM)	**semi thin slice**	**thickness 3 µm**	*
transmission electron microscopy (TEM)	**ultra thin slice**	**1x1 mm, thickness 50-100 nm**	*

* Microtomed at Institute for Electron Microscopy of the Graz University of Technology, Graz Centre for Electron Microscopy

3.2 Mechanical characterizations under monotonic loading conditions

In the following sections, the test equipments and the process of each experiment are described, and the testing machines used are presented, too. The fundamental theory of the mechanical material behaviour has been introduced in Section 2.1.5. The experimental results are documented and discussed in Section 5.

3.2.1 Uniaxial tensile tests

The uniaxial tensile tests are used to determine the stress-strain relationship and provide the values of tensile modulus, yield stress, yield strain, as well as the stress at fracture, strain at fracture. An uniaxial test was carried out at constant temperature and loading velocity. For this work three different testing temperatures were chosen: -30 °C/25 °C/80 °C, and the loading velocity was 0.01 mm/s. The standard uniaxial tensile tests (ISO 527) were performed on an Instron 5500R (High Wycombe, UK) test machine (**Fig. 23**) in the laboratory of the Institute of Material Science and Testing of Plastics at the University of Leoben. The specimens used were standard multipurpose dumbbell tensile specimens. For the estimation of the lateral strain of the dumbbell specimen, additional FFSA (full field strain analysis) measurements were made with help of the ARAMIS optical deformation analysis system (GOM, Braunschweig, Germany). The details of such FFSA measurements please refer to [Feichter, Major and Lang, 2007].

Fig. 23: Instron testing machine, type INSTRON 5500R, (Fa. INSTRON LIMITED; High Wycombe, UK).

3.2.2 Planar tensile tests

The planar tensile tests (pure shear tests) provide deformation information of a sample under planar strain state. The state of pure shear exists in the specimen at a 45° angle to the tension direction. The aspect of a FWPS specimen is shown in **Fig. 24**, it is much shorter in the direction of stretching than the width which is 200 mm, whereas the distance between two fixtures is only 16 mm. Therefore the specimen is perfectly constrained in the lateral direction so that specimen thinning occurs only in the thickness direction if stretched. The planar tensile tests were performed on a servo hydraulic MTS 831.59 Polymer Test System (**Fig. 25**), (MTS System GmbH, Berlin, Germany).

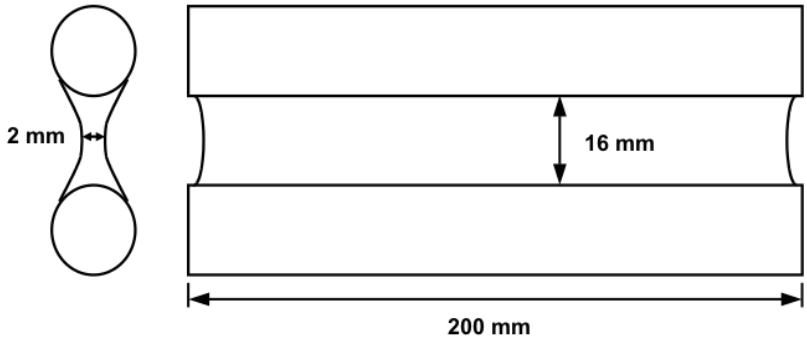

Fig. 24: Illustration of a FWPS (faint-waist pure shear) specimen.

Fig. 25: The servo hydraulic MTS 831.59 Polymer Test System of the Institute of Material Science and Testing of Plastics at the University of Leoben.

3.2.3 Equibiaxial tensile tests

Equibiaxial tensile tests create a strain state in a sample equivalent to the pure compression. The equibiaxial strain state can be realized by stretching a circular disc sample from incompressible material. Equibiaxial tensile tests can be well applied to characterize the elastomers of which the Poisson's ratio is approximately 0.5, while that of most polymers is between 0.35 and 0.45 [Saechtling, 1995].

In this study, the equibiaxial tensile tests of the PP-elastomer compounds have been performed and analysed. During the experiments, the strain field of the disc specimens was measured with the same ARAMIS optical deformation analysis system used in the uniaxial tensile tests and in the pure shear tests. The test set-up with pressure measurement (**Fig. 26**) was developed by Feichter and Major [Feichter, Major and Lang, 2006]. As shown in **Fig. 26**, the disc specimen was placed between a metal ring and a cylinder of the same inside diameter of 140 mm. The specimen was blown up by air, and the non-contacting full field strain measurement system Aramis detected the deformation and documented the strain change. In **Fig. 27** one sees different stages of the strain field measurement.

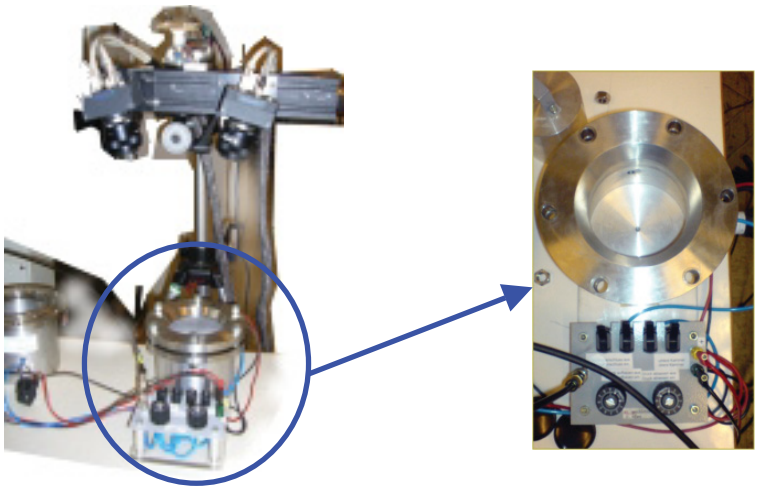

Fig. 26: The equibiaxial tensile test set-up [Feichter et al., 2006; Mach et al., 2008].

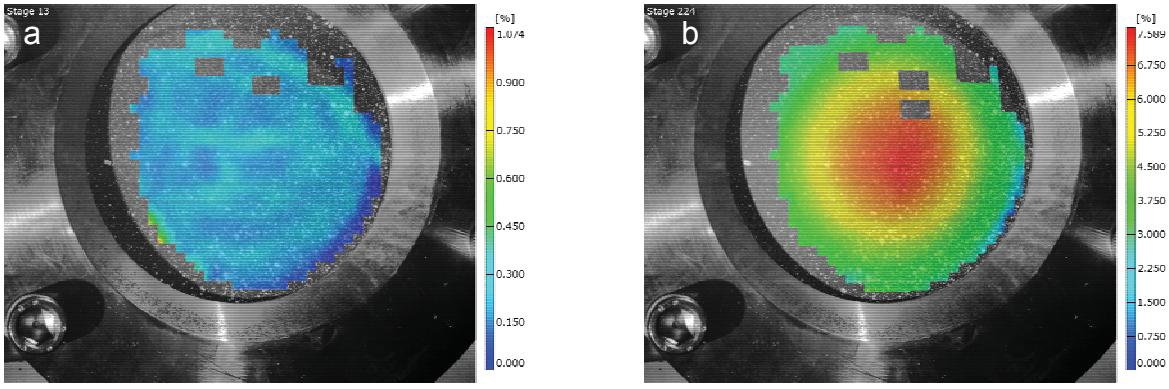

Fig. 27: Two stages of a strain field analysis; **a** low pressure – small deformation; **b** high pressure – large deformation.

3.3 Dynamic mechanical analysis

Attention must be separately paid to the dynamic loading in the application of a material. A material may fail in the dynamic loading with lower stress amplitude than the stress amplitude in a monotonic loading. The tires for instance mainly consist of elastomers are subjected to continuously changeable loading that leads to the wear and eventual failure of the product. The dynamic mechanic properties of the elastomer filled PP compounds have thus been studied by means of tensile DMA (dynamic mechanic analysis). And the effect of the fillers on the response of the compounds to cyclic loading will be presented in terms of the filler volume fraction in each compound.

The test device is a Bose Electro Force 3450 (Bose Co., Minnesota, USA) shown in **Fig. 28**. The specimens for the dynamic tensile tests are standard multipurpose tensile dumbbell specimens that are also used in the monotonic uniaxial tensile tests. The monotonic uniaxial tensile tests and cyclic DMA tests were thus applied to the exactly same compounds, where the compounded material has the same morphology (injection moulded), so that the comparability of the test results of both monotonic and dynamic tests can be guaranteed.

Fig. 28: The Bose Electro Force 3450 DMA testing machine with tempering chamber. (image copied from www.bose-electroforce.com)

Before performing a DMA on a polymer, it is recommended to determine the boundary of linear-viscoelasticity of the material (see **Fig. 29**). The maximum stress in specimen and the maximum deformation of the specimen caused by the applied force of a DMA experiment should not exceed this limit, since the measurements make sense only if the linear-viscoelasticity as prerequisite has been guaranteed [Ehrenstein, Riedel and Trawiel, 1998]. In the amplitude scan, the linear-viscoelastic limit will be determined.

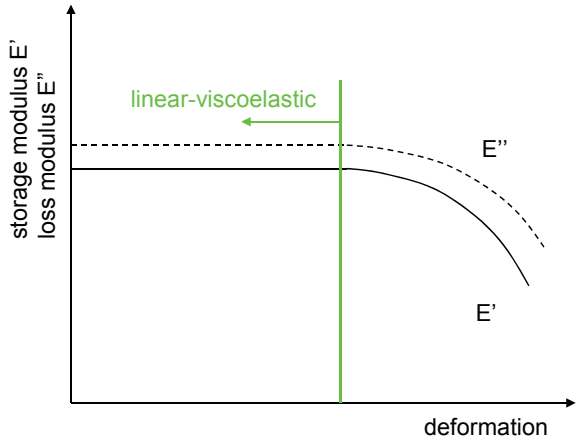

Fig. 29: Schematic illustration of the linear-viscoelastic deformation limit of materials in DMA measurements.

In the temperature scan, the storage modulus and the loss tangent of the resin, the filler and the compounds have been measured in function of temperature with a constant testing frequency of 1 Hz. The mechanical properties of constituents and compounds under the same testing conditions were compared with each other. Pilz [Pilz, 2001] demonstrated diverse thermo dynamic analyses and discussed the technique of data reduction and interpretation in his dissertation. For more information about dynamic measurement and the data manipulation please refer to [Strobl, 1996; Pilz, 2001].

3.4 Morphological investigation

The morphological investigations provide optical information of the material structure. The light microscopy (LM) can be used to study the crystallinity of the semi crystalline polymeric materials like the PP. The scanning electron microscopy (SEM) yields overall visual images of material microstructure and especially of the 3D surface structure because of the depth of view, whereas the TEM with higher resolution offers more details of micro structure of an object.

Both elastomers and PP are composed of C (Carbon) and H (Hydrogen) and components of a multiphase system like the elastomer-PP compound can therefore not be distinguished from each other in SEM. Therefore the TEM was employed for the microstructural study of the compound.

In this work thin sections cut from the multipurpose tensile dumbbell specimen of the compound were observed in LM as well as in TEM to determine the surface layer thickness depending on the cooling rate on the cavity wall in processing. The TEM micrographs also reveal the microstructure of the compounds, and suggest the shape, size, orientation and distribution of the elastomer fillers in the PP matrix. The TEM experiments were carried out on a TEM Tecnai 12 (**Fig. 30**) at the Institute for Electron Microscopy of the Graz University of Technology (www.felmi-zfe.tugraz.at)

Fig. 30: TEM testing device, at the Institute for Electron Microscopy of the Graz University of Technology. (image copied from www.felmi-zfe.tugraz.at).

The preparation of specimen for TEM observation has been carried out as follows. First, a cross section was taken from the middle or the edge area of the dumbbell tensile specimen with a saw. A small piece about 5x5x15 mm (**Fig. 31**) was then

separated from the cross section with a saw and utility knife. The slab was then embedded into epoxy resin and sharpened to have a 1x1 mm tip like blue circled in **Fig. 31** by glass microtome at room temperature after the solidification of the resin. After that the tip was stained with RuO_4 solution over night. Prior to staining, the surfaces of the piece were varnished with epoxy resin except the 1x1 mm tip, to avoid the overhardening of the edges of the slices that were to be microtomed next. The contrasted sample was cryogenic microtomed using a diamond knife at about –100 °C. The necessary low temperature was generated by liquid nitrogen so that the original microstructure could be maintained without melting due to heating during the cutting. The ultra-thin slices were placed on a copper mesh as carrier. The thickness of the slice varies between 10-100 nm with respect to the particular purpose of observation. For example to investigate the PP spherulites, thicker slices (about 100 nm) will be recommended, the thickness of a slice is about 60 nm in the study of elastomer phase structure in an elastomer-modified PP blends.

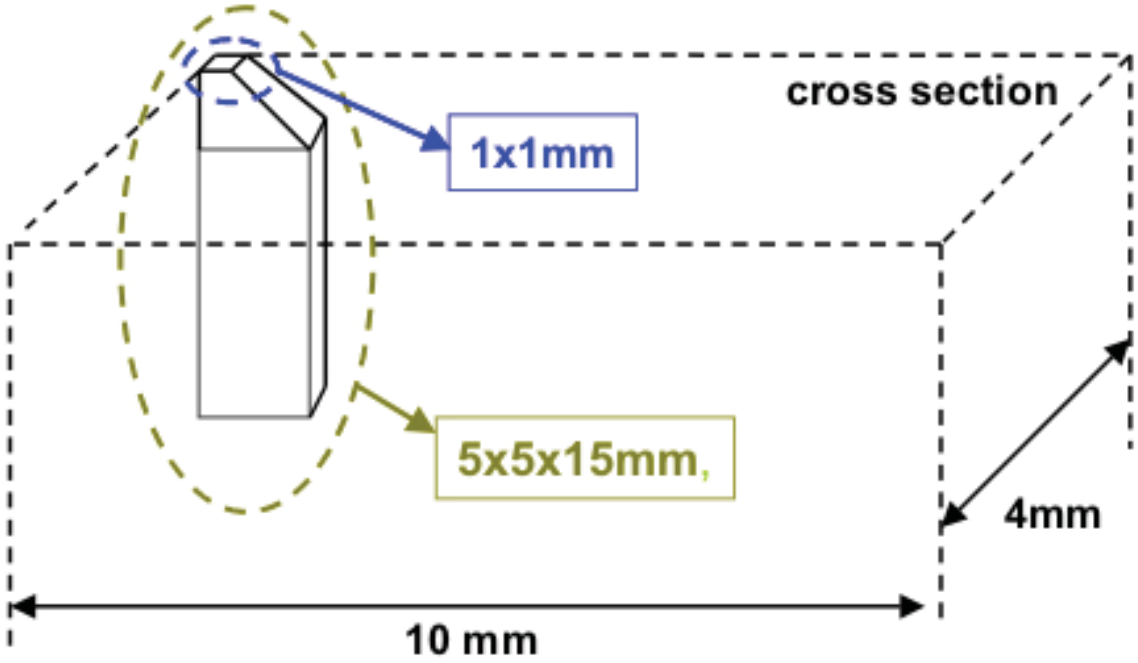

Fig. 31: Specimen sectioning for TEM investigation of the microstructure of the cross section of an injection moulded dumbbell tensile specimen (4X10X50(effective length) mm).

4 SIMULATION

The modeling and simulation of the mechanical material behaviour of the compound are based on the experimentally determined characteristic material parameters of each constituent. In the software DIGIMAT (e-Xstream Engineering S.A., Louvain-la-Neuve, Belgium) one can vary the volume fraction or loading conditions to exam the results of the performed experiments or to predict the compound performance under conditions that are different from the experiments. Gastl [Gastl, 2008] has schemed the procedure as shown in **Fig. 32**. For the polymer blends, the types of elasticity can be classified as shown in **Fig. 33** according to the intrinsic property of each constituent.

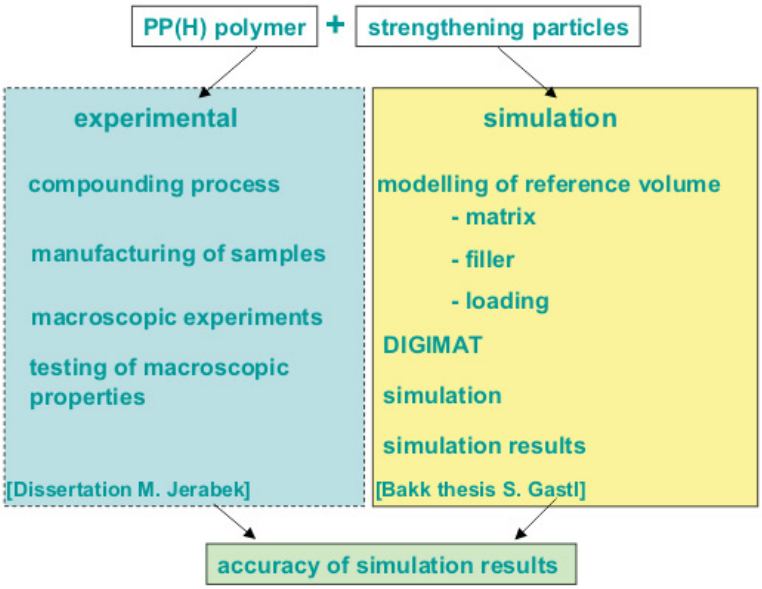

Fig. 32: The procedure of simulation with DIGIMAT [Gastl, 2008].

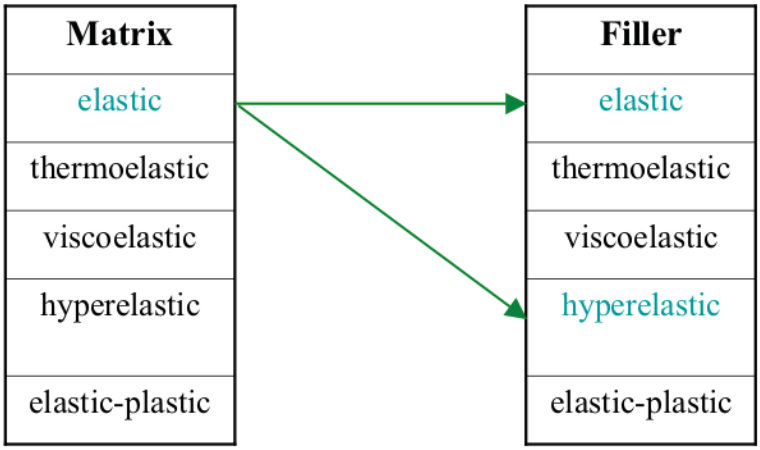

Fig. 33: The models of elasticity for the matrix material and the filler material.

In this work the compounded matrix material is polypropylene whose tensile behaviour can be modelled by elastic-plastic or elastic-elastic in the simplest approximation, as illustrated in **Fig. 34**. A hyperelastic model (Mooney model) will be used to depict the tensile behaviour of the elastomer (Section 2.1.2.3).

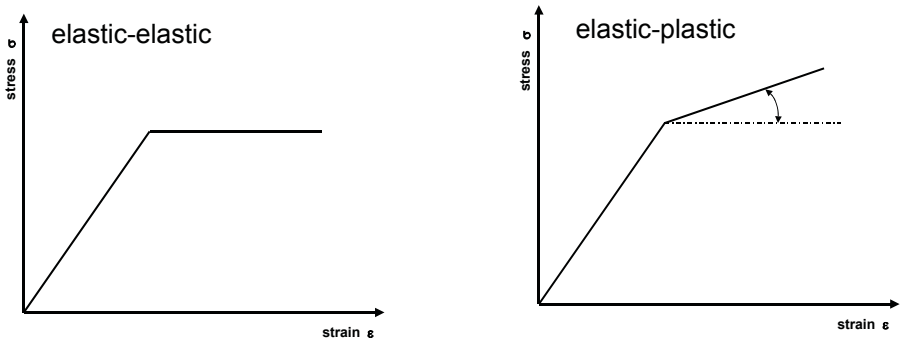

Fig. 34: The models of elasticity for describing the tensile behaviour of polypropylene.

Regarding the chosen material model for simulation in the software, different material parameters will be required (**Table 4**) as input signals. Here in this work, the elastic model was used for polypropylene and elastomer and the tensile modulus, E, and the Poisson's ratio, ν, of PP and the elastomer were used as input data for the simulation of small-strain deformation behaviour of the compounds, while for the hyperelastic model for large deformation of elastomer the Mooney energy function W (λ) will be needed. For the usage of the software DIGIMAT and its application properties in the polymer engineering, please refer to the Bachelor Thesis by Gastl [Gastl, 2008].

Table 4: Material models and corresponding simulation required input parameters.

Material Model	Parameters
elastic	E, ν
thermoelastic	E, ν and CLTE
viscoelastic	G(T) and K(T)
hyperelastic	W(λ)
elastic plastic	E, σ_y, ε_y, n

5 RESULTS AND DISCUSSION

In the following part of the work, the testing results are presented and interpreted in terms of property relationship between the constituents and compounds. Conventionally impact tests of notched specimens will be employed to investigate the toughened polymer compound, because the effectivity of toughening effect is the objective of most research works. In this work, however, the mechanical behaviour together with the microstructure of elastomer-toughened PP system are emphasized. As indicated in the introduction (see Section 1), this work is only an integral part of the research project that aims to establish a simulation approach for a systematic study and prediction of polymer compounds properties. The complete research activities will be reported elsewhere by Major et al. in the near future [Major et al., to be published].

5.1 Monotonic mechanical tests

In the foregoing theoretical sections, the microdeformation mechanisms of a polymeric material have been depicted. Monotonic experiments are characterised by constant testing conditions, i.e. the testing parameters like loading magnitude, loading rate and temperature are constant during a single experiment. The fundamental material parameters like stiffness and tensile strength will be derived from monotonic measurements. With respect to this work, the uniaxial, planar, and biaxial tensile tests of the constituents and compounds should provide the material behaviour under respective strain states, i.e. stress state.

5.1.1 Uniaxial tensile tests

The uniaxial tensile tests on multipurpose dumbbell specimens of the constituents and the compounds are presented in this section. There were three testing temperatures: -30 °C, 25 °C (RT), 80 °C. All of the uniaxial tensile tests have been performed at the loading rate of 0.01 mm/s. For the fundamental of uniaxial tensile tests please refer to Section 3.1.1.

The continuous phase of the compound is the thermoplastic PP. The nominal stress-strain relationship of the PP(H) in dependence on temperatures is presented in **Fig. 35**. The uniaxial tensile behaviour of the elastomer R(PEO) which constitutes the dispersed phase of the compounds is shown in **Fig. 36**. The nominal stress-strain relationship of the compounds RPP(3.5) and RPP(7) is revealed in **Fig. 37** and **Fig. 38**, respectively.

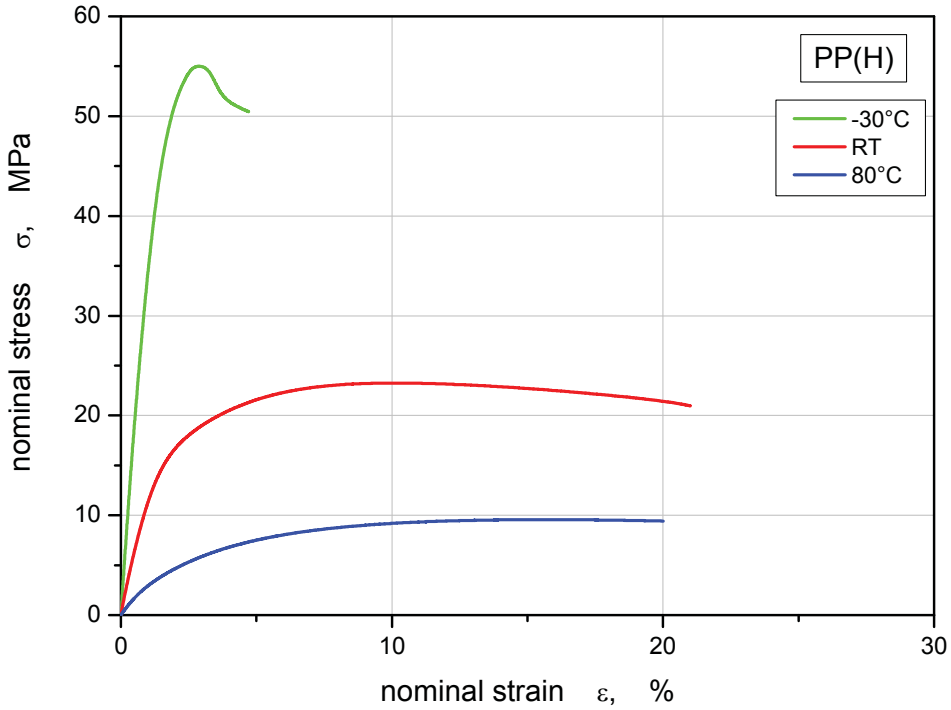

Fig. 35: Nominal stress-strain relationship of uniaxial tensile tests on PP homopolymer, PP(H).

The polypropylene homopolymer PP(H) shows a temperature dependence, at a constant loading rate of 0.01 mm/s. Generally the yield point is defined as the point where the dσ/dε of the stress-strain curve is zero. Preceding the yield point, the deformation behaviour of most materials can be characterized by elasticity, that is to say the deformation is recoverable, whereas plastic flow occurs after the yield point, followed by ultimately material fracture. At room temperature, the yield stress was about 23 MPa at a yield strain of about 10 %. After yielding at RT, the PP did not show significant strain softening. On the contrary, the mobility of the molecules must be dramatically reduced at –30 °C, which leads macroscopically to an increase of the yield stress to about 55 MPa an d a decrease of yield strain to 3 %. The tensile modulus rises from 1300 MPa at RT to 4000 MPa at –30 °C. Besides, an immediate drop of the slope of the stress-strain curve can be seen at –30 °C, which coincides normally with necking (cold drawing) of the specimen. Necking occurs, when the stress concentration localizes. The stress concentration localization of PP at the strain rate of 0.01 mm/s was not captured during tests at RT and at 80 °C until the strain reached 20 %. While a lower temperature stiffens the material, a high temperature softens it. This effect can be proved by comparison of the material response at the three testing temperatures. At 80 °C yielding occurred as the strain reached 16 %, and the yield stress was only 10

MPa. The tensile modulus of the PP fell at 80 °C to about 360 MPa.

The glass transition temperature T_g of the material is the temperature, at which the material undergoes the transformation between the glassy and rubbery states. Thermoplastic materials like PP are rigid and fragile in the glassy state (at below T_g), and otherwise soft and tough in the rubbery state (at above T_g). The T_g of the PP homopolymer is 0 °C. Obviously lower temperatures are critical for PP and restrict its application. The poor low temperature performance of neat PP derives from its inherent semi-crystallinity. The classical toughening agent, the elastomer, offers considerable improvement.

The elastomer particles were dispersed into PP and they are the second constituents, the so-called discrete phase. The uniaxial tensile tests of the elastomer R(PEO) (ethylene-octene copolymer) are presented in **Fig. 36**, where the nominal stress-strain relationship of the elastomer R(PEO) are shown at two temperatures.

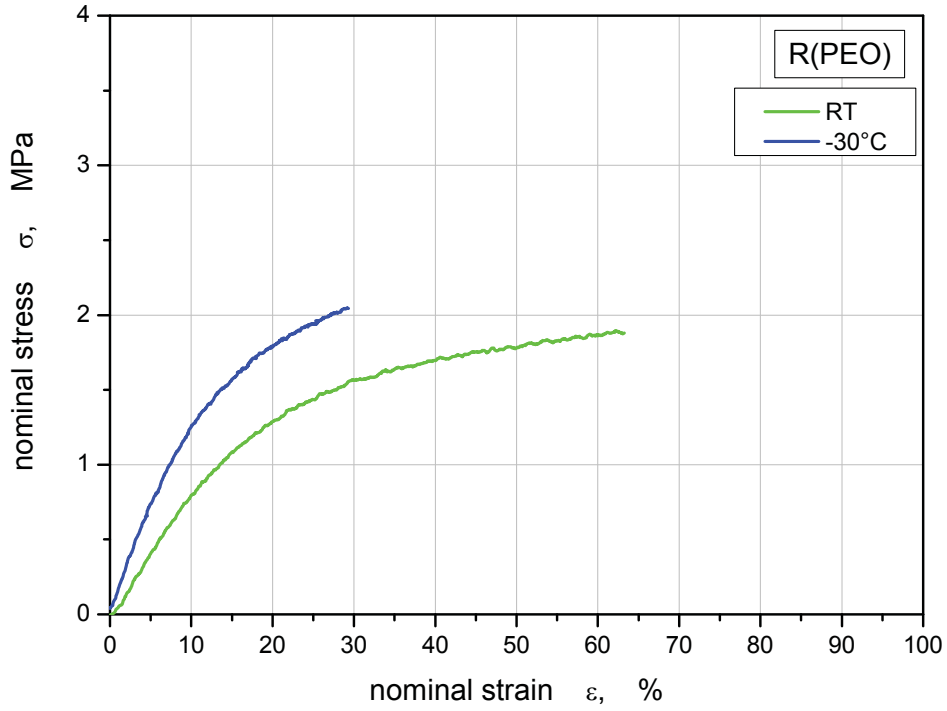

Fig. 36: Nominal stress-strain relationship of uniaxial tensile test on elastomer (ethylene-octene copolymer), R(PEO).

The dumbbell tensile specimens were injection moulded. The R(PEO) is a thermoplastic elastomer and its specimens retract into smaller size at 80 °C due to the recovery of orientation that was frozen in by rapid cooling during moulding. Therefore an uniaxial tensile test was not accomplished at 80 °C. The intrinsic

widely meshed network structure of elastomers is beneficial for absorption of deformation energy. The work of the force during deformation can be stored as elastic energy and released again if the force is removed. The elastomer particles are hyperelastic and ductile even at lower temperatures. The T_g of the elastomer R(PEO) is –52 °C according to data sheet information of DOW. The excellent elasticity of the R(PEO) can be seen in **Fig. 36**. The elastomer can be stretched to large strains beyond 60 % at RT. Unlike neat polypropylene PP(H), the R(PEO) maintains its deformation ability and toughness even at –30 °C. The tensile modulus of R(PEO) at RT is about 10 MPa, compared to that of PP of 1300 MPa at RT. The modulus difference between the two materials implies a stiffness variation of the compounds that are comprised of these two materials. Empirically, the PP will be loaded with 5-20 % (by volume) elastomers without remarkable sacrifice of stiffness and strength.

The behaviour of polymeric material always depends on rate and temperature. In most cases an increasing rate and decreasing temperature have an equivalent effect on material response, and vice versa. The temperature dependence of the elastomer can be deduced by contrasting the two stress-strain curves in **Fig. 36**. The lower temperature of –30 °C results in an elevated elastic modulus and higher stress at the comparable strain level with RT. One may analogously forecast that modulus and tensile strength of the elastomer would decline if tested at high temperatures, e.g. 80 °C.

The question is in which degree the properties of a compound will be adapted when it is composed of the two constituents. The PP and the elastomer are nearly immiscible in melts; but the modification of elastomer to PP can be only sufficient, if the elastomer phase is well bonded to the PP phase. Other decisive factors should also be taken into account in design of new compounds. The average elastomer particle size and the content of the elastomer in particular compound are of special importance and interest. The former can be theoretically determined by microscopy analysis, and the latter should be fitted to the intended application. The particle size should be optimized by processing to perform two basic functions as mentioned in Section 2.1.3. On the one hand, well-dispersed elastomer particles should induce the necessary stress concentration to trigger minute crazes throughout the whole sample. On the other hand, elastomer particles must be able to inhibit the growth of crazes to avoid premature failure. Jang et al. suggest the critical particle size of an elastomer toughening system to be 0.5 µm [Jang et al., 1985]. But Wu has proposed that the critical interparticle distance is a characteristic material property of the matrix of an elastomer-toughened system and is the essential criterion for the efficiency of the toughening effect [Wu, 1985]. Yet no single explanation has met universal acceptance so far. The results of the uniaxial tensile tests of compounds are presented in **Fig. 37** and **Fig. 38**.

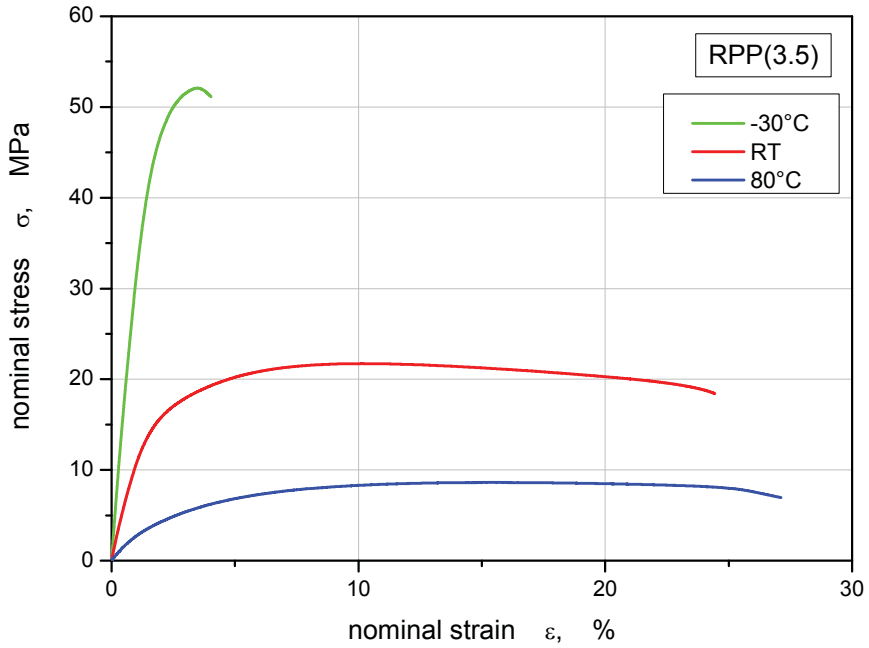

Fig. 37: Nominal stress-strain relationship of uniaxial tensile testson compound RPP(3.5) (PP(H)+3.5vol% R(PEO)).

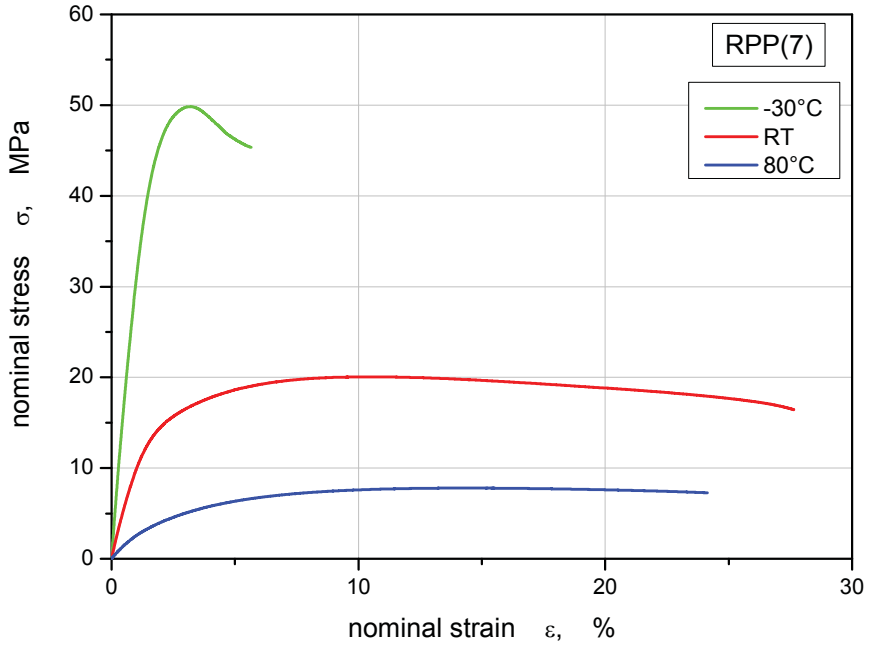

Fig. 38: Nominal stress-strain relationship of uniaxial tensile tests on compound RPP(7) (PP(H)+7vol% R(PEO)).

In this work the elastomer contents of both compounds are small. Nevertheless, a toughening effect can be perceived, if one compares the matrix behaviour under uniaxial tension in **Fig. 35** with that of the two compounds in **Fig. 37** and **Fig. 38**. As temperature ascends, the tensile modulus and the yield strength of the compounds at each temperature descend merely with increasing elastomer contents. The yield strain of the compounds increases at both temperatures of 25 °C and –30 °C coupled with decreasing yield stress. The unexpected fall of yield strain of the compounds at 80 °C may be the result of stress concentration caused by elastomer particles. As explained in the preceding part (see Section 2.1.3), elastomer particle induced stress concentration has been inclined to trigger the formation of subcritical crazes, which contributes to energy absorption and hence promotes the yielding of matrix. This effect may be supported by higher temperature, at which the mobility of matrix molecules has been activated so that the crazes initiation in matrix can readily benefit from the existence of filler particles. The nominal stress-strain relationship of the measurements discussed above (**Fig. 35** to **Fig. 38**) are compared in **Fig. 39** below. The solid curves are of PP(H); the dashed curves are of RPP(3.5); and the dotted curves are of RPP(7). The three testing temperatures –30 °C, room temperature (RT) and 80 °C are represented by green, red and blue, respectively. The influence of soft elastomer particles was shown in **Fig. 20**, and the composite plot of the tensile stress-strain relationship of the PP(H), RPP(3.5) and RPP(7) in **Fig. 39** is in agreement with that.

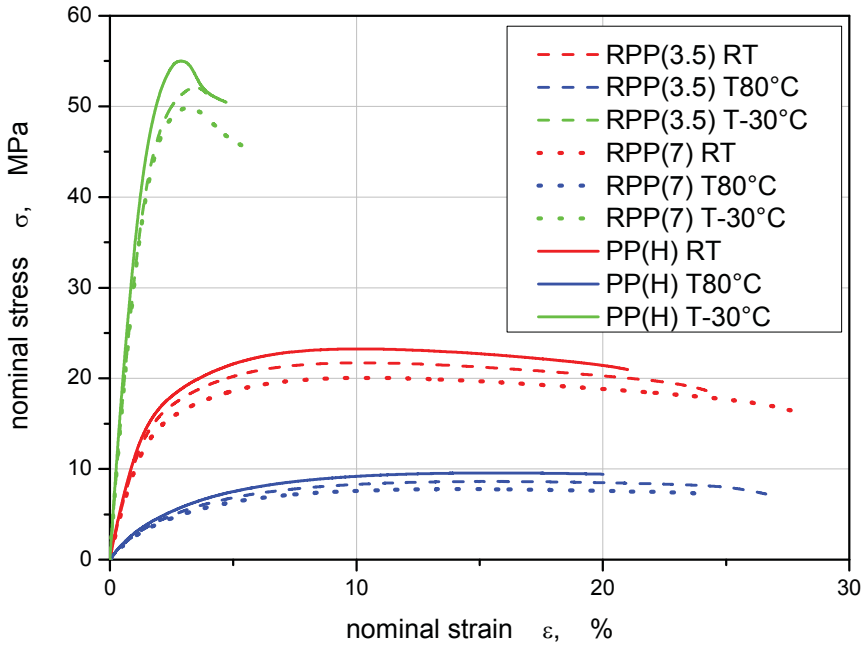

Fig. 39: Alteration tendency of the tensile behaviour of neat PP(H) with varying loading of elastomer (0vol%→3.5vol%→7vol%), at three temperatures.

Through the comparison of the uniaxial tensile behaviour of the neat matrix material PP(H) and of the two compounds, it can be deduced roughly that with increasing elastomer content, the stiffness and the tensile strength sink slightly. The characteristic material parameters that are determined by uniaxial tensile tests are tensile modulus, yield stress and yield strain. These values of the two constituents and the two compounds have been summarized in the **Table 5**.

Table 5: Characteristic material parameters from uniaxial tensile test.

	Temperature	Abbreviations	Volume Fraction [vol%]	Yield Stress [MPa]	Yield Strain [%]	Tensile Modulus [MPa]
matrix	-30°C	PP(H)	0	55	3	4000
	25°C	PP(H)	0	23	10	1330
	80°C	PP(H)	0	10	16	360
compound						
	-30°C	RPP(3.5)	3,5	52	3,6	3600
	-30°C	RPP(7)	7	45	3,3	3500
	25°C	RPP(3.5)	3,5	22	10,5	1250
	25°C	RPP(7)	7	20	11	1160
	80°C	RPP(3.5)	3,5	9	15,5	330
	80°C	RPP(7)	7	8	14	330
filler	25°C	R(PEO)	100	1,9	60	10

In the following three figures (Figs 44-46), the values of **Table 5** are plotted to visualize the tendency of each material parameter in function of filler volume fraction. In every plot, the three testing temperatures –30 °C, 25 °C and 80 °C are indicated with green, red, and blue, respectively. In the legend, the abbreviation RPP refers to the compounds that are elastomer (R(PEO)) modified polypropylene PP(H). The deviation of single measurement points is integrated, too. All the experiments have been repeated under same testing conditions three times to ensure the plausibility of the results. It can be seen that the tensile modulus, E (**Fig. 40**), and the yield stress, σ_y (**Fig. 41**), decrease while the yield strain, ε_y (**Fig. 42**), increases with increasing filler content. The accuracy of the measurement of yield

strain of uniaxial tensile tests was low, so **Fig. 42** shows no clear tendency.

In addition, a consideration, which governs the research activities throughout this work, is that the matrix PP can be regarded as a virtual compound with 0 % filler, and the elastomer filler can be considered as a virtual compound with 100 % filler. Keeping this consideration in mind, one may assume that the properties of the compounds should fall somewhere between the two extremes represented by the two constituents. Most important is however the sensitivity of the matrix material to given loading conditions in application of a compound. The influence of a filler or reinforcement on particular properties of a composition is usually moderate. In many cases an enhancement of a property is at cost of another, the design and engineering of polymer compounds are in this sense to find a compromise. To these aspects, the various experiments in this work should contribute to a better understanding.

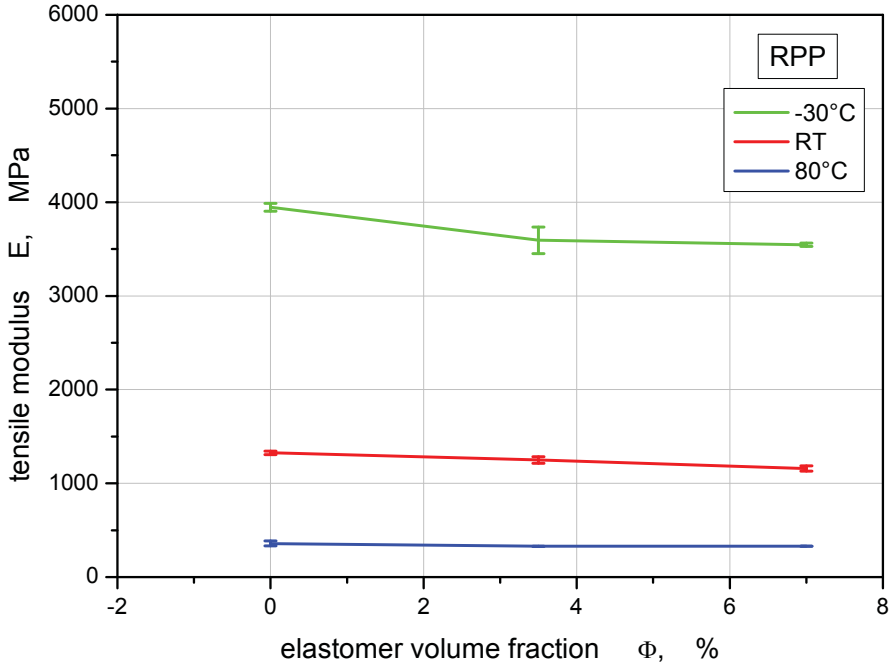

Fig. 40: The change of elastic modulus, E, in function of elastomer volume fraction, Φ, at three testing temperatures.

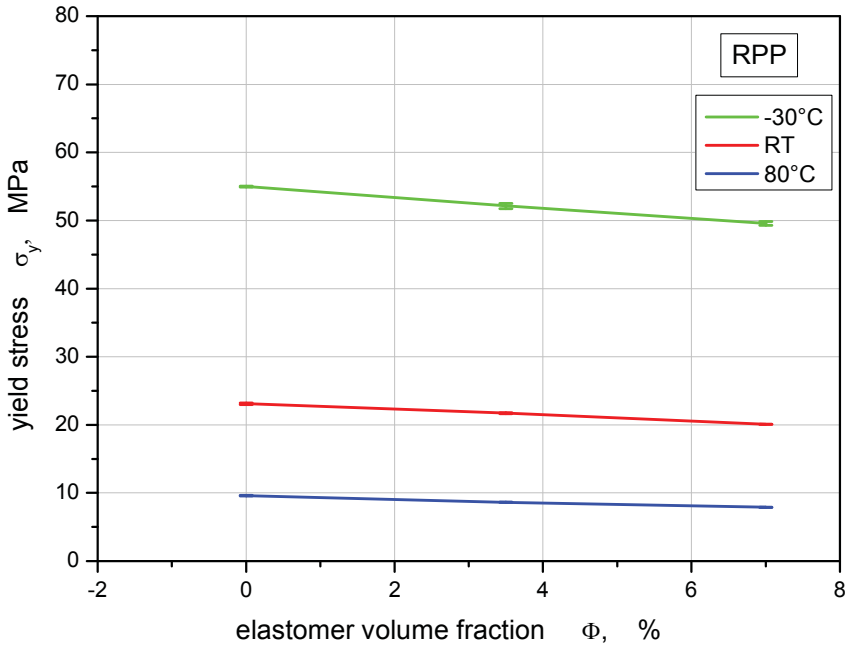

Fig. 41: The change of yield stress, σ_y, in function of volume fraction, Φ, at three testing temperatures.

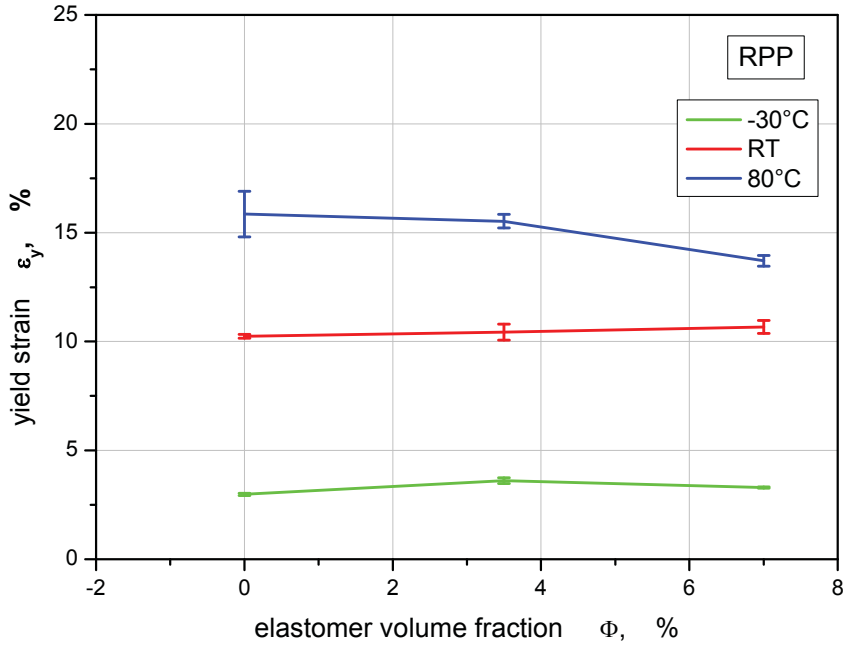

Fig. 42: The change of yield strain, ε_y, in function of volume fraction, Φ, at three testing temperatures.

Based on the uniaxial tensile experiments, the Poisson's ratios, ν of the PP(H) and the R(PEO) have been estimated and documented (see **Table 7** page 79). The values of Poisson's ratio have been determined by FFSA with Aramis. In the following the temperature dependence of the Poisson's ratio will be revealed in **Fig. 43**, where the Poisson's ratio of PP(H) raises with increasing temperature, but the R(PEO) has a constant Poisson's ratio of about 0.5 at all temperatures due to its incompressibility. The measurement of the Poisson's ratio of the R(PEO) at room temperature delivers the value 0.48. The Poisson's ratio of the R(PEO) has not been measured at other temperatures successfully due to technical difficulties.

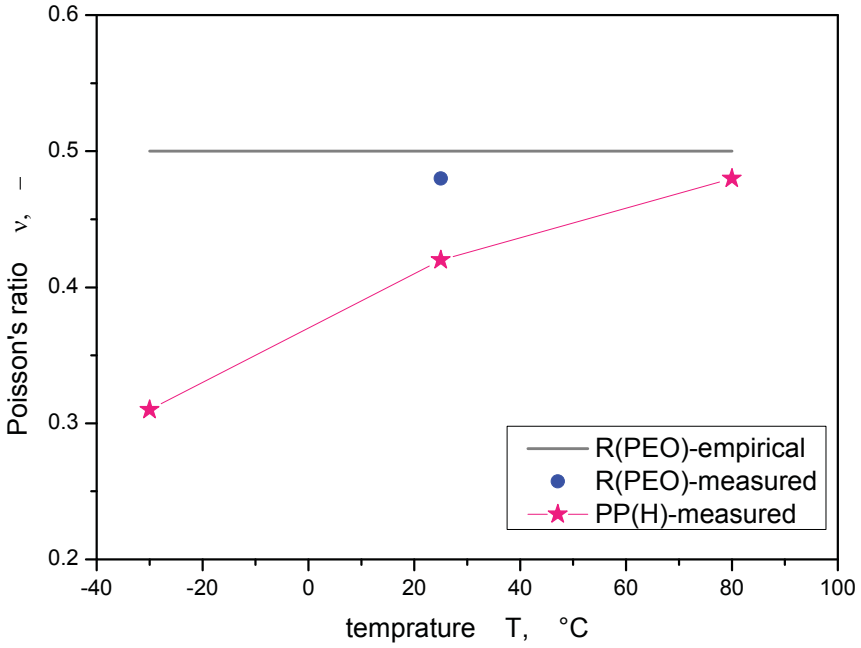

Fig. 43: Poisson's ratio, ν, of PP(H) and R(PEO) in dependence on temperature, T.

5.1.2 Planar tensile tests

The planar strain state can be realized by stretching the FWPS specimen (**Fig. 24**), as the effective part of specimen is much shorter in height (16 mm) than in width (200 mm). During tension parallel to the axis of the height, the contraction in width will be inhibited and hence be negligible. This means that the thinning only appears in the thickness.

The pure shear tests of elastomer R(PEO) were carried out at two temperatures: 25 °C and 80 °C. At each temperature the FWPS specimens were tested at two strain rates: 0.01 mm/s and 1 mm/s. The operation of the pure shear experiment was described in Section 3.2.2. The results of pure shear tests on R(PEO) are documented in **Fig. 44**. The dashed curves refer to strain rate 1 mm/s, and the solid

curves to 0.01 mm/s. The red stress-strain curves correspond to a room temperature of 25 °C, while the blue curves to 80 °C. One sees that a higher testing rate leads to a stiffening of the material, because the relaxation of the molecule chain does not have enough time to take place or only occurs of a limited level. The rate effect is especially pronounced at 80 °C.

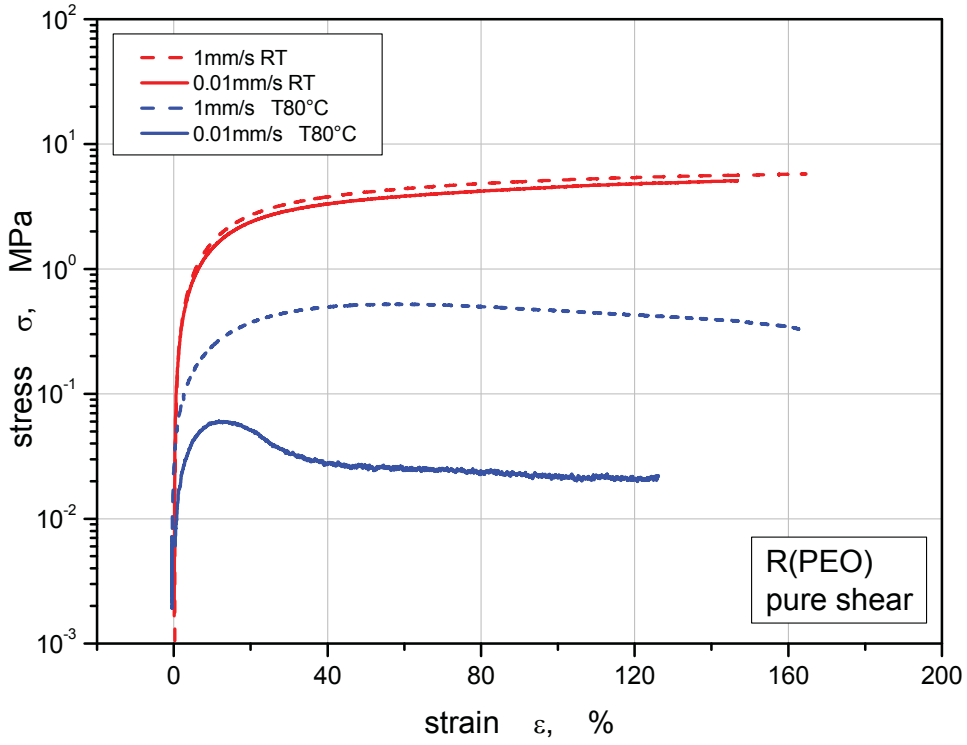

Fig. 44: Stress-strain curves of pure shear tension on FWPS specimens of elastomer R(PEO).

The temperature dependence shows the same tendency at both testing rates, namely the material is stiff at lower temperatures and soft at higher temperatures. Moreover, the rate effect is more obvious at a temperature of 80 °C, if one compares the two blue stress-strain curves in **Fig. 44**. This observation reflects the thermal property of the elastomer. According to the data sheet of DOW chemical company in the appendix, the T_g of the elastomer R(PEO) is about –52 °C, and its DSC melting point T_m determined at 10 °C/min is 60 °C. By contrast, the PP resin is a very rigid material. Some research reports show that the thermo stability of PP could be enhanced to a certain extent by elastomeric phase [Karger-Kocsis, 1995].

During tension, whitening in the specimen accompanies material yielding. As shown in **Fig. 45**, at room temperature and at testing rate of 0.01 mm/s, the whitening appears at a strain of about 50 % and implies the onset of inhomogenous deformation of the specimen. As the elongation reaches about 100 %, a

remarkable void formation of material manifested. In general elastomers are tough in a wide temperature range and withstand large deformation.

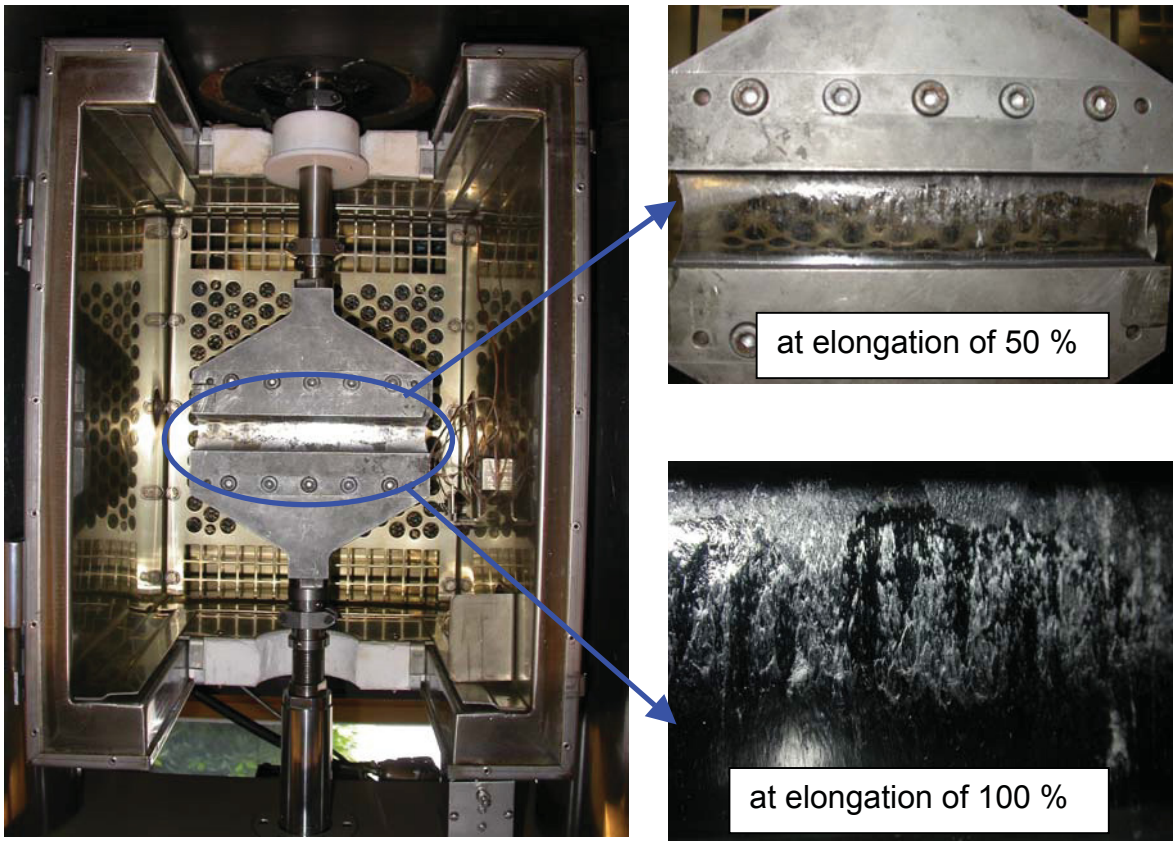

Fig. 45: Whitening of R(PEO), observed in the pure shear (planar tension) experiment at a loading rate of 0.01 mm/s and at RT.

5.1.3 Equibiaxial tensile tests

In Section 3.2.3 the test device together with examples of strain field analysis have been shown. It is worth mentioning that the practical handling of the equibiaxial tensile test is of particularly difficult. The fixture-induced stress concentration will more or less affect the testing and the results. Some brittle specimens fracture abruptly at the clamps during loading. Another problem is, the testing device is applicable in the strict sense only to the incompressible materials such as elastomers. Further, the polymeric materials fail more rapidly, that is to say after reaching the yield point less force is needed principally in order to cause the same elongation of the sample as before yielding. Loading in the uniaxial and planar tensile tests is applied under displacement controlling to guarantee the monotonic loading conditions. In the equibiaxial tensile test, however, the loading by gas blowing from beneath the gripped disc specimen cannot be kept constant. The calculated stretch rates of the equibiaxial tensile experiments with the two

compounds are shown in **Fig. 46**. In this work, the measurements of the strain field have been made in the centre of the disc specimens during biaxial tension.

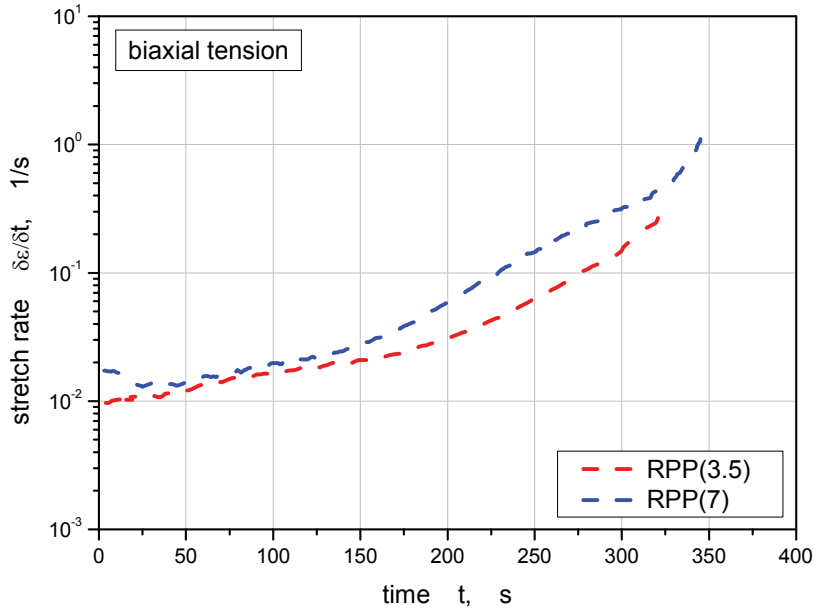

Fig. 46: Calculated stretch rates of equibiaxial tensile tests with the two compounds.

The stress-strain relationship of the performed tests is plotted in **Fig. 47**. As shown in **Fig. 47**, the two compounds distinguish merely from each other in the linear elastic region (the green circled region in **Fig. 47**) but do differentiate in the nonlinear elastic region (the black circled region in **Fig. 47**). Based on this observation, one may conclude that the matrix material governs the elastic behaviour of the compounds, whereas the nonlinear, irreversible large deformation will be more strongly influenced by elastomer fillers. Hence the deviation of the two stress-strain curves in **Fig. 47** appears at a strain of about 4 %. At larger deformation, the compound RPP(7) with 7 vol% elastomer fillers has a smaller stress resistance but a better fracture behaviour; it fails at a strain of beyond 40 % in the biaxial tensile test. In contrary to RPP(7), the compound RPP(3.5) with 3.5 vol% elastomer fillers fails at strain less than 20 % in the biaxial tensile test. The volume fraction of the elastomeric phase of a PP compound can reach normally up to 20 vol%, where the toughness can be further improved without loss of the stiffness with a higher filler content of the compounds. In this work, both compounds are low-loaded, but the toughening effect of elastomers can still be identified by contrasting the two compounds (**Fig. 47**). Because of the brittleness of the neat polypropylene, biaxial tensile tests on PP(H) were not carried out successfully.

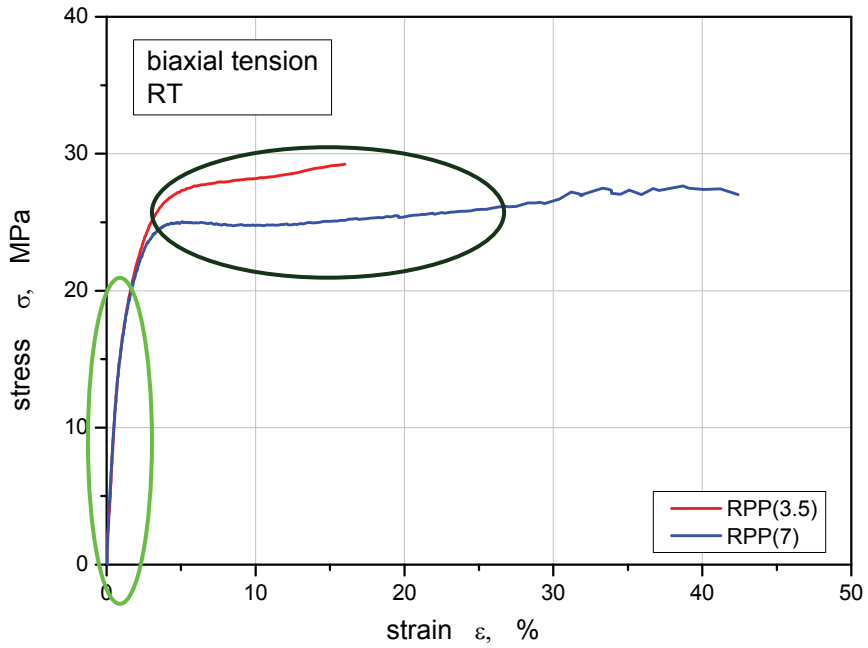

Fig. 47: Comparison of the equibiaxial tensile behaviour of the compounds RPP(3.5) and RPP(7), at room temperature.

5.1.4 Comparison of material behaviour at different strain states

In Section 2.1.3 the three fundamental strain states were explained. Results of the experiments at each strain state were interpreted one by one in Sections 3.2.1 to 3.2.3. In this section, the results of the three strain states will be compared with one another in terms of the effect of strain conditions on the material behaviour (refer to **Fig. 12**).

In **Fig. 48** the material behaviour of the uniaxial tensile test and the pure shear test of the elastomer R(PEO) are presented. The loading of both tests was applied at room temperature with a loading rate of 0.01 mm/s. It can be seen that the tensile strength of the elastomer has been approximately doubled in planar tensile (pure shear) state in contrast to the uniaxial tensile state. This phenomenon is called strain state dependence and shall be taken into account while studying the mechanical properties of polymeric materials.

The distinction between the uniaxial and biaxial tensile tests provides another evidence of the strain state dependence. The results of the two types of strain state that have been applied to the two compounds RPP(3.5) and RPP(7) is shown in **Fig. 49** on the next page. The pink curves correspond to RPP(3.5) and the cyan curves correspond to RPP(7). The dot-line curves refer to the biaxial tension tests and the solid curves to the uniaxial tension tests.

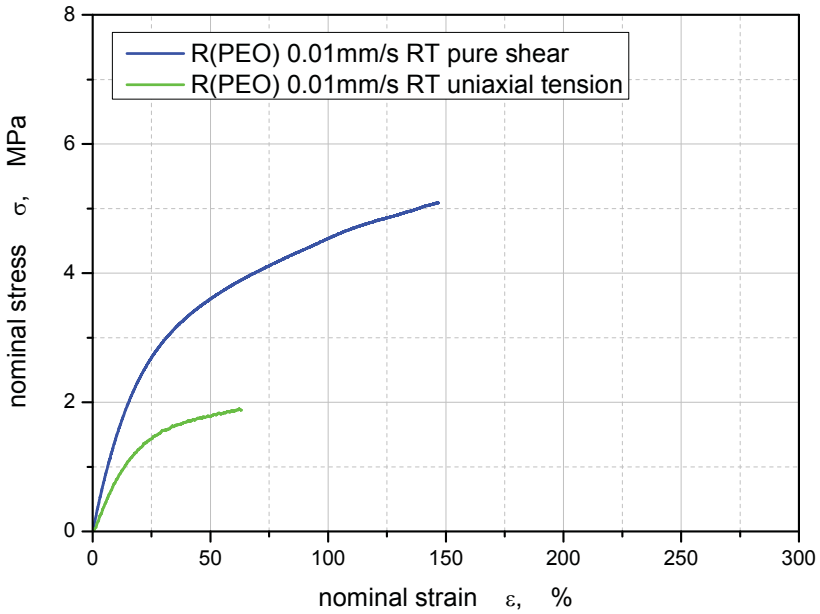

Fig. 48: Stress-strain relationship of the uniaxial tension and the pure shear experiments that were carried out at room temperature where the same loading rate 0.01 mm/s was applied.

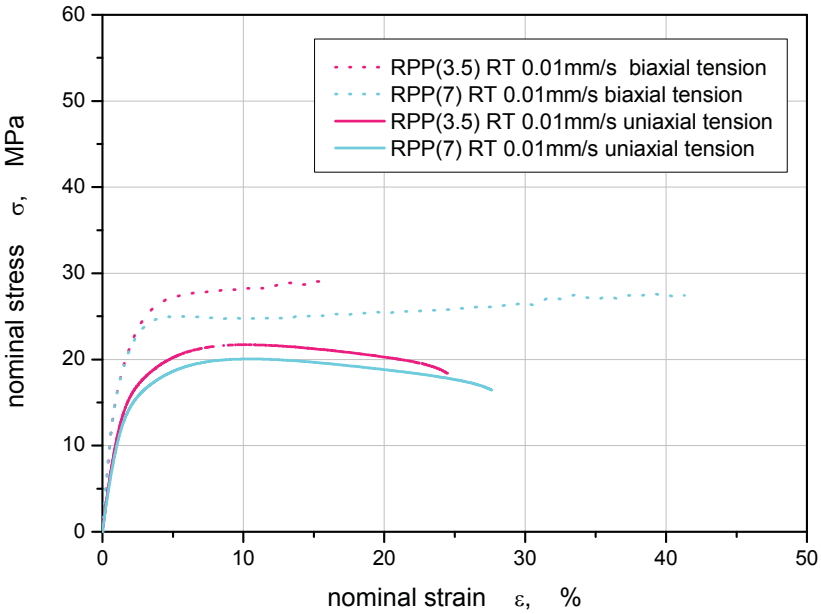

Fig. 49: Stress-strain relationship of the uniaxial tension and the biaxial tension experiments on the compounds where the same loading rate 0.01 mm/s was applied at room temperature.

The uniaxial tension refers to loading in only one direction, whereas the biaxial tension is a multiaxial loading procedure in which the loadings in two orthogonal directions are of same magnitude. It can be derived from the stress-strain relationship in **Fig. 49** that the biaxial strain state leads to upgrade in stiffness (elastic modulus) and tensile strength (yield stress) relative to the uniaxial strain state. In addition, irrespective of strain state, the yield strain seems dependent mainly on material. Different strain states do not result in different yield strain of single material, neither of elastomer nor of compounds as shown in **Fig. 49**.

5.1.5 Data extraction for simulation

The rubber elasticity and relevant material law (the simplified Mooney-Rivlin strain energy function) have been generally described in the Section 2.1.2.3. Treloar has in his book “the physics of rubber elasticity” introduced the development of the theories for large elastic deformation of rubber and also discussed the restraint of various proposals [Treloar, 1975].

The Mooney plot of the elastomer R(PEO) is presented in the **Fig. 50** based on the uniaxial tensile test, where the loading velocity was 0.01 mm/s and the testing temperature was 25 °C. The red straight line is the linear fitting on the experimental curve in green and yields the values of Mooney constants C_1 and C_2.

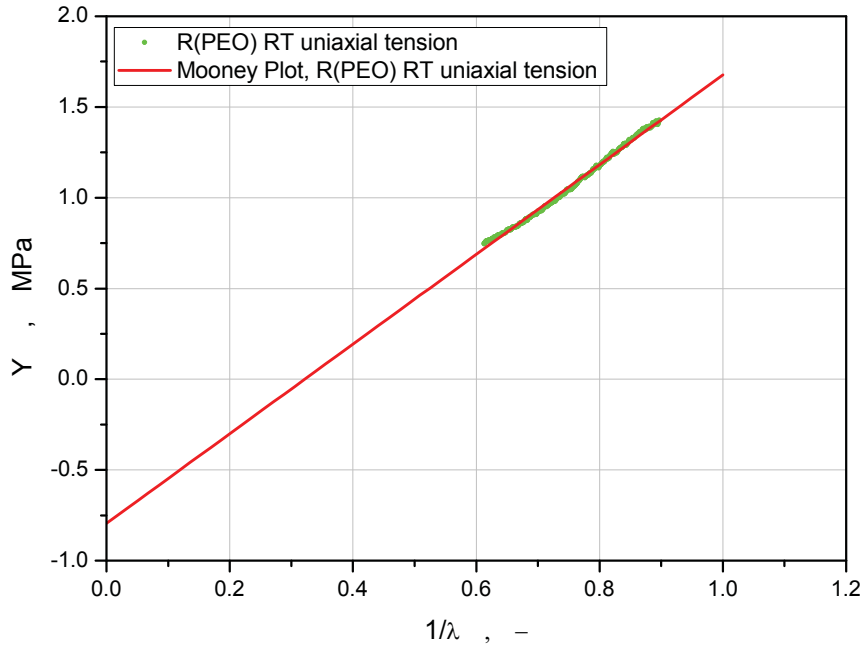

Fig. 50: Mooney plot on the basis of uniaxial tensile test of elastomer R(PEO), the testing conditions were: room temperature and stretch rate of 0.01 mm/s.

According to statistics by Treloar, the empirical value of C_1 ranges from 0.10 MPa to 0.31 MPa, whereas the C_2 remains approximately constant (0.10 MPa). The experiment shown in **Fig. 50** yields values of C_1 and C_2 those are unlike the empirical values. For the elastomer R(PEO), C_1 is about –0.8 MPa and C_2 approaches 2.5 MPa. The difference between the empirical and the experimental values may depend on the material. The empirical values have been based on uniaxial tension of a series of vulcanized rubbers, but the elastomer R(PEO) in this work is a thermoplastic elastomer (see introduction in Section 2.1.2.2, pages 7 and 8). Since C_1 and C_2 are material specific constants, the individual test conditions such as temperature and stretch rate should not play a part in the deviation. The determination of the two constants by means of Mooney plot has been introduced in Section 2.1.2.3 (**Fig. 13**). In the later simulation, C_1 and C_2 are two of the inputs that are required by the chosen material law for the elastomeric phase.

5.2 Dynamic mechanical analysis

For the processing and application of polymeric materials, their viscoelasticity is of essential importance. Depending on the particular rate and temperature, the viscous, anelastic (retarded elastic deformation) and elastic responses of polymeric materials to loading have different weights in terms of deformation. The dynamic mechanical tests of polymers deliver complementary information of material behaviour to monotonic mechanical tests, because they deliver important information of the viscosity of a material. In this work, DMA (dynamic mechanical analysis) was employed to measure the material property dependence on variable frequency and on temperature. The input cyclic signals of all the DMA measurements in this work have been set in sinusoidal form that is generally considered the best waveform to reveal the properties of polymeric materials which show both viscous and elastic responses.

5.2.1 Amplitude scan and estimation of the linear viscoelastic limit

The amplitude scans of constituents and compounds are presented in Figs 51 to 54 on the following pages. **Fig. 51** shows the strain amplitude scan of PP(H), with a relatively large scattering of data points at small strain amplitudes. The tendency of the storage modulus, E', in relationship of the strain amplitude, A, was evaluated approximately, and the amplitude limit at which the storage modulus is no more constant was estimated. The same procedure was repeated in the determination of the applicable strain amplitude of the R(PEO) in **Fig. 52**, RPP(3.5) in **Fig. 53** and RPP(7) in **Fig. 54**. The strain amplitude limits of these materials were then plotted in **Fig. 55**. The test settings of the temperature scan (Section 5.2.2) is based on the estimated linear viscoelastic limits of the materials in the amplitude scan (see Section 3.3 and **Fig. 29**).

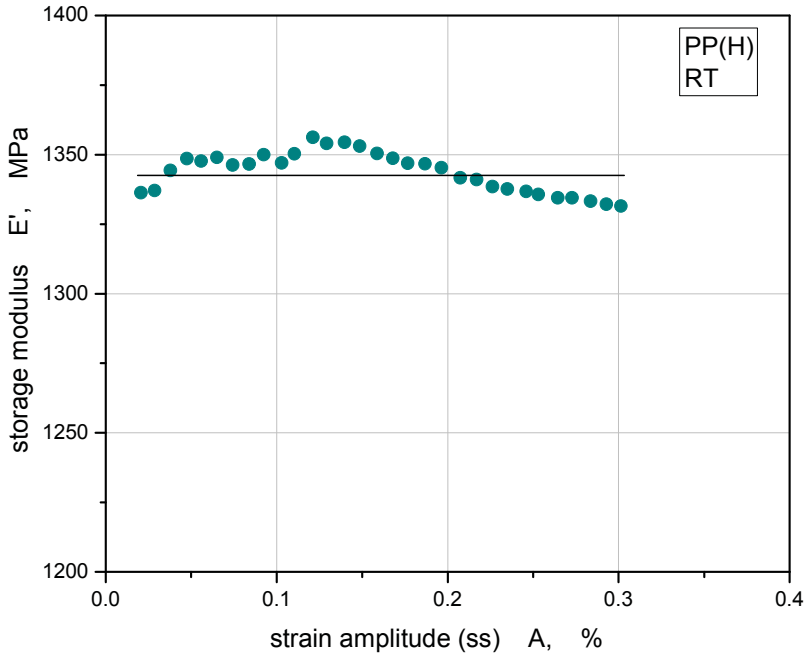

Fig. 51: Strain amplitude scan of resin PP(H), at room temperature.

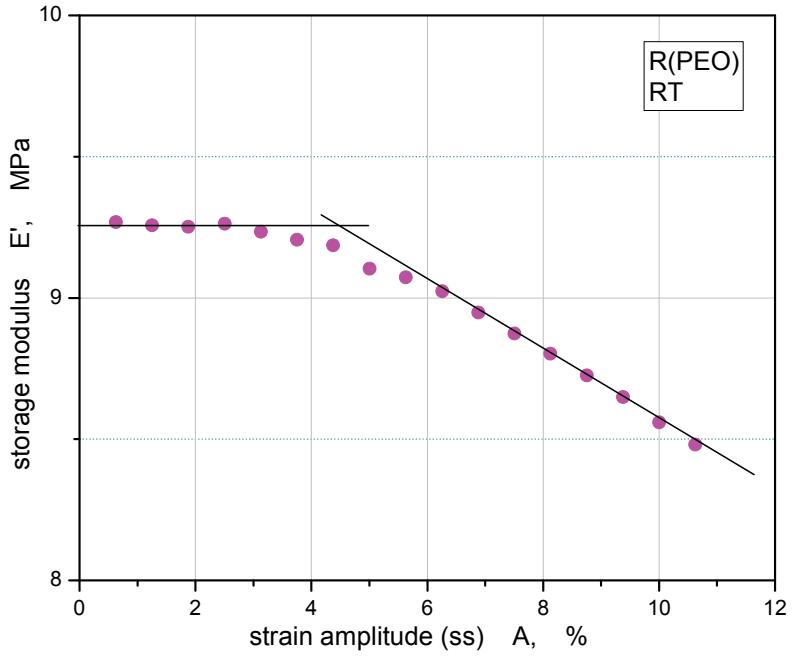

Fig. 52: Strain amplitude scan of modifier R(PEO), at room temperature.

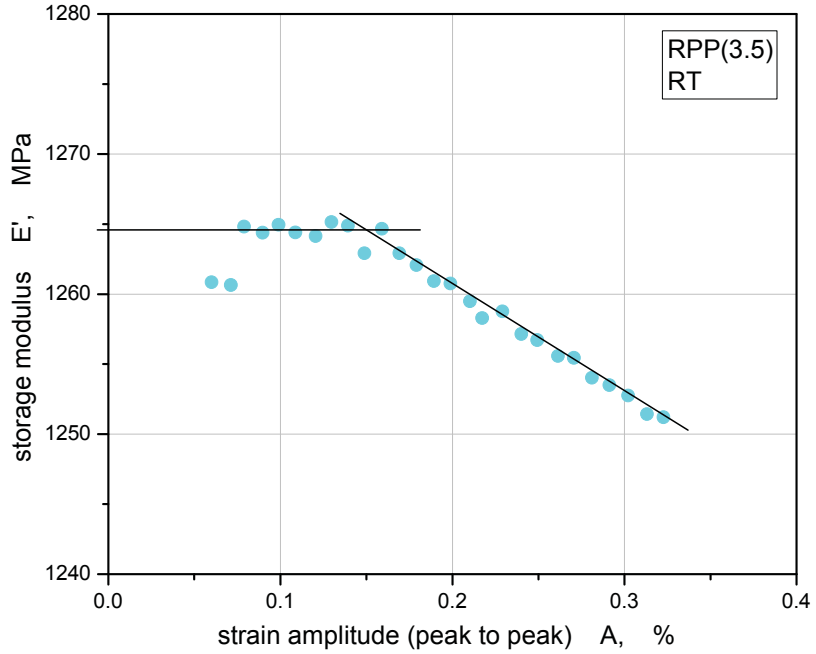

Fig. 53: Strain amplitude scan of compound RPP(3.5), at room temperature.

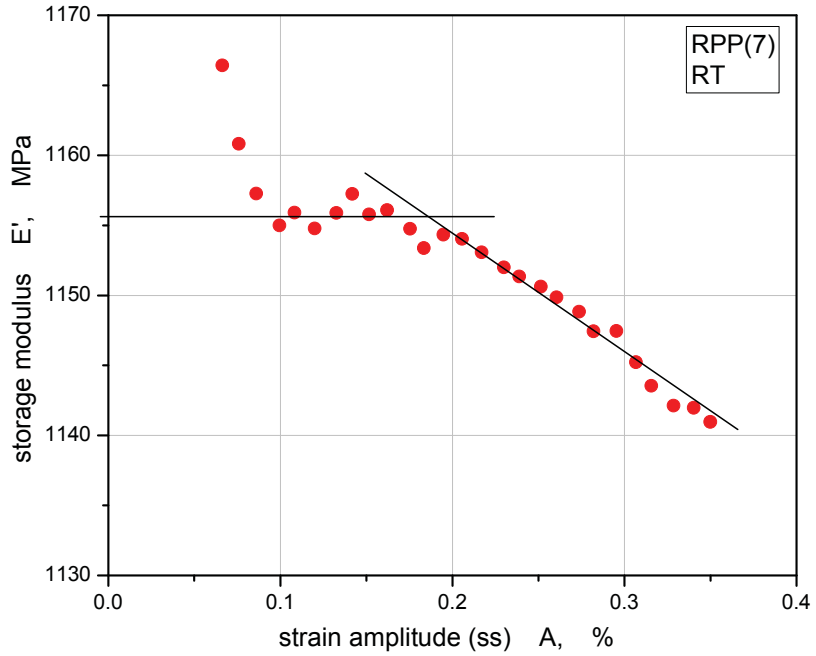

Fig. 54: Strain amplitude scan of compound RPP(7), at room temperature.

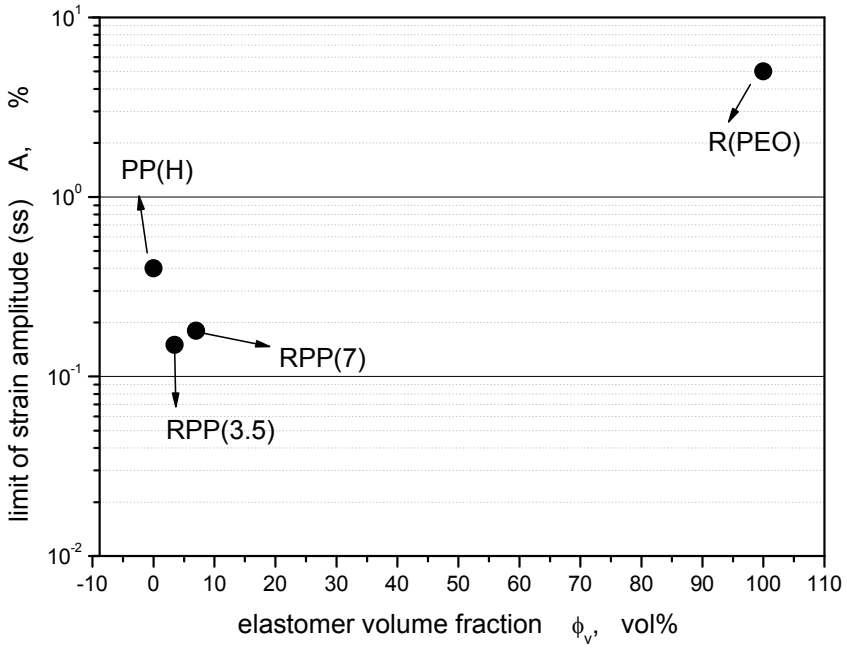

Fig. 55: Maximum limit of strain amplitude (peak-to-peak) for each material.

5.2.2 The temperature dependence

The temperature scan is a DMA measurement of one frequency, one force amplitude, with a temperature program. The temperature scan also offers information on the glass transmission temperature, T_g, that is one of the important parameters for the determination of the temperature application extent of a polymeric material.

The temperature scans (tensile DMA in this work) of the two constituents and two compounds with constant frequency of 1 Hz are displayed here in Figs 56 to 60, where the change of the storage modulus, E', and the loss tangent, tanδ, of each material depending on the temperature will be displayed separately. The applied force/displacement amplitude to each material has been checked to be below the linear-viscoelasticity limit (Figs 51 to 54). The cross section of the dumbbell specimens used is 40 mm^2 (4x10 mm). The temperature scans of the PP(H), RPP(3.5) and RPP(7) were under force control and have these testing conditions: the mean value of applied axial force F_{mean}=50 N, the peak-to-peak amplitude of applied axial force F_{ampl}=50 N, test frequency f=1 Hz. The temperature scan of the R(PEO) was however under displacement control due to the large variation of the storage modulus over the test temperature range. The testing conditions for R(PEO) are: the mean value of the axial displacement S_{mean}=0.75 mm, the peak-to-peak amplitude of the axial displacement S_{ampl}=0.5 mm, test frequency f=1 Hz. The storage modulus variations of materials in function of temperature will be

then contrasted with each other in the **Fig. 60** on page 64.

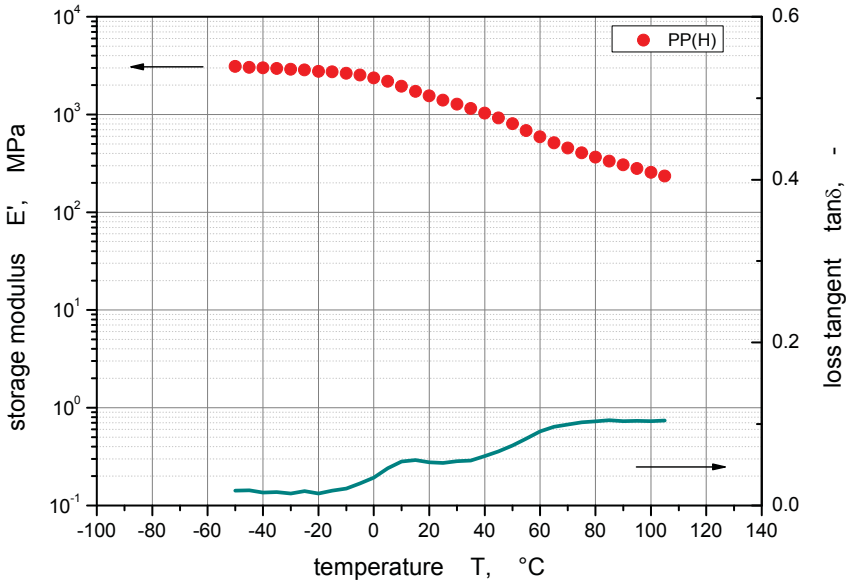

Fig. 56: Temperature scan of resin PP(H), showing storage modulus, E', and the loss tangent, tanδ.

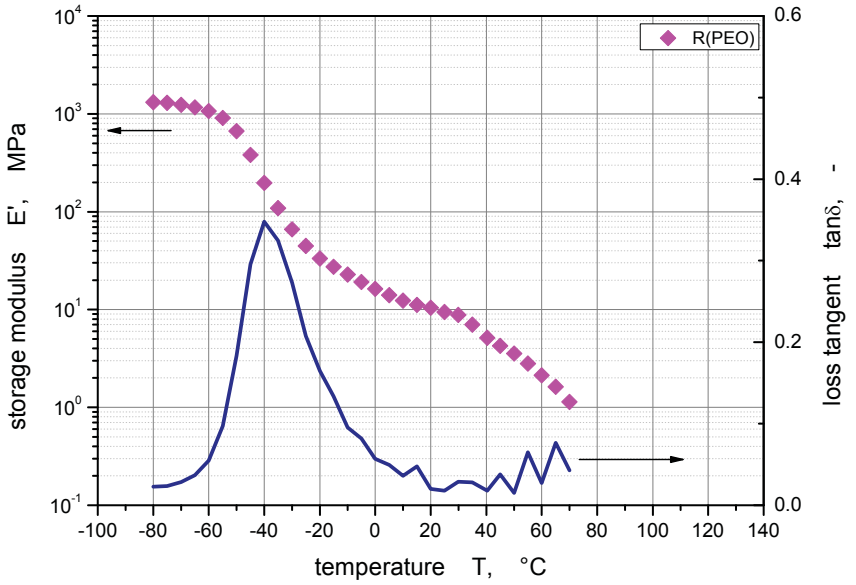

Fig. 57: Temperature scan of elastomer R(PEO), showing storage modulus, E', and the loss tangent, tanδ.

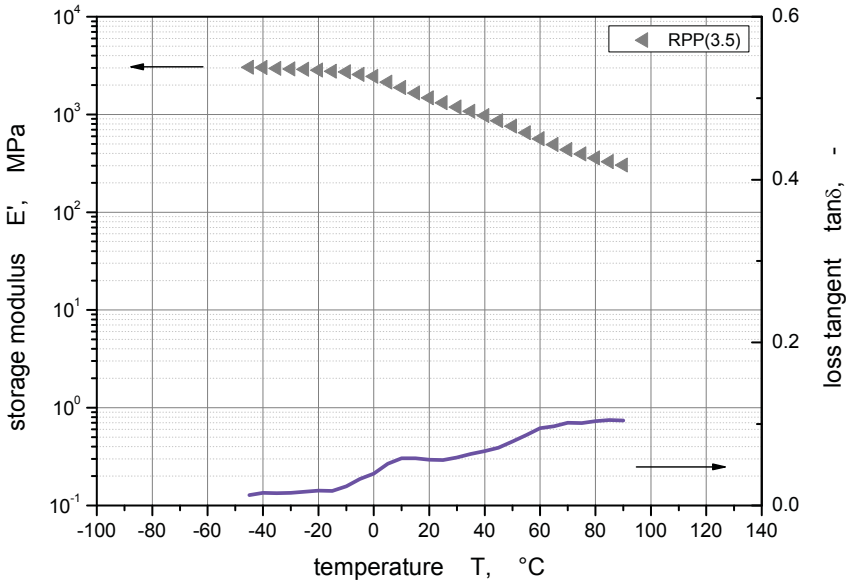

Fig. 58: Temperature scan of compound RPP(3.5), showing storage modulus, E', and the loss tangent, tanδ.

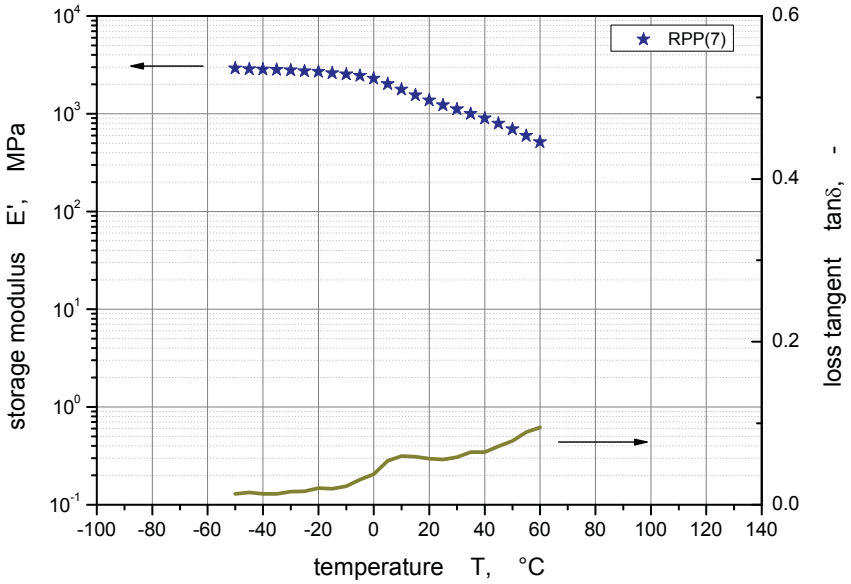

Fig. 59: Temperature scan of compound RPP(7), showing storage modulus, E', and the loss tangent, tanδ.

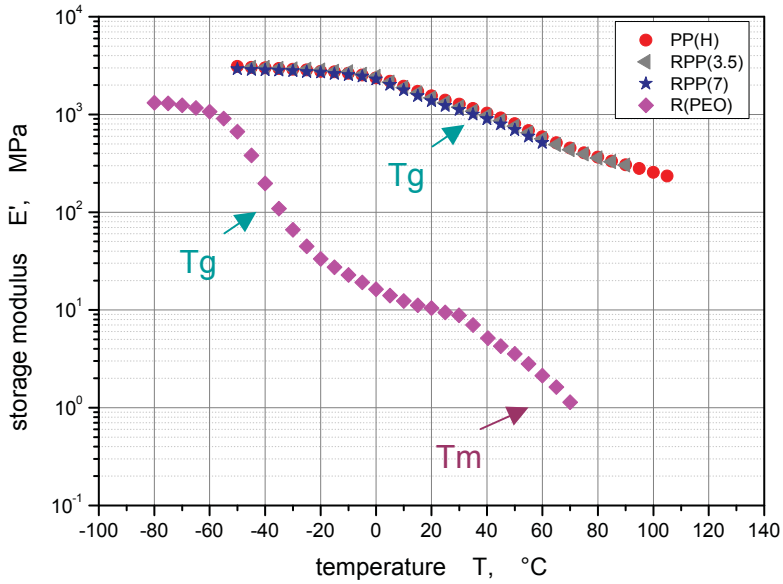

Fig. 60: Comparison of the temperature dependence of the storage modulus, E', of the materials.

By comparing the two constituents (**Fig. 60**), it can be derived that the elastomer R(PEO) (in magenta rhombus) reveals a dramatic drop of storage modulus as the temperature rises. On the contrary, the PP(H) (in red point) remains relatively rigid up to 100 °C. The T_g of R(PEO) at 1 Hz is about –40 °C, which is comparable with the data (T_g of R(PEO): -52 °C) offered by DOW chemical company. The melting temperature, T_m of R(PEO) is 60 °C according to DOW, which is the same as evaluated by the temperature scan at 1 Hz.

It is logical to infer that the dynamic mechanical properties of the compounds RPP(3.5) and RPP(7) may be in the interval built by the two constituents. This can be seen in **Fig. 60** where the storage modulus descends with ascending elastomer content, though the difference between the three materials (PP(H) in red point, RPP(3.5) in grey triangle, and RPP(7) in royal star) is very small owing to the relatively low filler contents in both compounds.

In the temperature scan (Figs 56 to 59) of the materials tested in this work compound properties are mainly determined by the matrix material PP(H) due to the small filler fractions. The temperature dependence of the storage modulus of the compounds are dominantly controlled by the matrix material PP(H) according to DMA experiments (**Fig. 60**), and so is the tensile behaviour (see Section 5.1.1).

5.3 Material morphology

Parallel to the mechanical experiments, the morphology of the compounds has been researched by means of LM (light microscopy) and TEM (transmission electron microscopy). The microstructure of a compound is basically determined by microstructures of the mixed constituents and by the process conditions along with the interaction between the constituents during processing. The micrographs will be presented in the following part and be interpreted in terms of structure-property relationships.

5.3.1 The microstructure of injection moulded dumbbell specimen

The light microscopy of the semi thin microtomed films of the compound RPP(3.5) shows the typical skin-core structure [Strobl, 1996] of the injection moulded dumbbell multipurpose tensile specimen. The measured skin layer is about 100-200 µm thick according to the size variation of the spherulites of the continuous phase, the PP(H) (see **Fig. 61**). Although there is no clear definition of the skin layer up to date, it is obvious (left image in **Fig. 61**) that there is a definitive abrupt change of the crystallite size in the material, which, for discussions in this work, may be defined as the boundary of the skin layer.

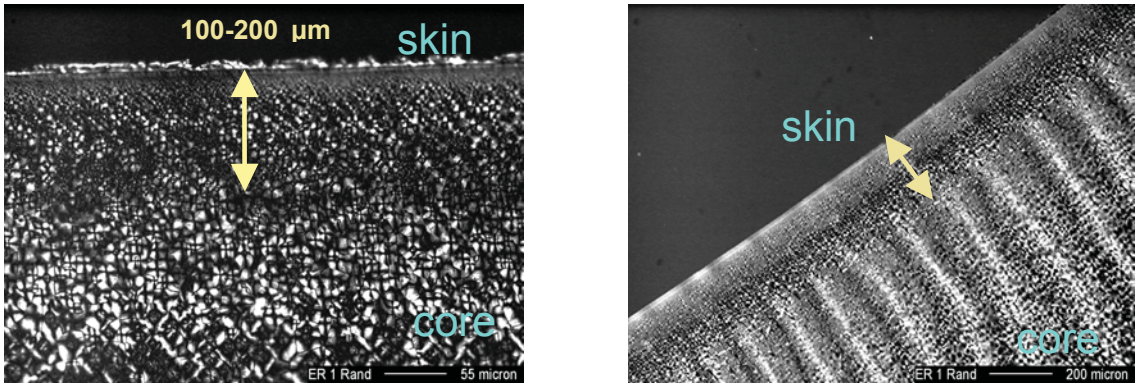

Fig. 61: Images that are taken from a semi thin microtomed film of the dumbbell specimen of the compound RPP(3.5).

An overview of the cross section of the dumbbell tensile multipurpose specimen of RPP(3.5) is shown in **Fig. 62**. The slice has been microtomed vertically to the direction of the material flow of injection moulding. The dark region in the middle of the film in **Fig. 62** suggests that the microstructure of the compound does not have a homogenous transition from skin to core. The microstructure of the core may be different from that of the skin and of the transition regions. The microstructure of the core layer is illustrated in **Fig. 63**, where the structureless features are presumably amorphous PP domain melted while sectioning of the thin slice at room temperature. Some studies reported that the elastomeric discrete phase might

influence the size of the PP spherulites but not the crystallinity of the continuous phase [Karger-Kocsis, 1995]. The TEM observations support argument this (see Section 5.3.2.2).

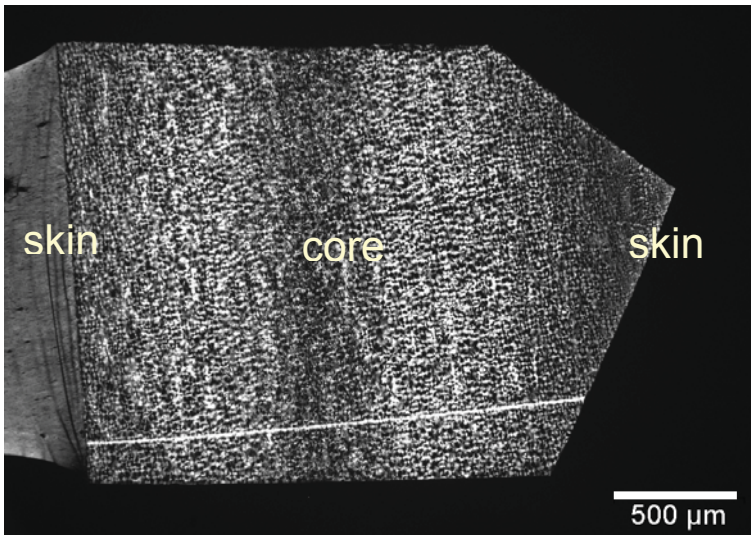

Fig. 62: Image of cross section of a dumbbell tensile multipurpose specimen of RPP(3.5).

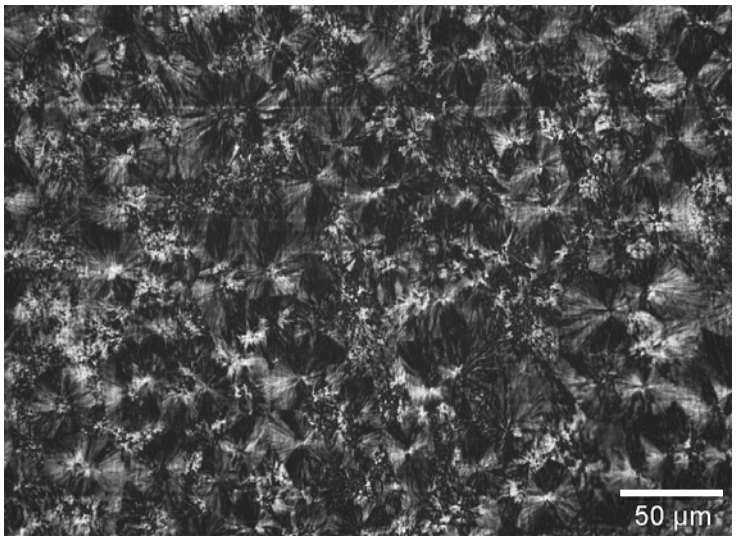

Fig. 63: Illustration of microstructure in the core of a dumbbell tensile multipurpose specimen of RPP(3.5), by polarized light microscopy.

5.3.2 Morphological observations of the compounds

In this section, TEM micrographs of the two compounds have been studied in order to know how the two principally immiscible phases are coexistent in the compound. The centre problem is the dispersion and the distribution of the discrete phase coupled with filler content and processing technique. Furthermore, the property of the interface (the interfacial adhesion) between the two phases in the compounds will be briefly discussed, too because of its importance for the bonding.

5.3.2.1 The particle size and shape distribution

Methods have been developed to enable the determination of the shape and size of filler particles and their distribution in a composite; some of the theories deal with the explanation of the three-dimensional morphology of filler particles and are successful in many cases [Xu et al., 2003]. Anyway, the exclusive resource for such a study or analysis is the micrograph. The single particles will be counted and classified in association with their size and shape. But only particles that can be recognized by the analysis tools used will be counted in statistics. In most cases the very tiny particles are neglected though the total number of small particles is larger than the total number of large particles (**Fig. 64**). The elastomer particles change their shape and size during processing which complicates the estimation. The accuracy and validity of such calculation of filler size and shape distribution based on micrographs will thus be quite impaired in practice. If the same operation or procedure of statistical analysis can be ensured, they can be applied for instance to compare the compounds with the same kind of filler but different filler contents. Above all, the statistics should be made by analysing large amount of micrographs, with careful regard of other factors like specimen preparation and operation of microscopy etc.

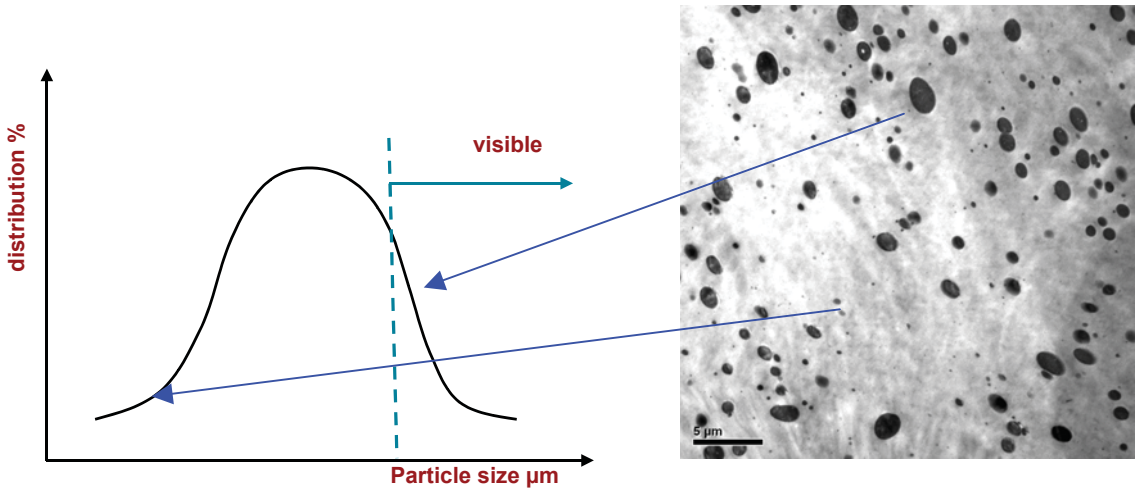

Fig. 64: Scheme of size distribution of elastomer particles in compounds.

By coincidence with observation by LM, the skin-core structure of the injection moulded dumbbell multipurpose tensile specimen finds its evidence in TEM micrographs, too. It can be identified by the transition of the elastomer particle shape. This can be viewed in **Fig. 65**, where the TEM micrograph of the compound RPP(3.5) has been made by using an ultra thin slice microtomed from dumbbell specimen perpendicularly to the flow direction. The skin layer thickness is about 60 µm according to the variation of the elastomer particle shape, while the skin layer thickness determined by the spherulite size variation is around 100-200 µm (see

Fig. 61 left). This phenomenon can owe to the distinct thermal properties of the two constituents, although they are subjected to the same cooling temperature history simultaneously in the mould. Compared with the resin PP(H), which crystallized on the wall of the mould at a relatively higher temperature during injection moulding, the elastomer particles remained molten until the temperature fell to below the T_g of the elastomer. Hence during cooling in the mould, the elastomer particles had enough time to relax, whereas the PP close to the wall was frozen-in in a very short time, so that the PP spherulites in a certain distance from the wall were not able to grow.

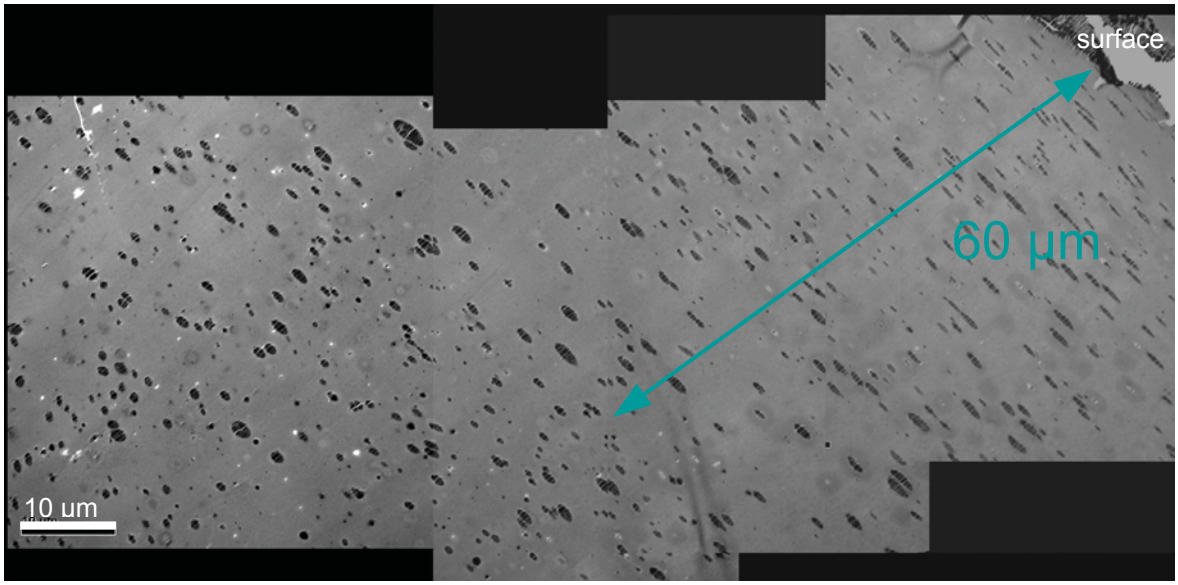

Fig. 65: Skin-core structure according to the particle size variation from surface layer (right) towards the core layer (left).

The ellipsoidal configuration of the dispersed elastomer particles together with the three dimensions a, b and c is illustrated in **Fig. 66**. If a < b < c, the c represents the flow (injection) direction, in which the largest deformation of elastomer particles appears, and the a and b are in the plane that is vertical to the c-axis. The a-b plane defines the cross section of the dumbbell specimen. The dumbbell specimens were injection moulded, but since the applied shear rate (injection velocity) and shear rate gradient as well as the cooling rate and the temperature gradient in the mould did not block the relaxation of the elastomeric phase significantly, the filler particles are quasi spheric in their solid state (after cooling). This can be proven by the TEM investigation of the samples sectioned from the dumbbell specimens of the compounds RPP(3.5) and RPP(7) in Figs 67 to 70.

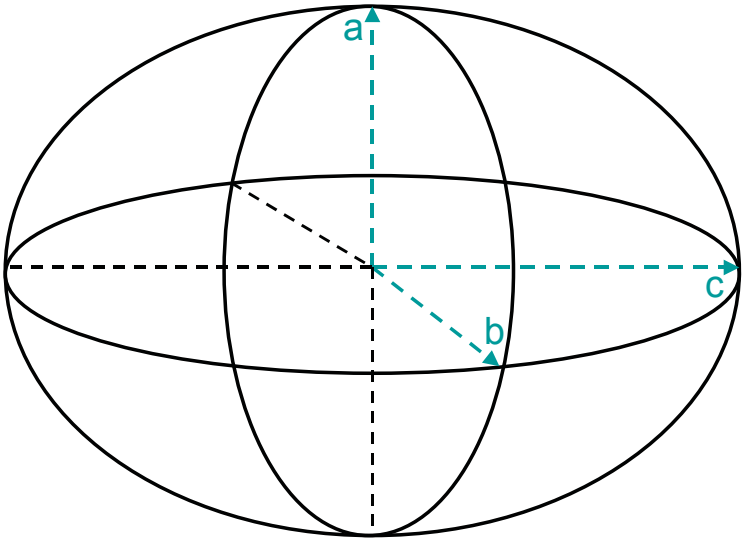

Fig. 66: Ellipsoidal configuration of the dispersed elastomer particles in the compound, c indicating the flow direction.

The elastomer particles in the skin layer were oriented, that is, in other words, elongated parallel to the flow direction. The micrographs are two-dimensional. In order to reveal the three-dimensional body of the particles, ultra thin microtomed slices that are in the two orthogonal planes were prepared. One of the planes is parallel to the c-axis which indicates the flow direction, and the other one is perpendicular to the c-axis. The aspect ratio denotes the degree of anisotropy of the dimensions of a particle. Two aspect ratios are defined in this work. The aspect ratio r_v equals b/a, of which the subscript v refers to vertical to flow direction. For simplification, the b/c and a/c can be represented by the same aspect ratio r_p, of which the subscript p means parallel to the flow direction. The orientation of filler particles is induced primarily by flow deformation, thus the relationship $r_p \geq r_v$ exists generally. Conclusion can be drawn from the observation of Figs 67 to 70 that $r_p \approx r_v \approx 1$ is valid in the core layer of dumbbell specimens of the two compounds RPP(3.5) and RPP(7). This means that the elastomer particles are approximately spheres in the core layer of the injection moulded dumbbell specimen. The morphology of particles in the skin layers of both compounds is shown in Figs 71 to 74, where large elongation of particles introduced by flow can be seen. Images in Figs 67 to 74 are of the same magnification.

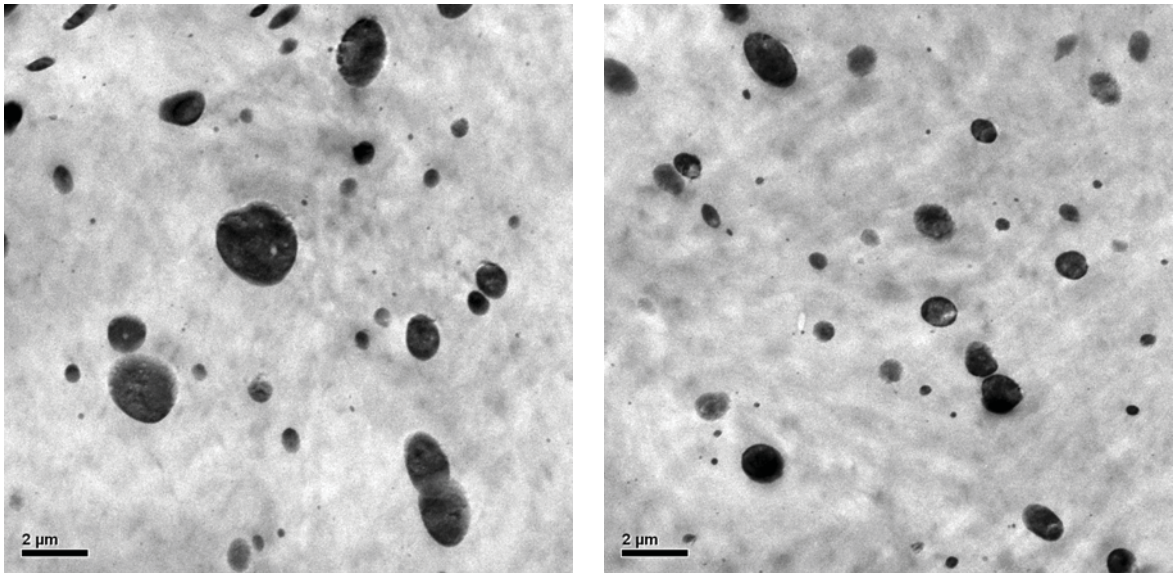

Fig. 67: Core region of the dumbbell specimen of RPP(3.5), parallel to flow direction. Particle diameter about 0.1-2 µm.

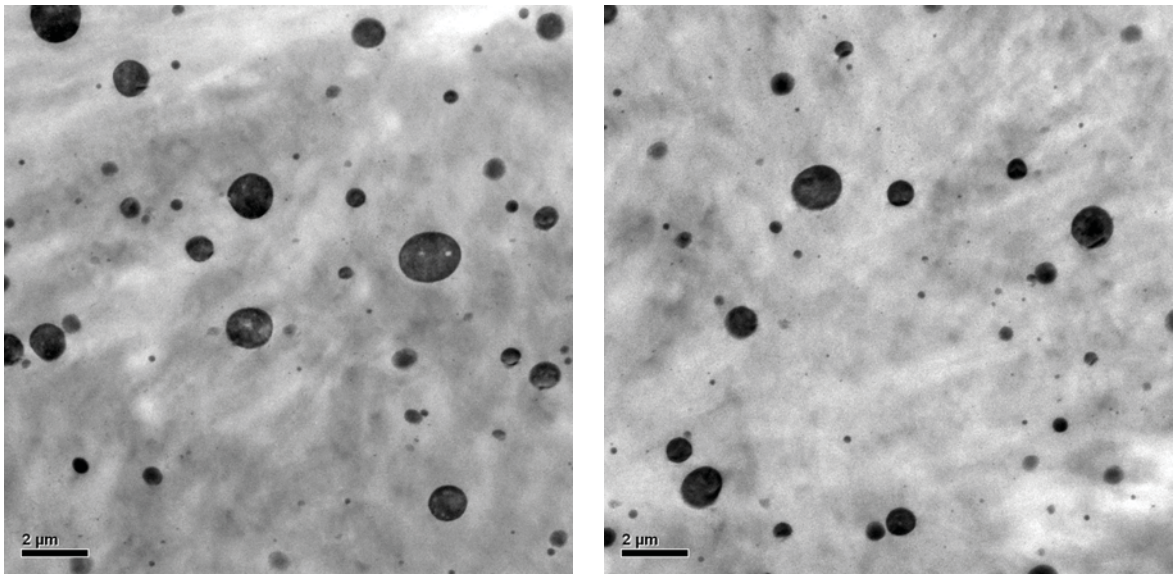

Fig. 68: Core region of the dumbbell specimen of RPP(3.5), vertical to flow direction. Particle diameter about 0.1-2 µm.

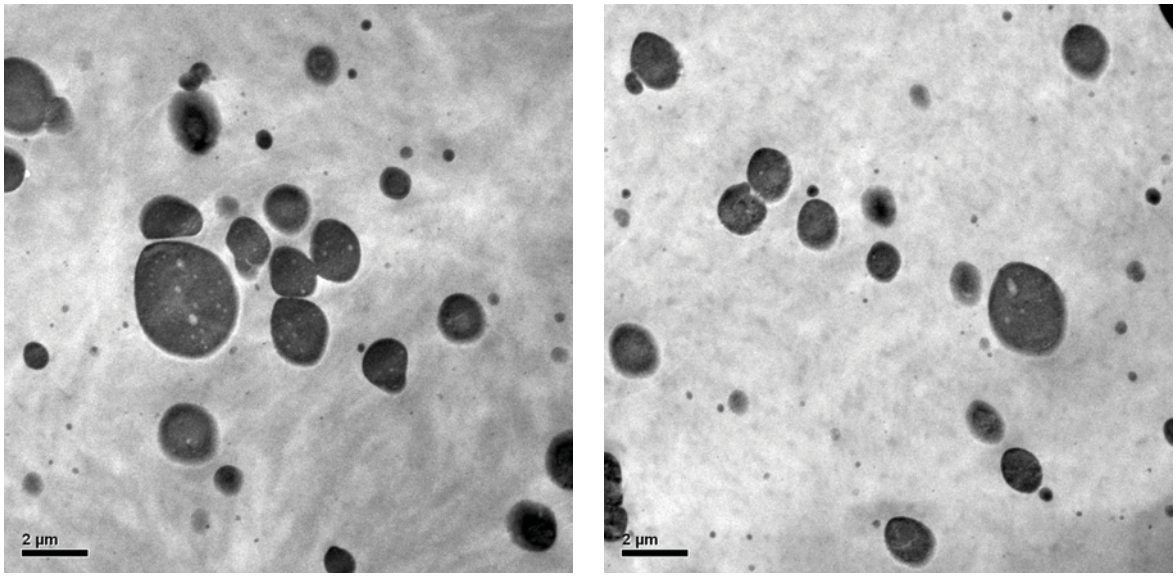

Fig. 69: Core region of the dumbbell specimen of RPP(7), parallel to flow direction. Particle diameter about 0.1-3 µm.

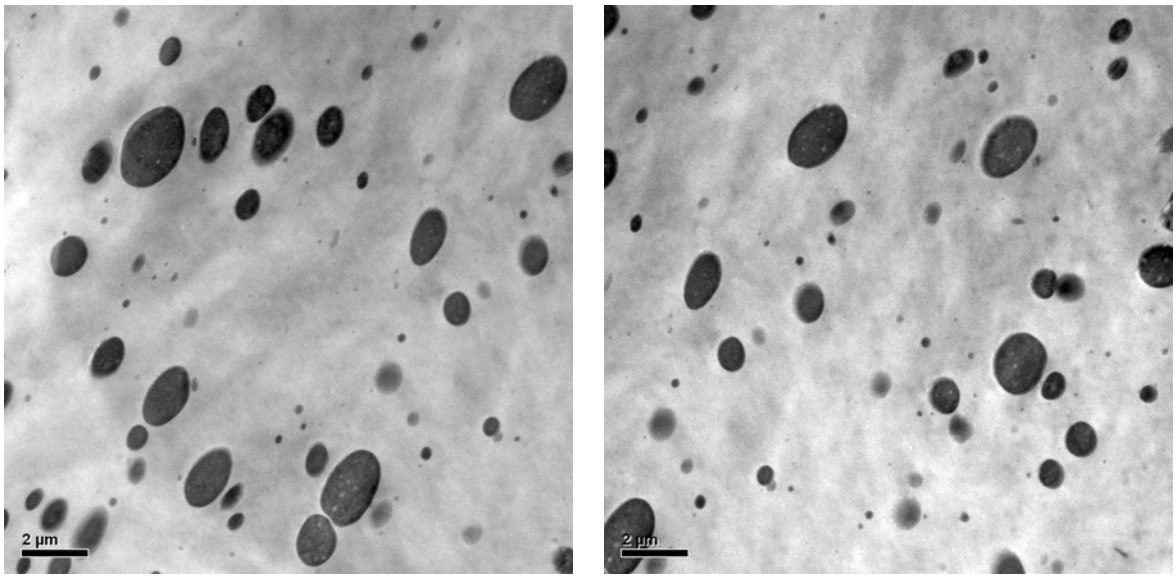

Fig. 70: Core region of the dumbbell specimen of RPP(7), vertical to flow direction. Particle diameter about 0.1-2 µm.

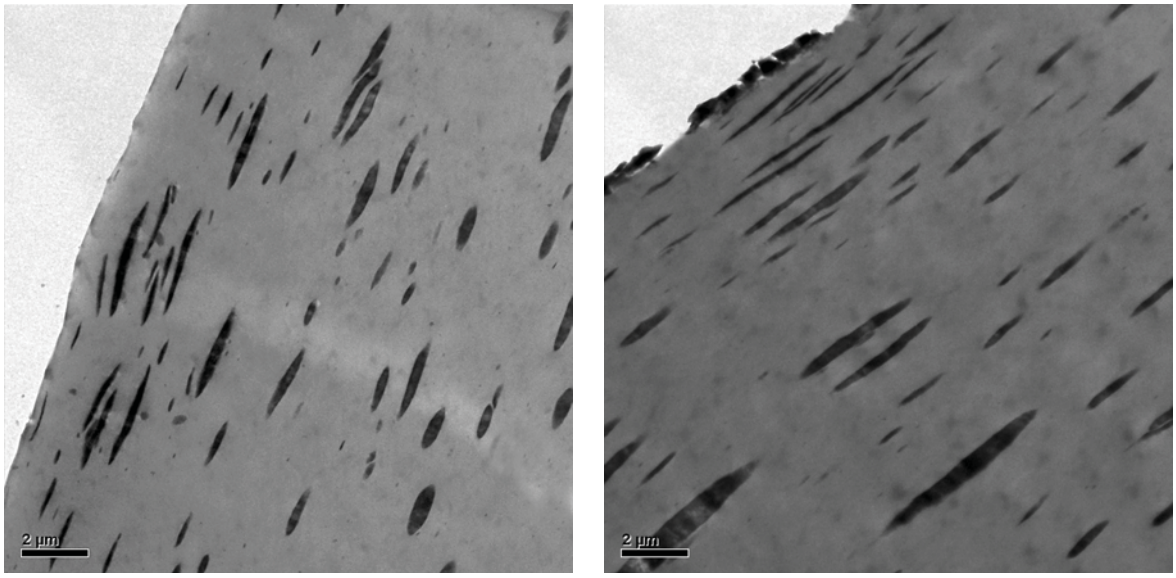

Fig. 71: Skin layer of the RPP(3.5), parallel to flow direction. Particle about 0.1-5 µm in length and 0.1-0.8 µm in width.

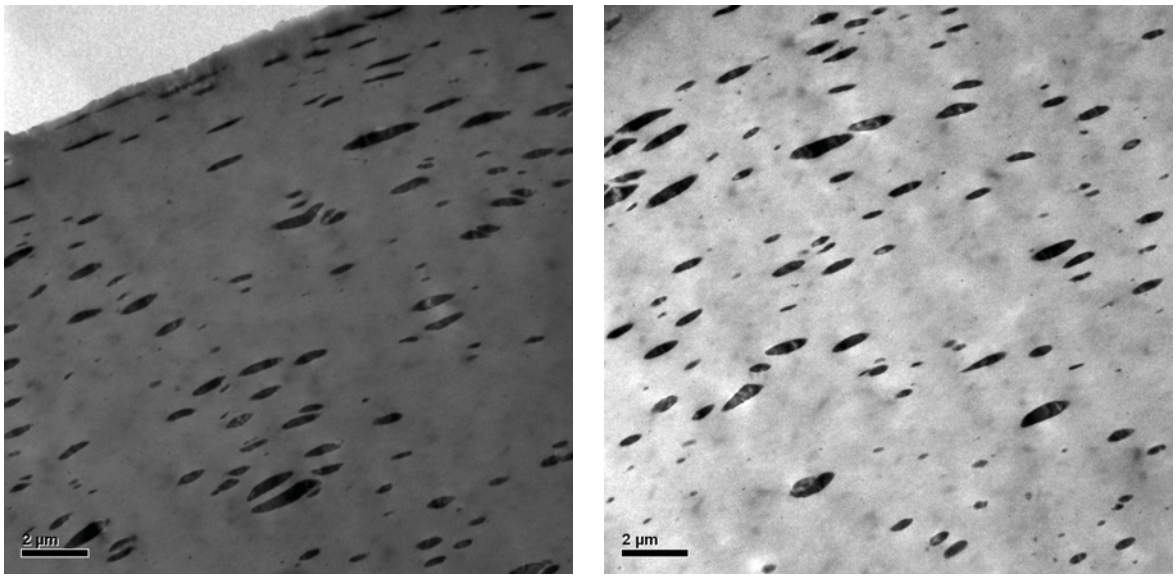

Fig. 72: Skin layer of the RPP(3.5), vertical to flow direction. Particle about 0.1-2 µm in length and 0.1-0.5 µm in width.

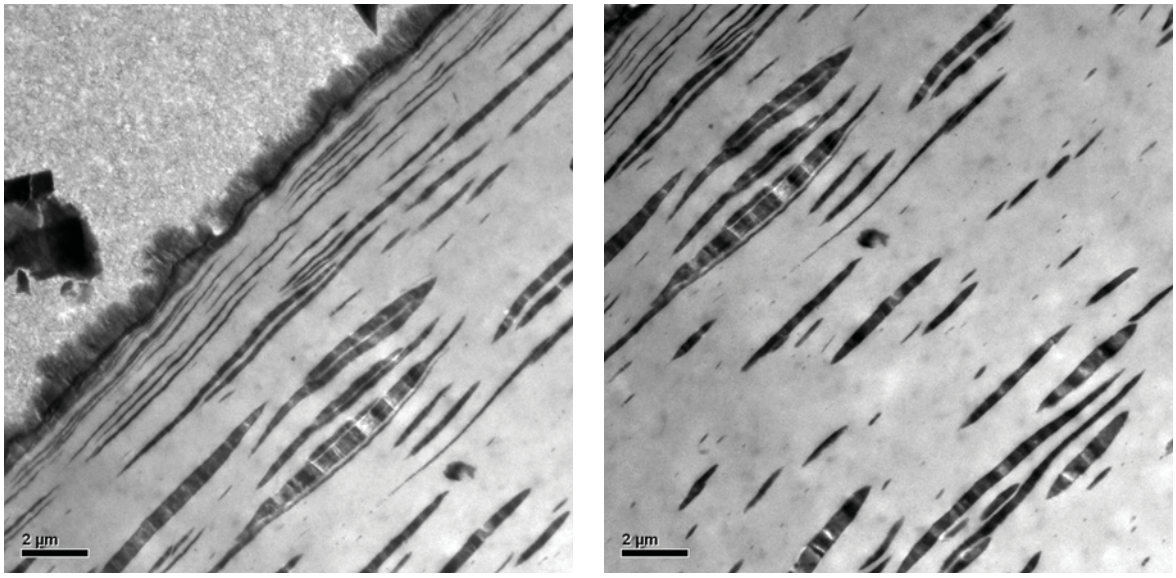

Fig. 73: Skin layer of the RPP(7), parallel to flow direction. Particle about 0.1-10 µm in length and 0.1-1 µm in width.

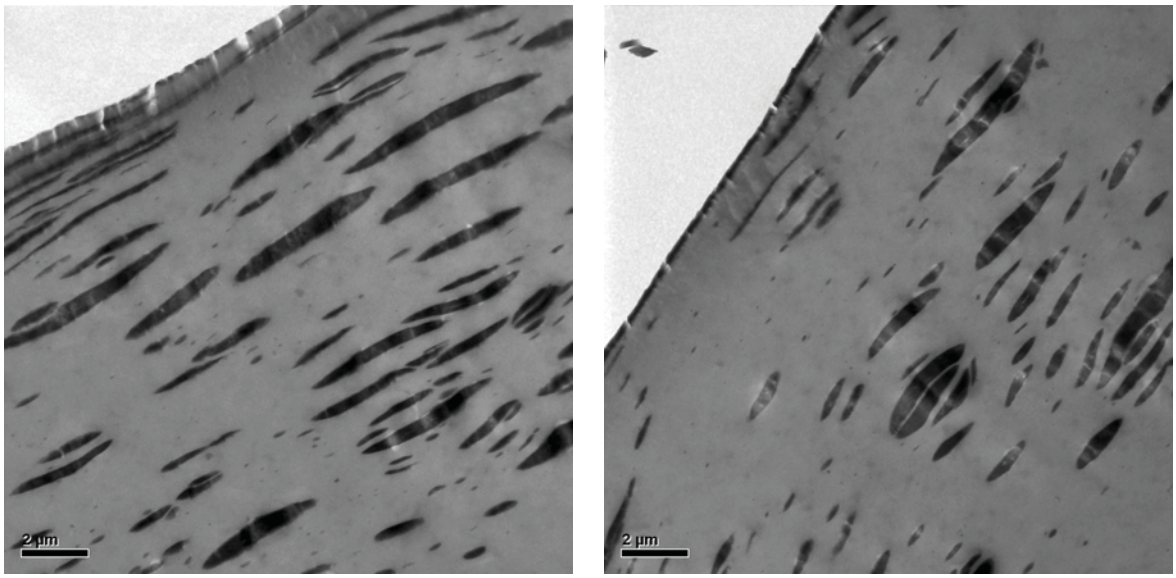

Fig. 74: Skin layer of the RPP(7), vertical to flow direction. Particle about 0.1-6 µm in length and 0.1-0.6 µm in width.

The following observations could be found by contrasting the TEM micrographs in Figs 67 to 74. The first observation is that in vertical and parallel directions the elastomer particles are elongated in the skin layer, where the values of the two

aspect ratios r_p and r_v are small (<<1), due to relatively large deformation (high orientation degree). The second observation is that the $r_p > r_v$ can be identified in the two compounds, indicating that the orientation parallel to the flow direction is more pronounced than the orientation vertical to the flow direction. The third observation, which can be seen in Figs 67 to 70 is, that the particle size and interparticle distance coincide with the filler particle volume fraction. Compared with RPP(3.5), the deformed particles of the skin layer in RPP(7) are thicker in the vertical direction and longer in the parallel direction. Not only in the skin layer but also in the core region, the filler particles of RPP(7) are in average larger than those of RPP(3.5) (see Figs 67 to 74). In addition, the distance between the particles in RPP(7) is smaller than in RPP(3.5).

Based on the TEM micrographs of the compounds, the aspect ratio r_p of the elastomer particles has been roughly estimated. The distribution of the aspect ratio r_p and the schematic illustration of the particle shape are plotted in **Fig. 75**. The statistic did not distinguish between the filler volume fractions; it is only of qualitative meaning due to the low accuracy available. One sees that the skin layer is very thin and the particle orientation has been well recovered without annealing except in the skin layer that is negligible in terms of the mechanical behaviour of the injection moulded specimens.

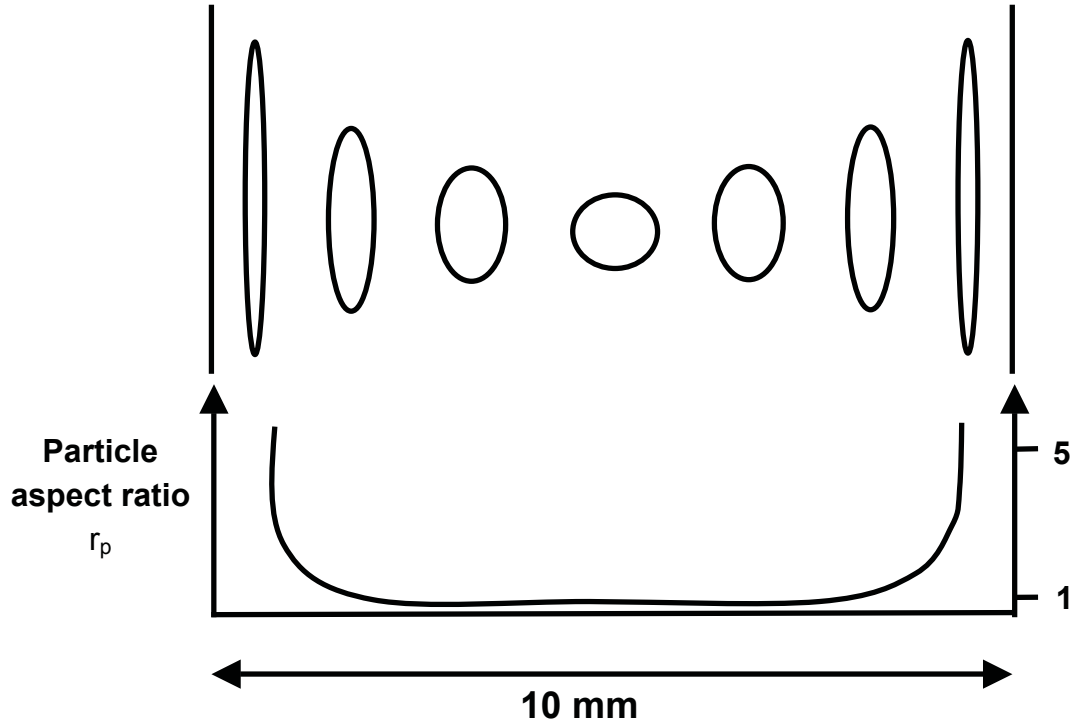

Fig. 75: Scheme of the particle shape distribution in compound, parallel to flow direction.

5.3.2.2 TEM observation of interface between two phases

As remarked at the beginning of Section 5.3.2, the interfacial bond is the key factor for the effectivity of the elastomer modification to a PP matrix. The stress transportation in the bulk material, diverse micro deformation and interaction mechanisms depend on whether the bonding between filler and matrix works sufficiently or not. The following figures show some interesting TEM micrographs in terms of interfacial bonding.

The images in **Fig. 76** should give an idea of the size ratio of the elastomer particles to the PP spherulites. As contrasted to the PP spherulites, whose diameters have an order of about 10-50 µm, the elastomer particles are only about 0.1-2 µm in diameter. The crystallinity won't be altered by elastomer particles that are too small to act as a nucleating agent or to cause a change in the spherulite type.

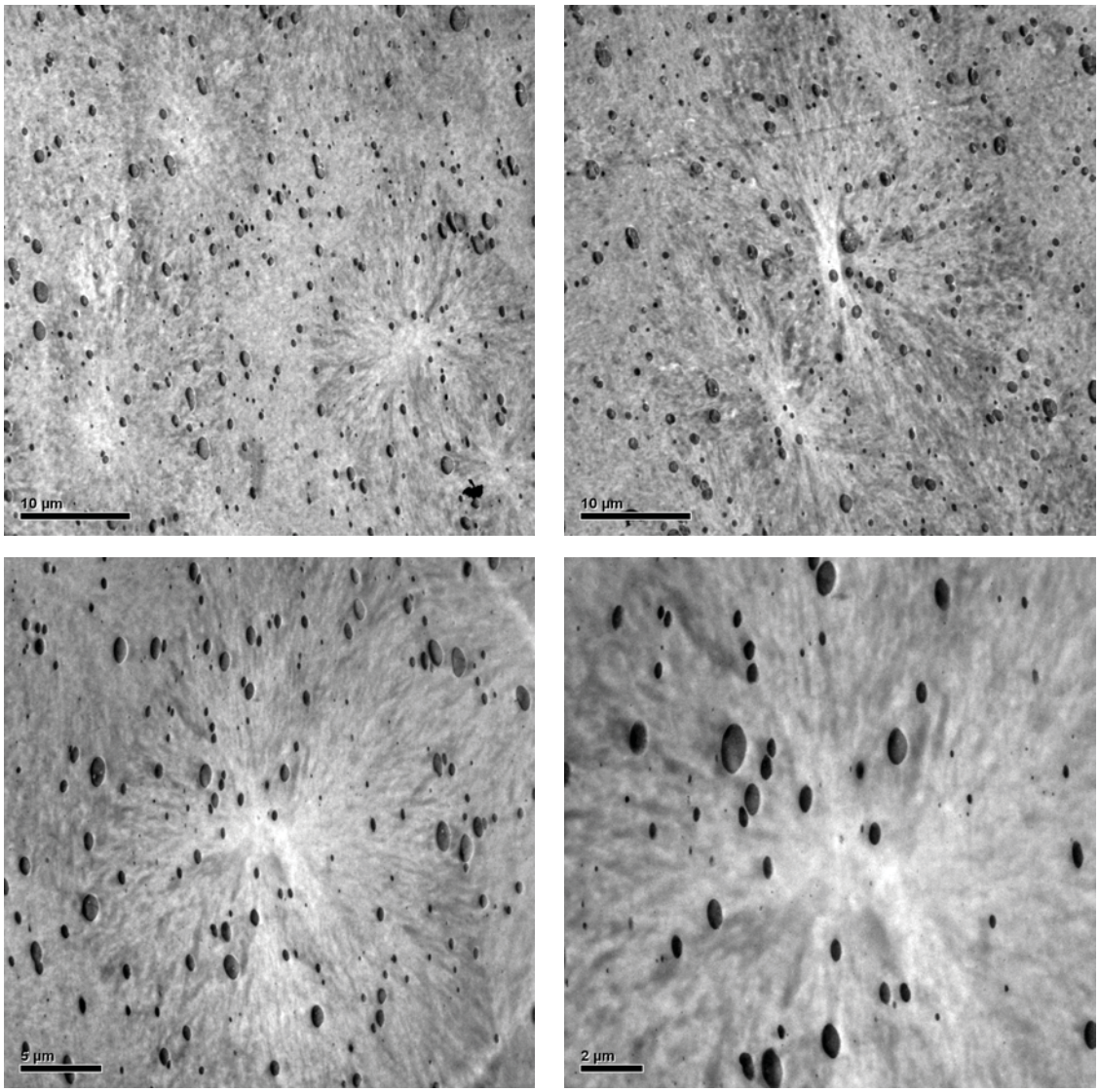

Fig. 76: TEM micrographs showing the size ratio of the elastomer particles to the PP spherulites of the compound (RPP(3.5)).

At higher magnifications, the microstructure of the compounds has been detected. The TEM micrographs in **Fig. 77** reveal some important details of the interface. **Fig. 77a** presents apparent lamellae of about 50-100 nm in length that coalesce the particle and the resin surrounding it. The interfacial lamellae play the chief role in linking the two phases in the compound. Even though we have not identified chemical bonding, entanglement between molecule chains of both phases may be formed and contribute to stress transportation. At the same time, the serrate lamellae protruding from the filler particles can gear the particle and the matrix so that the interfacial coalescence can be enhanced. The micrographs (**Fig. 77b, c, d**) are further examples which reveal the morphology of the interface.

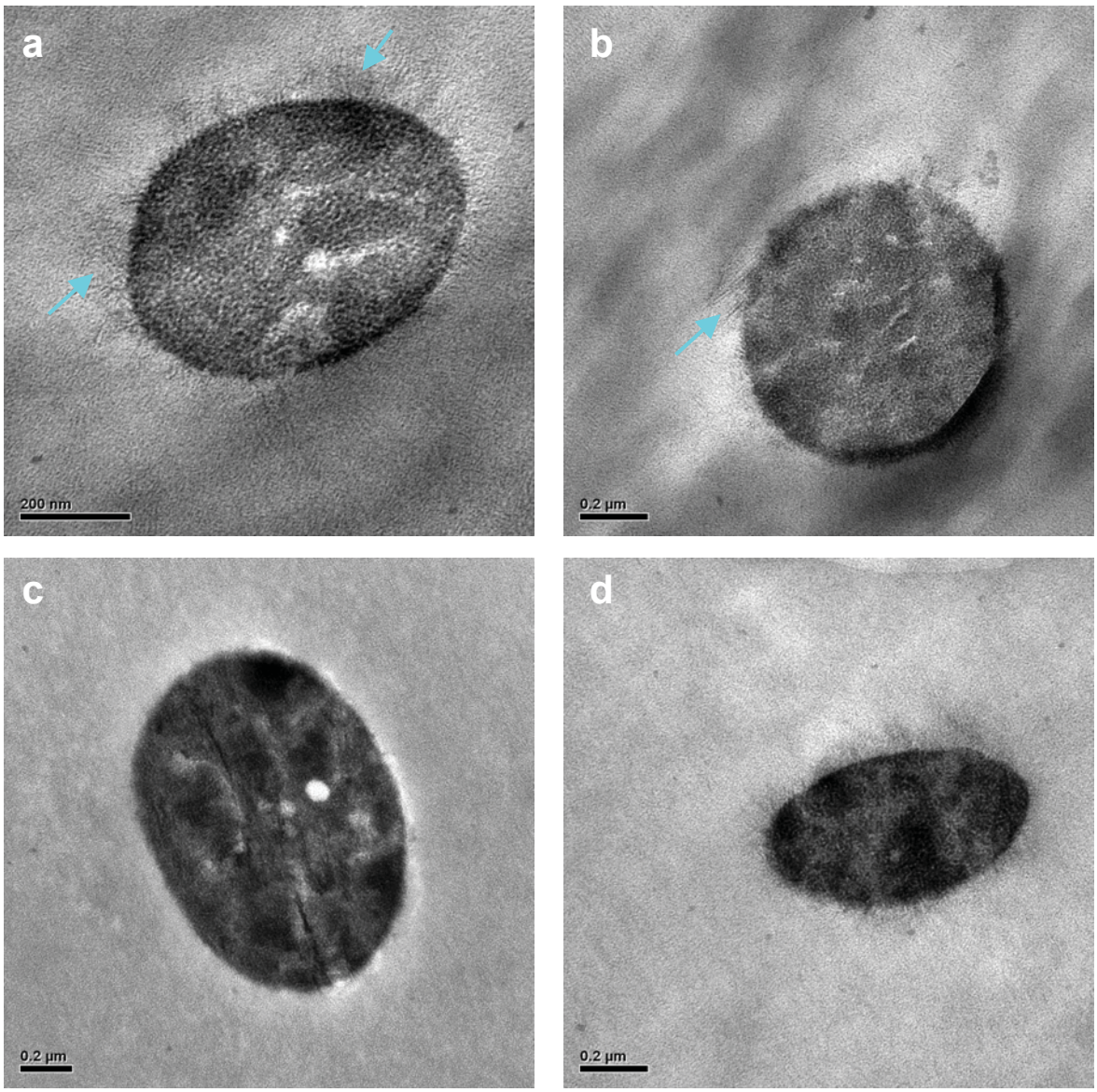

Fig. 77: TEM micrographs showing interfacial connections. The lamellae are about 50-100 nm in length.

In **Fig. 78**, three adjacent particles have been captured. It remains open if the particles will combine or will be isolated. The theories introduced in Section 2.1.4 may be used to investigate the formation and the size of an elastomer droplet in the melt during compounding and moulding. Nevertheless, the matter is beyond the scope of this work.

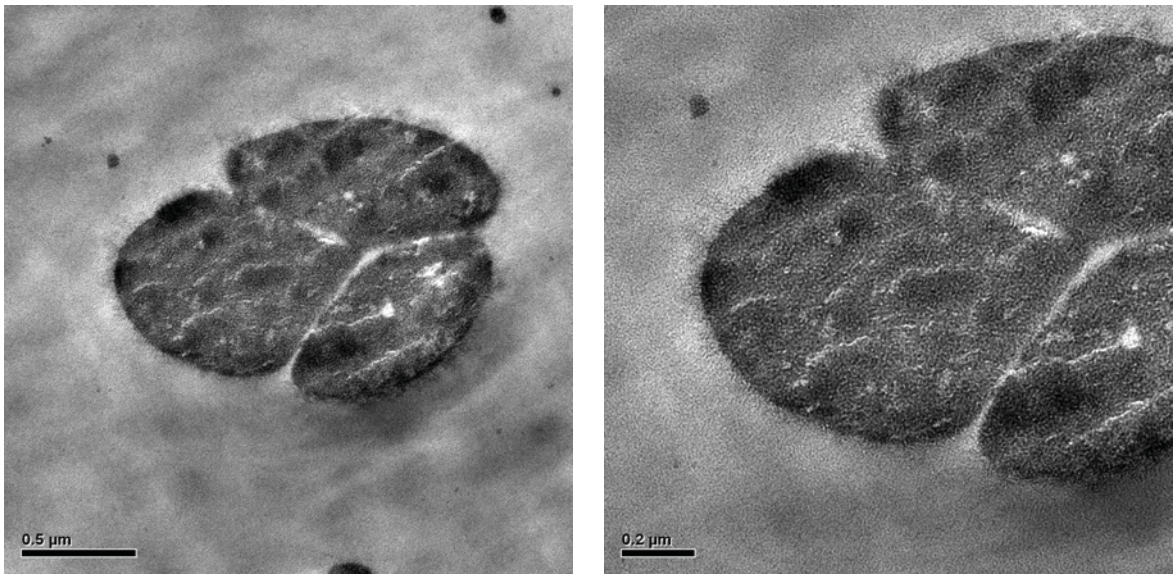

Fig. 78: TEM micrographs of three adjacent elastomer particles.

Before dealing with the next section, a brief review on the microscopic investigations shall be made here. The microstructures of the compounds have been successfully determined by means of LM and TEM. Due to lack of adequate analysing tools the attempt of obtaining the particle size distribution failed. The determination of the particle size distribution is problematic (**Fig. 64**) and requires adequate approach. At least, the comparison of the compounds with view to the effect of filler volume fractions could theoretically be carried out, if systematic or automatic procedure of image analysis were established. The approximate aspect ratio r_p will be used as one of the input signals in modeling and simulation. The next section focuses on modeling and simulating the mechanical behaviour of the compounds based on the information extracted from the experiments of constituents. The results of simulation of the compound behaviour will then be compared with the experiments on the compounds.

5.4 Simplified modeling and simulation of the mechanical behaviour of the compounds

Gastl introduced the practical operation of modeling and simulation of polymer materials with help of the software DIGIMAT MF in detail [Gastl, 2008]. Based on established concepts, the glass reinforced PP was investigated, where the glass represented the group of hard particle fillers [Gastl, Jerabek and Major, to be published]. In further investigations, polyester fibre reinforced and elastomer particles modified PP will be studied [Gastl, Jerabek and Major, to be published at the DIGIMAT user's meeting, Belgium, November 2008]. As mentioned in the introduction, the long-term objective of the research project, to which this work belongs, is to study the property relationship between the constituents (modifier and matrix) and the compound (a multiphase composition), and to bring out a modeling and simulation system for diverse applications in development of new compounds and for prediction of the compound performance.

In DIGIMAT MF there are various possible elasticity models (see **Table 6**), of which the simple combination for elastomer-filled PP were used in simulation of small deformation behaviour (see Section 4). It is assumed that the matrix is linear elastic and the filler obeys the hyperelastic material law and the properties are isotropically symmetric. Only the linear elastic behaviour has been simulated in this work, where it focuses on the small strain deformation of materials (refer to **Fig. 19**). The simulation results of large strain deformation will be discussed elsewhere [Jerabek and Major, to be published].

Table 6: Models of elasticity of constituents of the compounds.

Matrix	**Filler**
elastic	elastic
elastic	hyperelastic
elastoplatic	elastic
elastoplastic	hyperelastic

The input data are:

1.) Filler volume fraction:

RPP(3.5)-3.5 vol %

RPP(7)-7 vol %

2.) Temperatures:

-30 °C

25 °C

80 °C

3.) Material law:

Linear elasticity for PP(H) (refer to **Fig. 34**)

Linear elasticity for R(PEO) for small deformation

Mooney-Rivlin model for R(PEO) for large deformation

4.) The aspect ratio of elastomer particles:

r_p=b/c= a/c=1

(refer to **Fig. 66** on page 69 for definition of r_p)

5.) Experimentally determined mechanical parameters of material (see **Table 7**).

6.) Mooney constants for R(PEO) (for large deformation):

C_1 : –0.8 MPa

C_2 : 2.5 MPa

Table 7: Mechanical parameters of two constituents from experiments.

PP(H)	-30 °C	E = 4000 MPa	ν = 0.31
	25 °C	E = 1300 MPa	ν = 0.42
	80 °C	E = 360 MPa	ν = 0.48
R(PEO)	-30 °C	E = 33 MPa	
	25 °C	E = 10 MPa	ν = 0.48
	80 °C	E = 1 MPa	

The output data are the calculated mechanical parameters of the compounds. Below the results of simulation and the experimentally determined data will be compared (see Figs 79 to 82). Two mechanical parameters have been calculated by DIGIMAT MF; they are the tensile elastic modulus, E, and Poisson's ratio, ν. Poisson's ratio, ν, is the ratio of lateral strain (perpendicular to load direction) divided by the axial strain (load direction), referring to the uniaxial tensile test.

Comparisons of experimental and computational estimated E and ν of compound RPP(3.5) with 3.5 vol% elastomer fillers are shown in **Fig. 79** and **Fig. 80**. Comparisons of experimental and computational estimated E and ν of compound RPP(7) with 7 vol% elastomer fillers are presented in **Fig. 81** and **Fig. 82**.

A few simplifications have been made in the simulation procedure. The properties of the material are assumed to obey isotropic symmetry. The hyperelastic elastomer particles have been taken as elastic at small strain. Even the viscoelasticity of the resin PP has been ignored. But as E characterizes primarily the linear elastic behaviour of the material at a very small strain, such simplifications are reasonable. This is supported by the quite satisfactory agreement between the simulated and measured values of the two mechanical material characteristic parameters E and ν at each filler volume fraction. Only minimal discrepancies have been observed that shall be optimized by further adjustment of the simulation technique and the improvement of accuracy of input data.

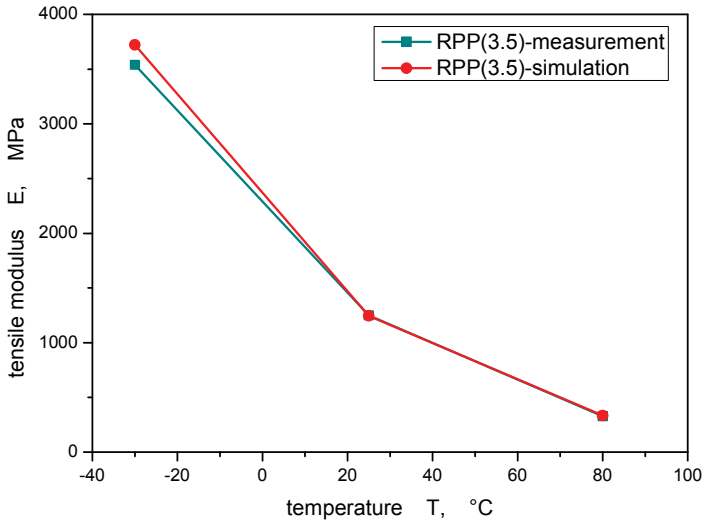

Fig. 79: Simulated and measured tensile modulus, E, of RPP(3.5) in function of temperature.

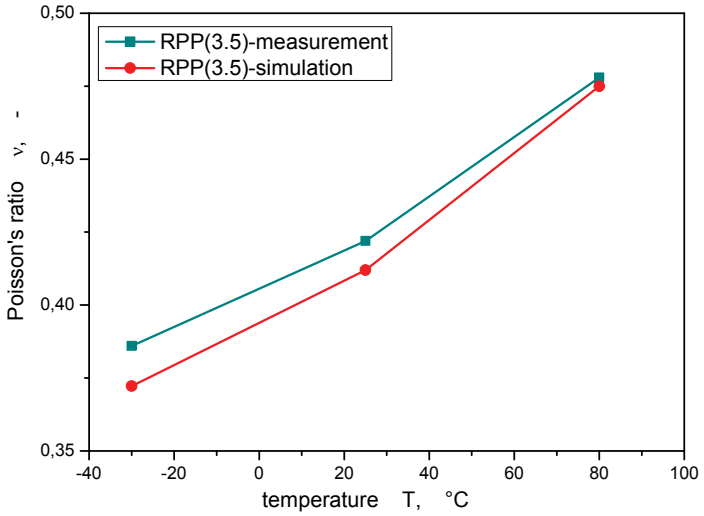

Fig. 80: Simulated and measured Poisson's ratio, ν, of RPP(3.5) in function of temperature.

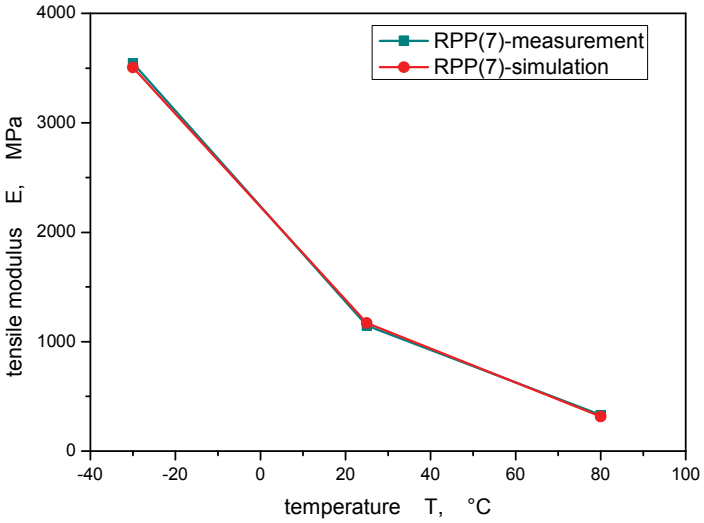

Fig. 81: Simulated and measured tensile modulus, E, of RPP(7) in function of temperature.

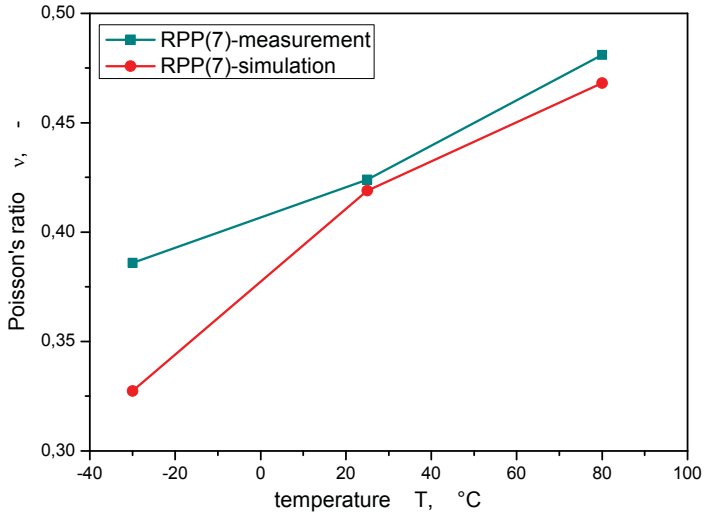

Fig. 82: Simulated and measured Poisson's ratio, ν, of RPP(7) in function of temperature.

6 SUMMARY AND CONCLUSIONS

For micromechanics-based material modeling and simulation of heterogeneous polymer compounds, adequate mechanical material data and microstructural parameters of the constituents are used as input data. Polymeric materials in general show highly non-linear, time and temperature dependent mechanical properties. Moreover, thermoplastic polymer and hyperelastic elastomer have significantly different time and temperature dependence in the reversible as well as in the irreversible deformation region. Therefore the mechanical behaviour of the polymer matrix in case of the hard-mineral-particle-filled polymer compounds and of both elastomer filler and polymer matrix in the case of the soft-elastomer-particle-filled polymer compounds should be characterized for modeling and simulation of the compound behaviour regarding their time and temperature dependence. To verify the results of simulation, the mechanical behaviour of compounds is to be characterized experimentally under conditions that are to be used in the simulation, too. Morphological investigations are required to determine the microstructural characteristic for modeling and simulation of the compound behaviour.

The modeling software offers various material elasticity models. The following material elasticity models are available in the DIGIMAT MF used for this work:

- elastic material
- thermoelastic material
- viscoelastic materil
- hyperelastic material and
- elastic-plastic material

Different material testing methods can be used to determine input data required by different models. For the elastic and elastic-plastic models used for thermoplasts like polypropylene, uniaxial tensile tests can be applied. For the hyperelastic model used for elastomers, monotonic tensile tests including uniaxial tensile test, planar tensile test and biaxial tensile test are normally applied to determine the large deformation behaviour of material under multiaxial strain states. For the viscoelastic material model, either experiments under static loading conditions (creep or relaxation) or conducting cyclic experiments in a small deformation range can be used. Dynamic mechanical analysis (DMA) was used in this work because it needed shorter testing time than static methods. This work focused on the small deformation behaviour of the compounds, thus the simulation used the simple elastic model for two constituents though they had different elasticities in general.

For the elastic model, tensile modulus and Poisson's ratio of the two constituents were determined using engineering stress-strain relationships of uniaxial tensile tests at testing temperatures of -30 °C, 23 °C and 80°C. The testing temperatures represent the temperature range of automotive applications where the compounds will be mainly used. The two Mooney-Rivlin parameters were estimated based on the engineering stress-strain relationship of uniaxial tensile test on the elastomer at room temperature. They can be used for simulation of deformation (strain) up to 25% according to the simple Ogden model. To describe the large deformation behaviour of the elastomer, complex models will be selected which need more than two parameters that can be determined by multiaxial tensile tests such as planar and biaxial tensile tests. In the DMA experiments, the limits of linear viscoelasticity of the two constituents and two compounds were determined by amplitude scan. In the temperature scan, the glass transition temperature and temperature dependence of storage modulus and loss tangent of materials were determined in temperature range of from –60 to 120 °C.

Based on monotonic mechanical tests, the neat polypropylene matrix PP(H) revealed a significant temperature dependence, tensile modulus and yield stress decreased with increasing temperature. PP(H) showed elastic-plastic characteristic according to uniaxial tensile tests, where necking and irreversible deformation of the specimens were observed after the yield point. As expected, the PP(H) matrix showed a typical temperature-dependent dynamic mechanical behaviour according to DMA. Monotonic tensile tests of the elastomer were carried out successfully. The two Mooney-Rivlin parameters were evaluated using the stress-strain relationship of uniaxial tensile tests of elastomer R(PEO). The results of planar and biaxial tensile tests were not used in the simulation in this work but they will be used in the further work of the project. The temperature dependence of the storage modulus and the loss tangent of elastomer R(PEO) was observed in DMA, too. Based on these results, mechanical behaviour of the two constituents can be combined in elastic-elastic, elastic-hyperelastic or viscoelastic-viscoelastic models for simulation.

Summarizing the results of the mechanical characterization of the matrix PP(H) and the filler R(PEO), the following conclusions may be drawn:

- PP(H) exhitbits thermoplastic mechanical behaviour and R(PEO) exihibits hyperelastic mechanical behaviour. PP(H) has a higher stiffness and higher strength than R(PEO). The tensile modulus and yield stress of compounds may reduce with rising filler content, and so do the storage modulus of the compounds.
- The mechanical behaviour of the two constituents is time and temperature dependent. The compounds are supposed to have similar dependences in application.

The results of the simulation of mechanical properties of compounds were compared with the experimental test results. As expected the two compounds RPP(3.5) and RPP(7) had a lower modulus and yield stress in monotonic tensile tests when compared with PP(H). Furthermore, the comparison of the master curves over a wide frequency range and the comparison of the storage modulus variation over a temperature range of the four materials showed that the elastomer phase reduced the storage modulus of the polypropylene matrix, but the dynamic behaviour of compounds was controlled by the matrix material at small filler fractions.

Particle filled polymeric materials may have a highly heterogeneous microstructure depending on processing and viscosities of constituents. The size distribution, shape, orientation of filler particles and the level of adhesion (quality of the interface) between matrix and filler particle highly influence the mechanical behaviour of compound. Hence, in addition to the mechanical characterization of the constituents, it is necessary to determine geometrical and spatial quantities of the heterogeneity to perform modelling for particle-filled polymer compounds. The relevant morphological parameters can be determined by microscopy of compounds.

Transmission electron microscopy (TEM) is a proper technique for establishing microstructure-property relationships. Based on the TEM investigations of injection moulded tensile dumbbell specimen of compounds, the following results were observed:

- PP is the continuous phase and the elastomer particles are dispersed and form the discrete phase in the compounds investigated.
- Size and shape (characterised by aspect ratio r_P) of the elastomer filler particles were relatively uniform except in the skin layer of the specimen. In most parts of the specimen, filler particles are nearly spherical (r_P =1), ellipsoid particles with r_P values of between 2 and 5 were observed in skin layer of specimens where all particles are oriented in flow direction.
- The filler particles are too small to affect the crystallinity of PP matrix. The diameter of PP spherulites is about 10-50 µm, but the elastomer particles are only about 0.1-2 µm in diameter.
- Interfacial lamellae were seen in compounds and good adhesion can thus be assumed.

In this work, the intended investigations were performed and delivered material parameters needed. Simulation of small deformation behaviour of compounds was carried out successfully using simple material models. Simulation showed good agreement with experiments. Large deformation behaviour of compounds will be characterized and simulated in the future work of the project.

REFERENCES

1. Amelinckx at el. (1997). "Electron Microscopy", VCH Verlagsgesellschaft mbH, Weihheim.
2. Amelinckx at el. (1997). "Handbook of Microscopy", VCH Verlagsgesellschaft mbH, Weihheim.
3. Birley et al. (1991). "Physics of Plastics", Hanser, Germany.
4. Briscoe.B.J et al. (1999). "A review of immiscible fluid mixing", Advances in Colloid and Interface Science 81 (1999) 1-17.
5. Bucknall.C.B, Smith.R.R (1965). Polymer 6 (1965) 437.
6. Bucknall.C.B et al. (1999). "Polymer Blends Volume 1: Formulation", John Wiley & Sons, INC, USA.
7. Bucknall.C.B (2006). "New criterion of craze initiation", Polymer 48 (2007) 1030-1041.
8. Coran.A.Y and Patel.R (1995), "Thermoplastic elastomers by blending and dynamic vulcanization", Polypropylene: Structure, blends and composites, edited by J. Karger- Kocsis, published by Chapman & Hall, London.
9. Ehrenstein.G.W, Riedel.G and Trawiel.P (1998). "Praxis der Thermischen Analyse von Kunststoffen", Carl Hanser Verlag München Wien.
10. Feichter.C, Major.Z, Lang.R.W (2006). "Deformation Analysis of Notched Rubber Specimens", Strain, Vol. 42, 299-304(6)
11. Gastl.S et al. (2008). " Microstructure simulation of hard particle strengthened PP ", bachelor's thesis, Institute of Materials Science and Testing of Plastics, University of Leoben, Austria.
12. Grellmann.W, Seidler.S, Kotter.I (2000). "Brittle-to-tough Transition in Toughened Polypropylene Copolymers", Polymer and Composites, No. 24, pp. 1-8.
13. G'Sell et al. (2004). "PP-PA 6-POE blends. Part 2: volume dilatation during plastic deformation under uniaxial tension", Polymer 45 (2004) 5785-5792.
14. Ha-Anh.T and Vu-Khanh.T (2005). "Prediction of mechanical properties of polychloroprene during thermo-oxidative aging", Polymer Testing 24 (2005) 775-780.
15. Herbst.H (2008). Ph.D thesis, to be published in 2008
16. Hertzberg, (1995). "Deformation and fracture mechanics of engineering materials", John Wiley & Sons, USA.
17. Jang.B.Z, Uhlmann.D.R (1984). J. Appl. Polym. Sci., 29, 3409.
18. Jang.B.Z, Uhlmann.D.R (1985). Polym. Eng. Sci., 25, 643.

19. Sternstein.S, Ongchin.L (1969). Polymer Preprints, Am Chem Soc Div Polym Chem;10:1117.
20. Jerabek.M, Major.Z, Herbst.H (2007). "Mechanical characterisation of particle-filled polypropylene compounds", 12th International Workshop on Advances in Experimental Mechanics, Portoroz, Slowenien.
21. Jerabek.M (2008). Ph.D thesis, to be published in 2008
22. Karger-Kocsis.J (1995). "Polypropylene Structure, blends and composites", Chapman & Hall, UK.
23. Kimberly et al. (2000). "Semicrystalline Blends of Polyethylene and Isotactic Polypropylene: Improving Mechanical Performance by Enhangcing the interfacial Structure", Journal of Polymer Science: Part B: Polymer Physics, Vol. 38, 108-121.
24. Lovell.P.A et al. (1993). "Multiple-Phase Toughening-particle Morphology", toughended plastics I, edited by Riew et al., American Chemical Society.
25. Ma et al. (1981). "Structure and Properties of polymers", Beijing.
26. Mach.E et al. (2008). " Characterization of Deformation Behaviour of NBR-PTFE Compounds and Simulation", bachelor's thesis, Institute of Materials Science and Testing of Plastics, University of Leoben, Austria.
27. Martuscelli.E (1990). "Rubber modification of polymers: phase structure, crystallization, porcessing and properites, in Thermoplastic Elastoemrs from Rubber-Plastic Blends", Ellis Norwood, London.
28. Martuscelli.E (1995). "Structure and properties of polypropylene-elastomer blends", Polypropylene: Structure, blends and composites, edited by J. Karger-Kocsis, published by Chapman & Hall, London.
29. McCrum.N.G et al. (1988). "Principles of Polymer Engineering", Oxford.
30. Moore.P (1996). "Polypropylene Handbook", Hanser, Munich.
31. Narisawa.I (1999). "Crazing and shear yielding in polypropylene", Polypropylene, edited by J.Karger-Kocsis, ISBN 0 412 80200 7.
32. Pilz.G (2001). "Viscoelastische Eigenschaften Polymerer Werkstoffe für Rohranwendungen", Ph.D. Thesis, Institute of Materials Science and Testing of Plastics, University of Leoben, Austria.
33. Poelt.P, Ingolic.E, Gahleitner.M et al. (2000). "Characterization of Modified Polypropylene by Scanning Electron Microscopy", Journal of Applied Polymer Science, Vol. 78, 1152-1161.
34. Pukanszky.B (1995). "Particulate filled polypropylene structure and properties", Polypropylene: Structure, blends and composites, edited by J. Karger- Kocsis, published by Chapman & Hall, London.
35. Rezaifard et al. (1993). "Toughening Epoxy Resin with Poly (methyl

methacrylate)- Grafted Natural Rubber", toughended plastics I, edited by Riew et al., American Chemical Society.
36. Saechtling (1995). "Plastics Handbook", Hanser, Munich Vienna New York.
37. Strobl.G.R (1996). "The physics of Polymers", Springer-Verlag Berlin Heidelberg.
38. Thomas.E.L and Talmon.Y (1978). Polymer, 19,225 (1978).
39. Treloar.L.R.G (1975). “the physics of rubber elasticity”, Clarendon Press, Oxford.
40. Utracki.L.A and Dumoulin.M.M (1995). "Polypropylene alloys and blends with thermoplastics", Polypropylene structure, blends and composites, edited by J. Karger-Kocsis, published by Chapman & Hall, London.
41. Van der Wal.A et al. (1998). "Polypropylenen-rubber blends: 1. The effect of the matrix porperties on the impact behaviour", Polymer 39 (1998), 6781-6787
42. Van der Wal.A et al. (1999). "Polypropylenen-rubber blends: 4. The effect of the rubber particle size on the fracture behaviour at low and high test speed", Polymer 40 (1999) 6057-6065.
43. Van der Wal.A, Gaymans.R.J (1999). "Polypropylene-rubber blends: 5. Deformation mechanism during fracture", Polymer 40 (1999) 6067-6075.
44. Varga.J, Schulek-Toth.F (1991). Angewandte Makromolekulare Chemie, 188, 11-25.
45. Verchere et al. (1993). "Rubber-Modified Epoxies", toughended plastics I, edited by Riew et al., American Chemical Society.
46. Vilgis.T.A. (2003). "Statistical Physics of Reinforced Nano Composite Materials", Mainz, Germany.
47. Wool.R.P (1995). "Welding and fracture of polypropylene interfaces", Polypropylene: Structure, blends and composites, edited by J. Karger- Kocsis, published by Chapman & Hall, London.
48. Wu.S (1985). "Phase structure and adhesion in polymer blends: A criterion for rubber toughening", Polymer Volume 26, Problem 12, November 1985, Pages 1855-1863.
49. Wypych.G (1999). "Handbook of fillers", CehmTec Publishing, Toronto-New York.
50. Xu.Y.H and Pitot.H.C (2003). "An improved stereologic method for three-dimensional estimation of particle size distribution from observations in two dimensions and its application", Computer Methods and Programs in Biomedicine /2 (2003) 1-20.
51. Yang.H et al. (2007). " Largely improved toughness ofPP/EPEM blends by adding nano-SiO_2 particles", Polymer, 48, 860-869.

52. Yokoyama.Y, Ricco.T (1998). "Toughening of polypropylene by different elastomeric systems" Polymer, Volume 39, Problem 16, Pages 3675-3681.
53. Zebarjad.S.M et al. (2006). " Modification of fracture toughness of isotactic polypropylene with a combination of EPR and $CaCO_3$ particles", Journal of Materials Processing Technology, Vol 175, Problems 1-3, 446-451.

APPENDIX: TECHNICAL INFORMATION ON POLYOLEFIN ELASTOMER BY DOW

Technical Information

ENGAGE 8100

Polyolefin Elastomer

ENGAGE™ 8100 Polyolefin Elastomer is an ethylene-octene copolymer that has excellent flow characteristics and performs well in a wide range of general purpose thermoplastic elastomer applications.

ENGAGE 8100 provides superb impact properties in blends with polypropylene (PP) and polyethylene (PE). ENGAGE 8100 provides high filler loading capability and outstanding peroxide cure capability. When cross-linked by peroxide, silane, or irradiation, it gives exceptional heat aging, compression set, and weather resistance properties, and may be used to produce high performance electrical insulation.

Main Characteristics

- Pellet form
- Excellent flow characteristics
- Improved impact in polypropylene and polyethylene
- High filler loading
- Peroxide, silane, and radiation curable
- Exceptional heat aging, compression set, and weather resistance when cured

Applications

- General purpose thermoplastic elastomers
- Wire and cable
- Impact modification

Properties(1)

Typical Physical	Test Method	Value
Melt Index, 190°C/2.16 kg, dg/min	ASTM D 1238	1.0
Density, g/cm^3	ASTM D 792	0.870
Mooney Viscosity, ML 1 + 4 @ 121°C	ASTM D 1646	24.1
Typical Molded(2)		
Ultimate Tensile Strength, MPa	ASTM D 638(3)	9.76
Ultimate Tensile Elongation, %	ASTM D 638(3)	810
100% Modulus, MPa	ASTM D 638(3)	2.9
Hardness	ASTM D 2240	
Shore A (1 Sec)		73
Shore D (1 Sec)		22
Flexural Modulus, MPa	ASTM D 790	
1% Secant		14.3
2% Secant		13.1
Tear Strength, Type C, kN/m	ASTM D 624	40
Typical Thermal		
Vicat Softening Point, °C	ASTM D 1525	45
DSC Melting Point, 10°C/min rate, °C	Dow Method	60
Glass Transition Temperature, °C	Dow Method	-52
Tc Peak, °C	Dow Method	45

(1) These are typical properties only and are not to be regarded as sales specifications.
(2) Compression molded
(3) 508 mm/min

Product Stewardship

The Dow Chemical Company and its subsidiaries ("Dow") has a fundamental concern for all who make, distribute, and use its products, and for the environment in which we live. This concern is the basis for our Product Stewardship philosophy by which we assess the safety, health, and environmental information on our products and then take appropriate steps to protect employee and public health and our environment. The success of our Product Stewardship program rests with each and every individual involved with Dow products — from the initial concept and research, to manufacture, use, sale, disposal, and recycle of each product.

Customer Notice

Dow strongly encourages its customers to review both their manufacturing processes and their applications of Dow products from the standpoint of human health and environmental quality to ensure that Dow products are not used in ways for which they are not intended or tested. Dow personnel are available to answer your questions and to provide reasonable technical support. Dow product literature, including safety data sheets, should be consulted prior to use of Dow products. Current safety data sheets are available from Dow.

Medical Applications Policy

NOTICE REGARDING MEDICAL APPLICATION RESTRICTIONS: Dow will not knowingly sell or sample any product or service ("Product") into any commercial or developmental application that is intended for:

a. long-term or permanent contact with internal bodily fluids or tissues. "Long-term" is contact which exceeds 72 continuous hours (or for PELLETHANE™ Polyurethane Elastomers only, which exceeds 30 days);
b. use in cardiac prosthetic devices regardless of the length of time involved ("cardiac prosthetic devices" include, but are not limited to, pacemaker leads and devices, artificial hearts, heart valves, intra-aortic balloons and control systems, and ventricular bypass-assisted devices);
c. use as a critical component in medical devices that support or sustain human life; or
d. use specifically by pregnant women or in applications designed specifically to promote or interfere with human reproduction.

Dow requests that customers considering use of Dow products in medical applications notify Dow so that appropriate assessments may be conducted.

Dow does not endorse or claim suitability of its products for specific medical applications. It is the responsibility of the medical device or pharmaceutical manufacturer to determine that the Dow product is safe, lawful, and technically suitable for the intended use. **DOW MAKES NO WARRANTIES, EXPRESS OR IMPLIED, CONCERNING THE SUITABILITY OF ANY DOW PRODUCT FOR USE IN MEDICAL APPLICATIONS.**

Disclaimer

NOTICE: No freedom from infringement of any patent owned by Dow or others is to be inferred. Because use conditions and applicable laws may differ from one location to another and may change with time, the Customer is responsible for determining whether products and the information in this document are appropriate for the Customer's use and for ensuring that the Customer's workplace and disposal practices are in compliance with applicable laws and other governmental enactments. Dow assumes no obligation or liability for the information in this document. **NO WARRANTIES ARE GIVEN; ALL IMPLIED WARRANTIES OF MERCHANTABILITY OR FITNESS FOR A PARTICULAR PURPOSE ARE EXPRESSLY EXCLUDED.**

NOTICE: If products are described as "experimental" or "developmental": (1) product specifications may not be fully determined; (2) analysis of hazards and caution in handling and use are required; (3) there is greater potential for Dow to change specifications and/or discontinue production; and (4) although Dow may from time to time provide samples of such products, Dow is not obligated to supply or otherwise commercialize such products for any use or application whatsoever.

Additional Information

North America
U.S. & Canada: 1-800-441-4369
1-989-832-1426
Mexico: +1-800-441-4369

Latin America
Argentina: +54-11-4319-0100
Brazil: +55-11-5188-9000
Colombia: +57-1-219-6000
Mexico: +52-55-5201-4700

Europe/Middle East +800-3694-6367
+32-3-450-2240

South Africa +800-99-5078

Asia Pacific +800-7776-7776
+60-3-7958-3392

www.dowplastics.com

This document is intended for use within GEOGRAPHIC AREA
Published May,2008

Form No. 774-00002-0508X